UNIVERSIDAD NACIONAL DE COLOMBIA

Production of n-butyl lactate by reactive distillation process: State-estimation, optimization and advanced control.

Cesar Augusto García Echeverry

Universidad Nacional de Colombia
School of Engineering, Doctoral Program in Chemical Engineering.
Bogotá, Colombia
2023

Production of n-butyl lactate by reactive distillation process: State-estimation, optimization and advanced control.

Cesar Augusto García Echeverry

Thesis proposal presented as partial requirement to qualify for the Doctoral degree in
Chemical Engineering.

Advisors:
Ph.D. Iván Darío Gil Chaves-Universidad Nacional de Colombia.
Ph.D. Argemiro Resende Secchi-Universidade Federal do Rio de Janeiro/Brasil.
Co-Advisor:
Ph.D. Silvia Mercedes Ochoa Cáceres-Universidad de Antioquia/Colombia

Research Topic:
Modelling and Simulation
Research Group:
Procesos químicos y bioquímicos/Lades

Universidad Nacional de Colombia
School of Engineering, Doctoral Program in Chemical Engineering.
Bogotá, Colombia
2023

I want to dedicate this work to my family, their emotional support through time, and the difficulties th at ma ke me st rong. I want to dedicate to all the people who, in some instances and moments of these four years, have added some part of their lives to help me with advice, company, friendship, and collaborative work. Thank you all.

`Any man whose errors take ten years to correct is quite a man.` Robert Oppenheimer.

"You may encounter many defeats, but you cannot be defeated. Remember that your difficulties do not define you. They strengthen your ability to overcome."Maya Angelou.

Acknowledgement

I want to thank my advisors, Iván Gil, Silvia Ochoa, and Argimiro Secchi, for their advice and knowledge shared throughout this work. Without them, it couldn't carry out this process. I want to thank all my friends and partners from Laboratorio de procesos quimicos y bioquimicos. Especially to Daniela Yusti and Jessica Velandia for helping me with the experimental part and writing papers. Especial thanks to Juan Pablo Galindo for his friendship and help with some parts of my code and to all my research group partners Liliana Avila, Victor, Angela, and Miguel. For being with me in this hard process, especially in the complex moments of my life.

I want to thank Universidad Nacional de Colombia y Universidad Federal do Rio de Janeiro for the double degree and all the nice moments. I want to thank my partners of Lades at UFRJ, especially Sergio Castaño, for helping me with a part of my code and for his friendship.

I want to thank all the guys of Semillero InnovaCodingUN; I feel very proud of you all.

I want to thank Fundación Ceiba and Gobernación de Bolivar for their financial support.

I want to thank my parents, Alberto García and Maria del Socorro Echeverry, and my brother Jose García and sister Adriana Garcia.

Finally, I want to thank life for this experience and the people I met and lost. All are an important part of this process. For the hard and complex moments that make me the person I am.

Abstract

Green chemistry has been gaining popularity to produce bio-based products and reduce environmental impact. This study examines the production of n-butyl lactate through reactive distillation at a pilot plant scale. The isobaric vapor-liquid equilibrium for the binary mixture n-butanol + n-butyl L-lactate at 1 and 5 kPa was evaluated, followed by an analysis and a new methodology to obtain maps of reactive and non-reactive residue curves for producing n-butyl lactate; results showed that it is possible to obtain n-butyl lactate with a purity of 97 % w/w. A dynamic model of the reactive distillation column was developed and validated. The model includes a mass and energy balance equation set, the NRTL thermodynamic model, and a pseudo-homogeneous kinetic equation. The model was validated against experimental data and literature data. Based on the modeling analysis and operability of the pilot plant, an advanced control strategy, a Non-linear Model Predictive Controller (NMPC), to improve n-butyl lactate production was tested in silico; this was evaluated and compared with a classic MIMO PID strategy and a Linear Model Predictive Controller (LMPC). Then, a state estimator using an Artificial Neural Network (ANN) was implemented to filter the signal from the measurements and estimate the final product composition, providing a viable scenario to predict and maintain the final product quality. The conclusion of the controller comparison showed that the NMPC presented the best performance indices, ITSE, and ITAE. However, the LMPC control was sufficiently good to be evaluated *in silico* at pilot plant scale.

Resumen

Producción de lactato de n-butilo por destilación reactiva: estimación de estado, optimización y control avanzado

La química verde ha ido ganando popularidad para producir productos biológicos y reducir el impacto ambiental. Este estudio examina la producción de lactato de butilo, a través de la destilación reactiva a escala de planta piloto. Se evaluó el equilibrio vapor-líquido isobárico para la mezcla binaria n-butanol + butil L-lactato a 1 y 5 kPa, seguido de un análisis y una nueva metodología para obtener mapas de curvas de residuos reactivos y no reactivos para producir butillactato; los resultados muestran que es posible obtener lactato de butilo con una pureza del 97 % p/p. Con los resultados del análisis, la columna de destilación reactiva se modeló y validó utilizando un modelo dinámico que incluye un conjunto de ecuaciones de balance de masa y energía y utiliza el modelo termodinámico NRTL y una ecuación cinética pseudohomogénea. El modelo se validó con datos experimentales y previamente se presentaron datos bibliográficos. Sobre la base del análisis de modelado y operabilidad de la planta piloto, se probó una estrategia de control avanzada para mejorar la producción de lactato de butilo en silico; esto se evaluó y comparó con una estrategia clásica de MIMO PID y un controlador predictivo de modelo lineal (LMPC) contra un controlador predictivo modelo no lineal (NMPC). La implementación de un estimador de estado, utilizando una Red Neuronal Artificial (ANN), para filtrar la señal de las mediciones y estimar la composición final del producto proporcionó un escenario viable para predecir y mantener la calidad del producto final. La conclusión de la comparación del controlador muestra que el NMPC presentó el mejor índice de rendimiento ITSE e ITAE. Sin embargo, el control de LMPC es lo suficientemente bueno para ser implementado en la planta.

Palabras clave: solventes verdes, lactato de butilo, destilación reactiva, modelado y simulación, control avanzado.

Contents

List of Figures

List of Tables

List of Symbols

Symbols with latin letters

Symbol	Descriptions	SI Unit
A	Area	m^2
A_{BET}	Internal area of the solid	$\frac{m^2}{g}$
A_g	Cross-sectional area of the gas phase	m^2
A_s	Cross sectional area of the bulk cargo	m^2
a	Coefficient	1
c	Carbon content	1
D	Diameter	m
E_A	Activation energy	$\frac{kJ}{mol}$
F	Volatile matter fraction	1
Fr	Froude number	1
$\overrightarrow{g}$	Acceleration of gravity	$\frac{m}{s^2}$
H	Enthalpy	J
H_o	Higher calorific power	$\frac{MJ}{kg}$
h	Hydrogen Content	1
K	Equilibrium coefficient	1
L	Length	m
L	Reactor Length	m
m	Mass	kg
$\dot{m}$	Mass flow	$\frac{kg}{s}$
n	Quantity of matter	mol
P	Pressure	Pa
Q	Heat	kJ

Symbol	Description	SI Unit
T	Temperature	K
t	Time	s
x_i	Fraction of the Quantity of matter	1
V	Volume	m^3
$\vec{u}$	Velocity	$\frac{m}{s}$
w_i	Mass fraction of component i	1
$w_{w,i}$	Moisture content of substance i	1
Z	Compressibility factor	1

Symbols with greek letters

Symbol	Defining	SI Unit
α_{BET}	Surface factor	$\frac{m^2}{g}$
β_i	Degree of formation of component i	1
γ	Wandhaftreibwinkel (Stahlblech)	1
ϵ	Particle porosity	1
η	mittlere Bettneigungswinkel (Stürzen)	1
θ	Bed tilt angle	1
θ_O	Avalanche top angle	1
θ_U	Avalanche lower angle	1
κ	Heat rate	$\frac{K}{s}$
ν	Stoichiometric coefficient	1
ρ_b	Bulk density	$\frac{kg}{m^3}$
ρ_s	Apparent density	$\frac{kg}{m^3}$
ρ_w	True density	$\frac{kg}{m^3}$
τ	Dimensionless time	1
Φ_V	Volumetric flow	$\frac{m^3}{s}$

Symbol	Defining	SI Unit
ω	Angular velocity	$\frac{1}{s}$

Subscripts

Subscripts	Meaning
bm	Organic material
DR	Dubinin-Radushkevich
E	Experimental
g	Gas phase
k	Condensed
Ma	Macropores
P	Particle
p	Pore
p	Pyrolyzed
R	Reaction
t	Total
wf	Water free
waf	Water and ash free
0	Baseline state

Superscripts

Superscripts	Term
n	Coefficient x

List of Abrevations

Acronym	In full
$VOCs$	volatile organic compounds
$VCPs$	volatile chemical products
LA	Lactic acid
$BuOH$	n-butanol
$BuLac$	n-butyl lactate
PSE	Process Systems Engineering
$LMPC$	Linear model predictive contro
$NMPC$	Non-linear model predictive contro
EKF	Extended Kalman filter
RTO	Real-time optimization
RDC	Reactive distillation column
VLE	Vapor-liquid equilibria
$VLLE$	Vapor-liquid-liquid equilibria
TAC	Annual total cost
CVP	Control vector parametrization
SQP	Successive Quadratic Programming
ILC	Iterative learning control
NLP	Non-linear programming
DAE	Differential-algebraic equation
GMC	Generic model controller
FID	Flame ionization detector
TDP	Distance to the tangent plane
$SSWR$	Sum of the square of weighted residual
IAc	Isoamyl acetate

Acronym	**In full**
AA	Acetic acid
IA	Isoamyl acetate
$NRTL$	Non-random two liquids
HOC	Hayden-O'Connell equation
RCM	Non-reactive residue curve maps
$RRCM$	Reactive-residue curve maps
Da	Damkohler number

1 State of the art and justification

1.1. Introduction

In the last ten years, an industrial interest has increased in a new type of solvents since traditional ones are considered hazardous because they include physical hazards such as explosiveness, flammability, and volatility; health hazards such as acute and chronic toxicity, carcinogenicity, mutagenicity, reproduction/developmental toxicity, ecological toxicity, and biodegradability Wypych [2014]. Taking a broader view of the emissions of all the volatile organic compounds (VOCs), according to the Canadian National Pollutant Release Inventory, only 0.7 % of the VOC emissions around the world come from the chemical industry. In contrast, 21 % come from the general solvent use outside the chemical manufacturing industry Jessop [2011].

According to McDonald et al. [2018], volatile chemical products (VCPs), including pesticides, coatings, printing inks, adhesives, cleaning agents, and personal care products, constitute half of the fossil fuel VOC emissions in industrialized cities. In the USA, the total emissions of VOC in 2014 were estimated at around 12 million tons Anand et al. [2014], which is related mainly to the chemical industry and road mobile sources. The European Commission on Environment has established certain legislation to reduce the industrial emissions of VOC into the air. They include technical changes in around 50000 chemical plants around the European Union, substituting chemical solvents for environmentally friendly solvents, and a strategy for implementing and encouraging a bio-based economy comission [2017].

There is a particular interest in lactate esters, especially from alcohols like n-butyl alcohols, due to their additional chemical properties, such as high boiling point, which allows their use in many applications. The most reported methods for lactate esters production include intensification technologies such as reactive distillation. Applying new technologies for producing green solvents, such as lactates and acetates, is a key point in the industry's transformation. The main drawbacks of the reactive distillation process are i) non-linearities are present, making the control problem difficult for assessing the end-product properties Valerica Taga et al. [2019], Castrillon and Ochoa [2018]. ii). The multiple steady states make a multivariable problem that should be studied and researched in depth to generate solutions in this area, especially for the production of lactates from higher alcohols like the obtention of n-butyl lactate from n-butanol, which is interesting lactate for industrial applications but without

enough kinetic and phase equilibria information and in many cases without the complete information Valerica Taga et al. [2019], Jiang et al. [2018], Peña-Tejedor et al. [2005a].

In Kumar and Mahajani [2007], the authors proposed a reaction process for the esterification of lactic acid with butanol to obtain n-butyl lactate, evaluating kinetic parameters. The process was carried out in batch and continuous stages, in a reactive distillation column at a laboratory scale, and compared with simulation in ASPEN Plus. In Wei, Y., Yu et al. [2020] the authors presented a novel synthesis method for ethyl lactate, a lactate ester commonly used as a green solvent. The authors used a sulfonated resin catalyst and optimized the reaction conditions to achieve high yield and purity.

To overcome the problems related to the residue and reactive curve maps and technical feasibility evaluation at the pilot-plant scale, it is necessary to develop advanced control strategies and soft-sensor predictions to fulfill economical, physical, and phenomenological constraints of the process Sharma and Singh [2014], Jana and Banerjee [2018], Kiva et al. [2003], Sánchez et al. [2020]. Additionally, according to Asthana et al. [2006], for design purposes, it is important to include the oligomer's kinetic reaction (lactic acid oligomers) to the kinetic and reactive distillation models to obtain more reliable predictions.

In this sense, Process Systems Engineering (PSE) is a very active research field to deal with those drawbacks related to the non-linearities and multivariable problems for the obtention of butyl lactate. There are many reports of the application of PSE tools for advanced control strategies such as non-linear model predictive control (NMPC), Extended Kalman filter (EKF), and real-time optimization (RTO) for obtaining lactates from primary alcohols in reactive distillation with high purity at low costs Mo et al. [2011], Valluru et al. [2015a]. However, most of these reports have been performed in silico, and only a few include lab-scale experiments Karacan [2018]. These do not allow determining a realistic scenario that integrates technical and economic evaluation to produce feasible information for and eventually implementation at an industrial scale.

This work presents the opportunity to engage with a pilot-plant scale reactive distillation column located at the chemical engineering laboratory at the Universidad Nacional de Colombia in BogotÃ¡. The isobaric vapor-liquid equilibrium for the binary mixture of n-butyl l-lactate and n-butanol at 1 and 5 kPa is attained to achieve this goal [Garcia et al., 2021]. Following this, were evaluated both reactive and non-reactive residue curve maps [Velandia et al., 2021]. This assessment was crucial in determining the technical feasibility of producing n-butyl lactate in the reactive distillation column at the pilot plant. Progressing forward, it was developed, simulated, and validated a phenomenological model for a reactive distillation column. This model incorporated a heterogeneous reaction alongside an equilibrium model. Advanced control strategies, such as linear and non-linear model predictive controllers, were

proposed for higher productivity. A state estimation technique employing an artificial neural network was implemented.

This thesis aims to develop advanced control tools and state estimators that can be implemented in real-time operations at a pilot plant scale. This serves as a foundation for further research on the topic and aims to determine optimal operating conditions to achieve the desired final concentration, estimate the reaction's progress, and reduce operational costs.

This doctoral thesis has made significant contributions in the domain of thermodynamic equilibrium. To begin with, it has generated equilibrium data for the binary mixture of n-butyl lactate and n-butanol at 1 and 5 kPa. This enriches the database of thermodynamic information, which is important for n-butyl lactate production. Furthermore, based on global optimization techniques, a novel strategy was conceived for generating both reactive and non-reactive ternary and quaternary residual curve maps. Such a move unlocks the potential to dissect the production of these esters in reactive systems, paving the way for a robust analysis of reactive distillation column designs. A dynamic state model has also been formulated for a pilot-scale reactive distillation column. This model has undergone rigorous validation through plant data, academic literature, and simulations in Aspen Plus. It's poised to lay the blueprint for optimal operating scenarios and appropriate control strategies, ensuring efficient n-butyl lactate production at the pilot plant scale. Conclusively, an advanced control strategy has been juxtaposed, weighing the merits of LMPC and NMPC controllers against MIMO PID, with LMPC showcasing a good performance through the intricate nonlinearities and operational constraints inherent to the system.

The rigorous research and development underlying the doctoral thesis have culminated in two significant publications thus far. The first one is titled, 'Isobaric Vaporâ€“Liquid Equilibrium for the Binary Mixture of n-Butanol + n-Butyl l-Lactate at 1 and 5 kPa' [Garcia et al., 2021] and the second, 'Reactive and non-reactive residue curve maps analysis to produce Butyl Lactate by catalytic distillation' [Velandia et al., 2021]. Furthermore, a third paper, dealing with the intricacies of modeling, validation, and advanced control, is currently in the writing phase.

The document has been structured for clarity and coherence in chapters. Chapter 1 serves as the introduction, offering a concise overview of the current state of the art associated with green solvent production. Chapter 2 dives into a comprehensive literature review concerning n-butyl lactate, intensified processes, reactive distillation, and the respective control strategies applied. Chapter 3 elucidates the methodology, encompassing the experimental parts like materials and methods, construction of ternary and quaternary diagrams, modeling, validation, and advanced control. Lastly, Chapter 4 showcases the research findings for each discussed theme.

2 Literature Review

2.1. Green solvents in the world

There is a long list of generic solvents that are considered green solvents. This group includes alcohols, esters, ethers, glycols, hydrocarbons, lactones, and a few other compounds Wypych and Wypych [2014]. Stringent regulations by the REACH, EPA, and DEFRA concerning toxicity content in conventional solvents have prompted the shift towards developing bio-solvents Grand View Research [2015]. In this sense, new natural resources have become important for getting the well-called green solvents. The global bio-based solvents (green solvents) market is growing in importance. Generally, the global solvent market between 2012 and 2013 was estimated at 2375 and 2505 kt, respectively. In 2015, it was in the order of 20 million metric tons, and in the same year, the global green and bio-based solvents market size were estimated at USD 5.44 billion. In 2016, it was estimated at USD 6.01 billion and was expected to reach USD 9.43 billion in 2022 and 13.7 billion in 2024. In 2015, European solvent production provided about one-quarter of the worldwide market, and the production and uses of bio-based solvents in the European Union were projected to grow to over one million metric tons by 2020, which was reached in the mentioned year Grand View Research [2015, 2016], market research [2017], Clark et al. [2015]. The most important industries for solvent production include paints and pharmaceuticals (Figure **2-1**). The uses of solvents include chemical formulations, chemical reactions, or chemical extractions. Therefore, a significant alleviation of non-renewable chemical dependence can be achieved by implementing green solvents.

In Afreen et al. [2021], the review paper discussed using lactate esters as green solvents for various organic synthesis reactions, highlighting their advantages over traditional solvents such as benzene and dichloromethane. The paper also covers recent developments in the synthesis and characterization of lactate esters. The authors in Ammar et al. [2019] investigated using lactate esters to extract bioactive compounds from natural sources such as plants and fruits. The authors found that lactate esters were effective solvents for extracting various compounds, including polyphenols, flavonoids, and carotenoids. They had advantages over traditional solvents, such as hexane and methanol, in terms of toxicity and biodegradability. In Almeida et al. [2019] discuss using lactate esters as green solvents for lignocellulose processing, an essential step in producing biofuels and bioproducts. The authors highlight the advantages of lactate esters over traditional solvents such as dimethyl sulfoxide

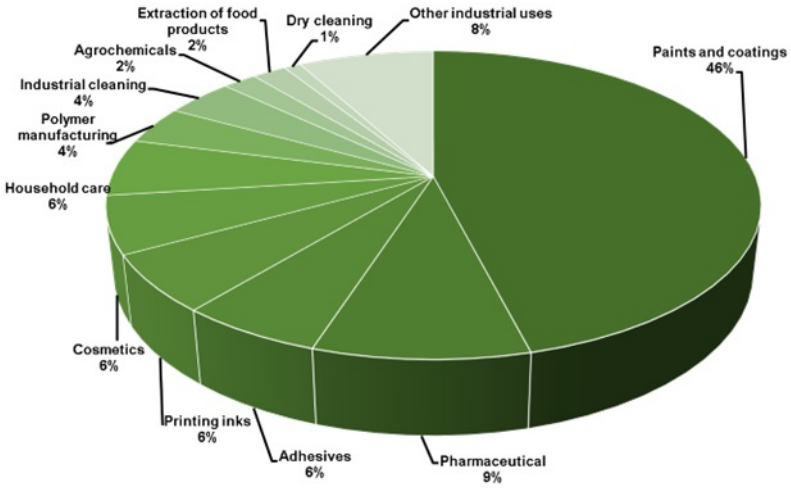

Figure 2-1: Industrial uses of solvents Clark et al. [2015].

and ionic liquids and discuss recent developments in their use for lignocellulose pretreatment.

One alternative for green solvent production appears in ethanol production plants that utilize the medium-chain-length alcohol fraction as raw material (fusel alcohols) from the distillery step. It consists mainly of iso-pentanol and isoamyl alcohol Eyerer et al. [2010]. Besides, it is possible to produce lactic acid in ethanol plants, another important component for green solvent obtention, such as lactates. This diversificate the products of sugar cane in the ethanol industry plants Tirpanalan et al. [2015].

Green chemistry can be defined according to Wypych and Wypych [2014] and Sharma [2015] as the design, manufacture, and application of chemical products and processes to reduce or eliminate the use and generation of hazardous substances. The Green Chemistry philosophy is based on 12 principles Anastas and Warner [2000]. Some of the most important are waste prevention, energy efficiency, renewable feedstock, benign chemistry, and pollution prevention (design for degradation). Based on the last principles, green chemistry define chemical solvents as the ones that are often volatile compounds from petroleum resources, bearing several health and environmental risks Häckl and Kunz [2018].

In this sense, green solvents can be defined as solvents that improve biocompatibility, sustainability, and biodegradability and avoid ecological toxicity and pollution, fulfilling the 12 principles of green chemistry of Anastas and Warner Häckl and Kunz [2018], Anastas and Warner [2000], Schuur et al. [2019].

Figure **2-2** shows that the three ideal conditions for obtaining a green solvent are the relation of the three main general topics of safety and legislation, environmental restrictions and effectiveness, and all their related topics that allow adequate use and application.

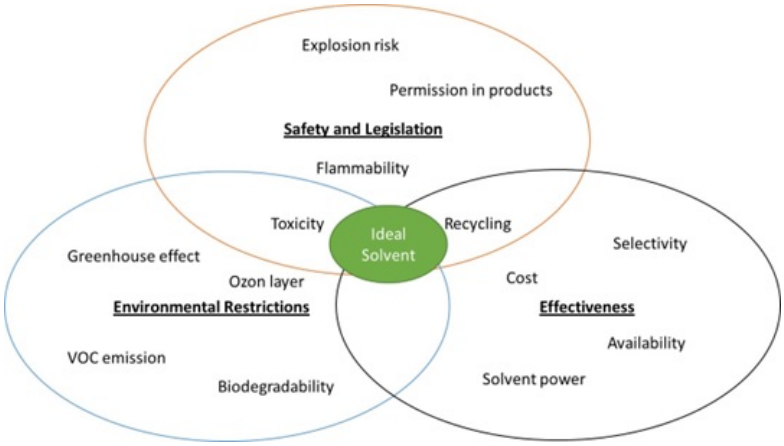

Figure 2-2: Relation for obtaining the ideal solvent Häckl and Kunz [2018].

2.2. Global market of lactate esters

Integrating the bio-refineries for obtaining and using second-generation products like fusel to obtain lactates allows for a diversified industry process to obtain green solvents Earle and Seddon [2000], Clark et al. [2009].

Applying short and long-chain alcohols as extraction solvents unites two important points. On the one hand, this liquid normally constitutes a surplus product with low market value. When used as an extraction solvent, the costs for alternative solvents are saved. Furthermore, this extraction solvent is less harmful to handle than the classical extraction solvents Edreder et al. [2010]. Besides, it is possible to generate new knowledge around the thermodynamic and kinetic properties of long-chain alcohols like butanol, propanol, and isoamyl.

Alcohols from fusel oil have been used to manufacture bioproducts in chemical industries, even for pharmaceutical applications, with the advantage of being environmentally safe, renewable, and in some cases, biodegradable Özgülsün et al. [2000]. In this aspect, Colombia has a significant advantage due to its bioethanol and beverage industries that allow good scenarios for green solvent obtention and applications Montoya et al. [2016].

In 2015, lactic acid production in a global market was estimated at 328.000 metric tons/year. By 2025, the utilization of LA for (bio) products obtention is expected to reach 50 % of total LA available in the global market Mohammad and Inamuddin [2012], Duque et al. [2016]. Globally, lactate esters dominated the industry with a revenue of over USD 1.48 billion in 2015. This segment is also expected to witness the highest growth during the forecast period,

driven mainly by increasing applications, easy availability of raw materials such as lactic acid, and low production costs Grand View Research [2016]. In 2016, lactate ester was a major type segment on account of the growing demand for printing inks, coatings, and industrial applications market research [2017] and the most important bio-solvent companies included The Dow Chemical Co., AkzoNobel N.V., E.I. du Pont de Nemours Co., Cargill Inc., BASF SE., Lyondell Basell, BioAmber, Huntsman Corp., Myriant Corp., Vertec Bio solvents and Florida Chemicals, among others Grand View Research [2016].

In this sense, lactate esters are a green and economically viable alternative to traditional solvents. Their extensive use and scale-up to the industrial level require a deep and accurate knowledge of its properties in wide pressure-temperature ranges Aparicio and Alcalde [2009]. Lactate esters can be obtained from the esterification reaction with alcohols (methanol, ethanol, propanol, iso-butanol, and isoamyl alcohol) with lactic acid Montoya et al. [2016]. They have been produced through both chemical synthesis and fermentation routes. This last process is the most common. However, lactates derived from fermentation broths require extensive purification processes that should be inexpensive and environmentally friendly Pereira et al. [2011].

2.3. Industrial production of lactate esters: Classical and intensified.

In 1926, Wood et al. [1926] evaluated the properties of butyl lactate and their isomer; two years later, Charles and Charles [1928] presented a patent for the obtention of butyl esters of lactic acid, and more particularly to the normal primary, butyl ester of alpha hydroxy propionic acid (fermentation lactic acid). The authors proposed an esterification reaction followed by distillation for dehydrating lactic acid. Shailer and Howard Shailer L. and Howard N [1934] presented the patent for obtaining secondary butyl lactate in a similar approximation to Charles L. and Charles. In 1948, Rehberg et al. [1948] evaluated the thermophysical properties of some alkyl esters, including butyl lactate. Later, Schulz et al. [1955] present a patent for an esterifying butyl lactate process, including an evaporating apparatus for carrying out the process. Besides, it is composed of a train of evaporating vessels, external heat exchangers, condensers, a separatory tank, a scrubber, and a distillation column (Figure **2-3**).

The process shown in Figure **2-3** includes many process units, which increases the process costs. For this reason, the production of n-butyl lactate based on this type of scheme is not an attractive process for industrial implementation. Despite this, other authors proposed alternative processes, methods, and technologies (including new catalysts) to make a feasible

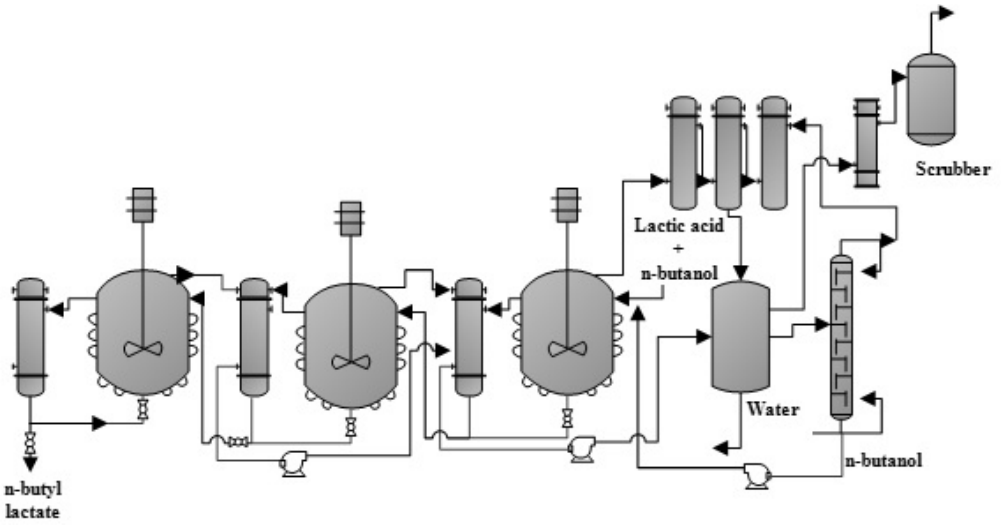

Figure 2-3: Process flow diagram for the production of ethyl lactate Serge et al. [2004].

production of n-butyl lactate Berg and Mont [1990], Dassy et al. [1994], Andersen [1998], Pirozzi and Greco [2006], Jianwu et al. [2009], Yuming and Yong [2015], Rui and Weilue [2018].

In Serge et al. [2004] presented an interesting approximation related to the process production of ethyl lactate with purity $\geq$97 % from lactic acid. According to these authors, this reaction should be catalyzed with acid. It is necessary to avoid the formation of lactic acid oligomers, which is an interesting topic to work on. According to the authors, the esterification of lactic acid with ethanol is complicated due to the formation of oligomers of lactic acid in the starting lactic acid compositions and the oligomerization of ethyl lactate with lactic acid and ethanol and an oligomer of lactic acid, which makes challenging to obtain purified ethyl lactate and reduces reaction yield.

Additionally, Serge et al. [2004] found that a water-ethyl lactate binary mixture can form an azeotrope, complicating water removal from ethyl lactate. Based on the mentioned problems, the authors proposed a methodology consisting of having a water content as low as possible during the esterification reaction of lactic acid and ethanol and then applying vacuum distillation. The distillation is carried out at a column base temperature ranging from 152 °C to 165 °C. Finally, the authors present an applied example feeding a stirred tank reactor with lactic acid (87 %), absolute ethanol, and 98 % sulfuric acid. Then the mixture was separated in a flash tank and later in a fractional distillation column with a diameter of 70 cm and 35 theoretical plates, and the ethyl lactate was recovered. This process is presented in Figure **2-4**, where the crude ethyl lactate is subjected to purification by fractional distillation under reduced pressure.

In this sense, Asthana et al. [2006] presented the kinetic model for the esterification of lactic

acid and its oligomers, where the esterification was performed with ethanol over Amberlyst 15 cation-exchange resin. The authors presented that the extent of oligomerization is inversely related to the water content of the solution. Based on this, for the production of lactate esters and design purposes, it is important to include and characterize oligomer reactions in the process model.

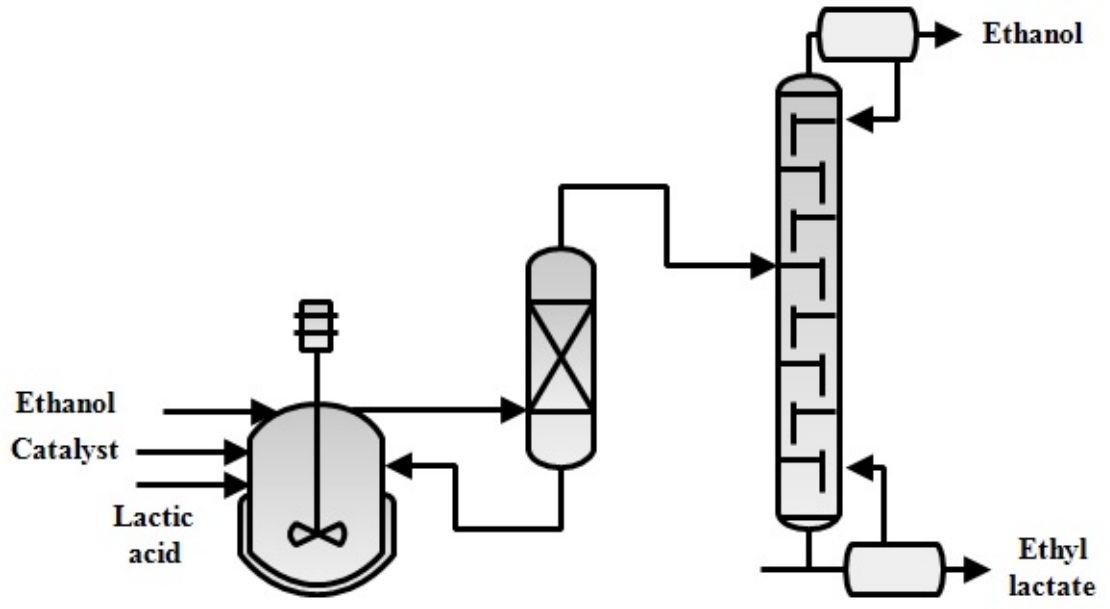

Figure 2-4: Process flow diagram for the production of ethyl lactate [Serge et al., 2004].

Other reports presented a similar approximation to Serge et al. [2004], where the different authors tried to propose, evaluate and implement different technologies that include catalyst, unit process, and equipment to improve the ethyl lactate yield in real process applications for ethyl lactate obtention Georges and Remy [2004], Jichu et al. [2005], Aparicio and Alcalde [2009], Delgado et al. [2010], Pereira et al. [2011], Bykowski et al. [2014], Fuquan [2017], Hu et al. [2019].

As a chemical synthesis, reactive distillation (RD) is a very attractive option to reduce investment and energy costs Lai et al. [2007]. According to Keller [2014], in 2009, the European chemical industry consumed approximately 19 % of the total energy of the continent, and approximately 40 % of the energy consumption in this sector was used in the separation proces, specifically in distillation units. In this sense, process intensification was created to design compact, safe, energy-efficient, and sustainable processes Stankiewicz and Moulijn [2013], being RD the most important example of process intensification.

For industrial purposes, it becomes pretty interesting to find different ways to reduce costs

and get higher profitability while predicting and controlling the main quality-related process variables. However, RD still has to deal with many complexities from an operational and control point of view. First, there exists a reaction scheme that should be solved with kinetic information. Second, a phase separation problem should be solved with phase equilibria information, which raises the nonlinearities and multiples stationary states in the process, reducing the economic feasibility in RD operation Valerica Taga et al. [2019], Castrillon and Ochoa [2018]. In many cases, the kinetic and phase equilibria information for the esterification reaction of long-chain alcohols like n-butanol is available only in a specific range of operation (90 to 101.4 kPa), and in another case, there is no information at all Valerica Taga et al. [2019], Kumar and Mahajani [2007], Peña-Tejedor et al. [2005a].

Thus, many types of research have been developed to solve RD's control and economic feasibility problem. In Mo et al. [2011] proposed an integrated design and control for the hydrolysis of methyl lactate and purification of lactic acid. They evaluated a dual temperature control for optimal operation. In Castrillon and Ochoa [2018] presented a similar methodology to achieve an integrated design and control of the process applied to a reactive distillation column to produce ethyl lactate. The proposed methodology allows the understanding that traditional designs present energetic inefficacy and low controllability. On the other hand, Valerica Taga et al. [2019] presented the trans-esterification of methyl lactate with isopropanol to obtain isopropyl lactate, considered a green solvent. Their methodology proposed to carry out the reaction in a reactive distillation column in an acid medium, in addition to using correlation models with the initial intention of obtaining kinetic data.

In Miller et al. [2006], the authors patented a process for producing organic acid esters using continuous countercurrent reactive distillation using acid catalysts in a structured packing in a single column. The authors evaluated two cases, methyl, and ethyl lactate production, at different operating conditions. Figure **2-5** and Figure **2-6** show the molar concentration, inlet reactants temperatures, and chemical ratio for the esterification reaction. Compared with the case of Figure **2-4**, the reduction in the process units can be easily observed, probably reducing the process's cost.

Sánchez et al. [2017] presented experimental vapor-liquid equilibrium data and thermodynamic modeling studies related to the separation and reactive synthesis of ester compounds from fusel oil mixtures. The authors measured isobaric VLE data for binary mixtures of isobutyl acetate with isoamyl acetate and ethyl acetate at various pressures. The near-ideal behavior was modeled well with NRTL, UNIQUAC, and UNIFAC-DMD activity coefficient models.

Sánchez et al. [2019] extended the equilibrium database, reporting new VLE measurements for the ethyl acetate + isoamyl acetate system at 50 kPa and 100 kPa. Modeling results

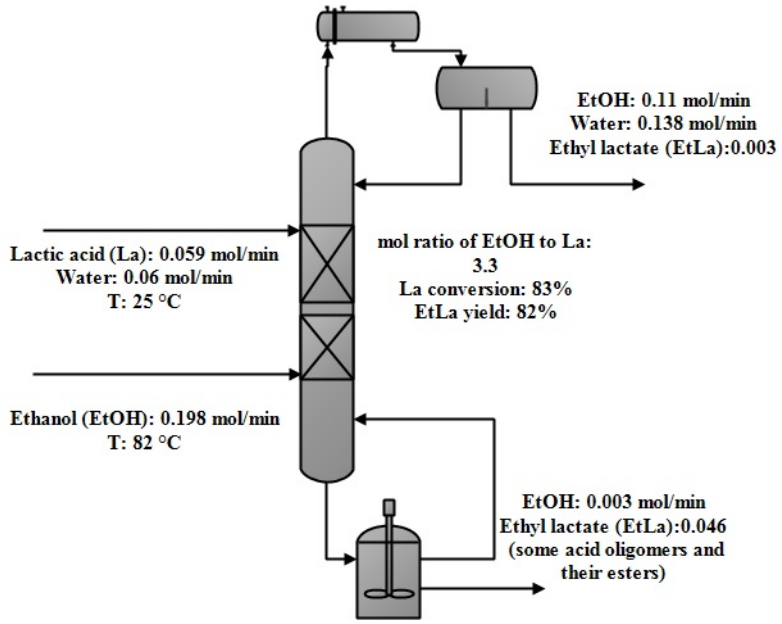

Figure 2-5: Ethyl lactate production in reactive distillation column Miller et al. [2006].

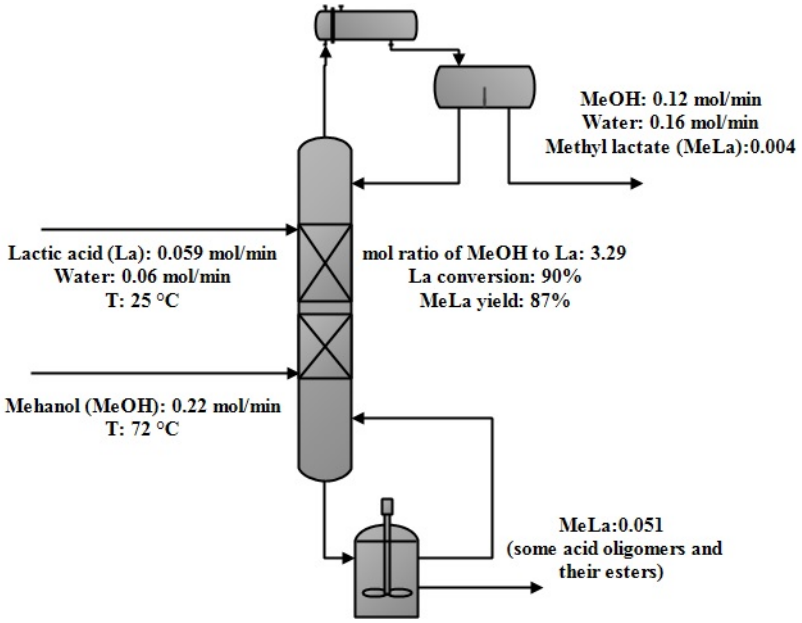

Figure 2-6: Methyl lactate production in reactive distillation column Miller et al. [2006].

again indicated near-ideal behavior that could be predicted by multiple activity coefficient models. Then, Sánchez et al. [2020] developed an improved NRTL model parameter set for the quaternary acetic acid + isoamyl alcohol + isoamyl acetate + water system, calibrated using available VLE, LLE and VLLE data. The model successfully predicted azeotropes and multicomponent VLE consistent with experimental reports, outperforming prior models from the literature.

Okasinski and Doherty [1997] explored the effect of reaction equilibrium constant uncertainty on the existence and location of reactive azeotropes for systems with a single chemical reaction. Using arc-length continuation, they generated bifurcation diagrams tracking reactive azeotrope branches vs. the equilibrium constant. Results for an esterification reaction showed three distinct phase behavior regimes depending on the constant value. The methodology enables rapid screening for reactive azeotropy and optimal conditions.

Overall, the works provide valuable phase equilibrium data, modeling, process insights, and analysis tools related to separation and reactive distillation syntheses of esters from fusel oil and other feedstocks. The improved understanding enables more accurate process simulations to evaluate and optimize these renewable chemical production pathways. Likewise, the construction of ternary reactive diagrams based on Michelsenâ€™s balance equations is presented, but there is not a sufficiently clear methodology in the literature for the construction of such diagrams [Doherty and Perkins, 1979, Michelsen, 1992].

2.4. Production of n-butyl lactate

In Kumar and Mahajani [2007] proposed a reaction process for the esterification of lactic acid with butanol to obtain n-butyl lactate, evaluating kinetic parameters and phase equilibrium. The process was carried out in batch and continuous stages, in reactive distillation equipment at a laboratory scale, and compared with simulation in ASPEN Plus V8. The kinetic parameters were estimated with the Pseudohomogeneous Activity-based model (Equation 2-1); Lee et al. [2002] evaluated the esterification reaction of propionic acid and n-butanol over Amberlyst 15. The authors obtained the estimated kinetic parameters, evaluating different models such as quasi-homogeneous, the Langmuir-Hinshelwood, the Eley-Rideal, and the modified Langmuir-Hinshelwood. They found that the Langmuir-Hinshelwood model best represent kinetic behavior. However, Kumar and Mahajani [2007] obtained, with their model, a confidence interval of 95 % presented in Table **2-1** in which the value of the objective function calculated by the mean square error (MSE) is presented.

$$r_{LA} = \frac{n_{LA}}{w_{cat}} \cdot \frac{dX_{LA}}{dt} = K_{f0} exp\left(\frac{-E_a}{RT}\right)(X_{La}X_{BuOH}) - K_{b0} exp\left(\frac{-E_b}{RT}\right)(X_{BuLac}X_w) \qquad (2\text{-}1)$$

where n_{LA} are the initial moles of Lactic Acid, W_{cat} is the weight of the catalyst, k_{f0} and k_{b0} are the preexponential factor, and E_a and E_b are the activation energies.

Table 2-1: Estimated kinetic parameters for the esterification reaction of lactic acid and n-butanol Kumar and Mahajani [2007].

Parameter	Value
$E_a(kj/mol)$	53.40±1,86
$E_b(kj/mol)$	52.24±6,01
$Ln(K_{f0})(mol/kgh)$	25.26±1,98
$Ln(K_{b0})(mol/kgh)$	$23.34 \pm 0,63$
Objective Function	2.02×10^{-4}

In Figure **2-7**, the batch reactive distillation performed by Kumar and Mahajani [2007] can be observed, as well as some results. The authors presented a set of equations related to the thermodynamic and mass balances for batch operation. The model was fitted with the experimental data for reactor compositions, temperature, and total water removed over time.

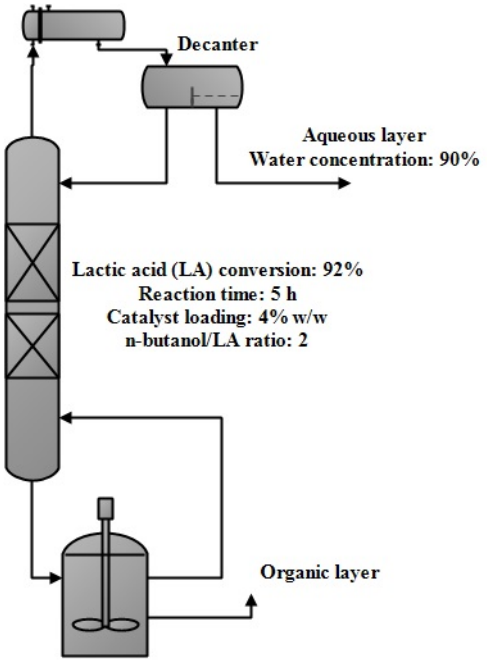

Figure 2-7: Batch reactive distillation for producing n-butyl lactate Kumar and Mahajani [2007].

In Kumar and Mahajani [2007] calculated the activity coefficients in the liquid phase using the UNIQUAC equation for all the binary interactions. The number of binary equilibrium data and interactions for the esterification reaction in the reactive distillation column is

important. Usually, the NRTL and UNIQUAC models are the most used for determining binary data in the esterification reaction of lactate esters. The models require at least two adjustable parameters. In this sense, two possible sources exist for obtaining phase equilibrium data, performing experiments or databases. Aspen Plus®is a software that contains NIST and DECHEMA databases where it is possible to find phase equilibria data for some components. There are not enough experimental reports in the open literature related to the phase-equilibrium data for the components in the esterification reaction of lactic acid with n-butanol to produce n-butyl lactate.

Table **2-2** presents the available and missing phase equilibrium data and binary interactions for the components in the esterification reaction for producing n-butyl lactate. Iwakabe and Kosuge [2001], the authors presented the vapor-liquid equilibrium (VLE) for the binary mixture of water-n-butanol at 101.3 kPa, and the reported data present thermodynamic consistency. Sanz et al. [2003] presented the VLE data from the binary mixture of water-lactic acid at 103.33 kPa. The authors evaluated the lactyl-lactic formation due to oligomerization and performed some correlations for determining the activity coefficients for the system water+lactic acid+lactyl-lactic acid, being UNIQUAC model, which was fitted better. Peña-Tejedor et al. [2005b] evaluated the VLE and excess volumes of the binary system ethanol+ethyl lactate, isopropanol+ isopropyl lactate, and n-butanol+n-butyl lactate at 101.325 kPa. The data present thermodynamic consistency, and the authors evaluated the UNIQAC model for predicting properties.

The VLE data presented by Peña-Tejedor et al. [2005a] is the most interesting for design purposes, but the authors reported 101.325 kPa. In real RD columns, it is necessary to operate at vacuum conditions to reduce the separation temperature and avoid the formation of oligomers. In this sense, it is necessary to generate VLE data at vacuum conditions for the mixture n-butanol-n-butyl lactate to get the most approximated model, which should be able to reproduce in a better form, the reactive-distillation process.

Finally, Jiang et al. [2018] presented the novel esterification reaction of lactic acid with isoamyl alcohol to produce isoamyl lactate, considered a green solvent with a high molar percentage in fusel oil. The authors evaluated four correlation models to obtain the kinetic data. The article is relatively simple, giving all the methodological information to reproduce the experimental set and the different model evaluations, and presents a research precedent in the area of green solvent production and data for model validation.

Table 2-2: Availability of binary phase equilibrium data for the esterification reaction producing n-butyl lactate.

	Lactic acid	**n-butyl Lactate**	**Water**	**N-butanol**
N-butanol	X	**	*	—
Water	***	X	—	*
n-butyl Lactate	X	—	X	**
lactic acid	—	X	***	X

*:measured by Iwakabe and Kosuge [2001]
**:measured by Peña-Tejedor et al. [2005b]
***:measured by Sanz et al. [2003]
X:without experimental report

2.5. Control, optimization, and state estimation applications in reactive distillation process

There are reports related to many problems in the control implementation in RD columns, one of these problems is because the traditional process design methodologies consider the control system and equipment design as two separate topics. In most real cases, the equipment is designed based on economic feasibility, optimization requirements, and steady-state information. Afterward, the process control system is designed to assure a good closed-loop performance at the selected set point to obtain some desired final product properties Castrillon and Ochoa [2018], Francisco et al. [2000]. In the operation of a reactive distillation column, implementing the process and its control system design sequentially can be a problem due to the resulting equipment. It is often difficult to control, especially because, in most cases, the proposed control system is based on the PID control law, which does not include the prediction of the main state variables. Besides, it is an inflexible system and presents problems when facing disturbances Balaban [2000].

Many efforts have focused on improving the control performance of RD in real-case applications. In Haßkerl et al. [2018a] and Valluru et al. [2015b], the researchers aim to apply in silico an adaptive NMPC integrated into RTO to an ideal case of reactive distillation. This application is interesting because the control has many deviations due to the kinetics and phase equilibrium. The proposed integrated control allows dealing with the non-linearity problems and the optimization to reach the maximum profitability fulfilling the productivity restrictions.

In Reddy et al. [2017], the authors proposed a case for the simulation of a reactive batch distillation for butyl acetate production using multi-objective optimization, which is solved by a non-dominated sorting Genetic algorithm. In Figure **2-8** (a), it can be observed the full model for RD process and in Figure **2-8**(b) can be observed the reduced order model proposed by the authors. One of the authors' objectives was to reduce the simulation time for this type of process.

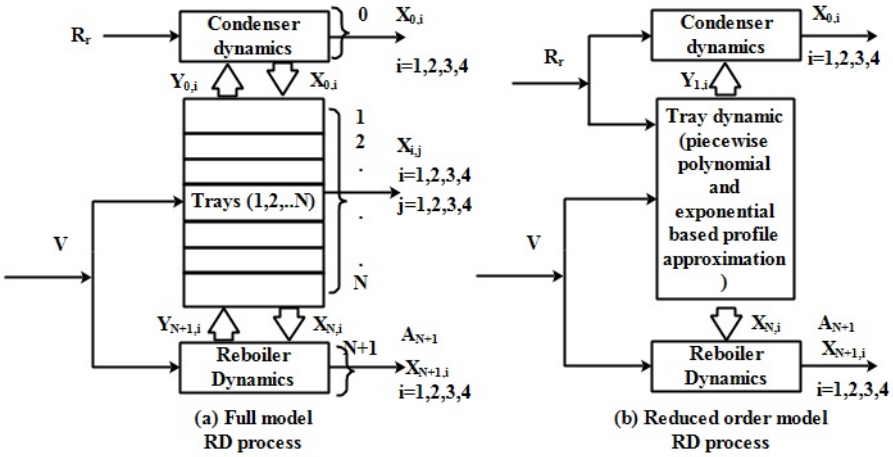

Figure 2-8: Schematic representation of the reduced order model proposed by Reddy et al. [2017].

In the same sense, Wahid and Putra [2018] proposed a multivariable model predictive controller applied to a reactive distillation for the obtention of dimethyl ether based on two-point control structures using rangeability analysis. The authors made a first-order system plus dead time. The linear model predictive controller (LMPC) plus dead time (FOPDT) was implemented based on simulation data generated by changes in the reflux flow rate and reboiler duty to obtain input-output data. The main conclusion is that multivariable MPC can attend to the non-linearities of the system, fulfilling the product features due to the dead time performance. It can also handle loop interactions. Figure **2-9** compare three different control configurations. Figure **2-9**a) and c) compare PI control with single and two control operations, Figure **2-9**b) present a multi-input-multi-output control scheme with a MPC. The control adapted with MPC presented the best performance with the smoothest response.

Marquez-Ruiz et al. [2019] proposed and implemented an alternative strategy based on LMPC developed *in silico* (using linear transformations to represent the non-linear system), which can handle the control and optimization of a batch reactive distillation process. They compared different literature methods applied to the same process, such as the order-reduction method and transforming variables. The main difficulty in applying control and

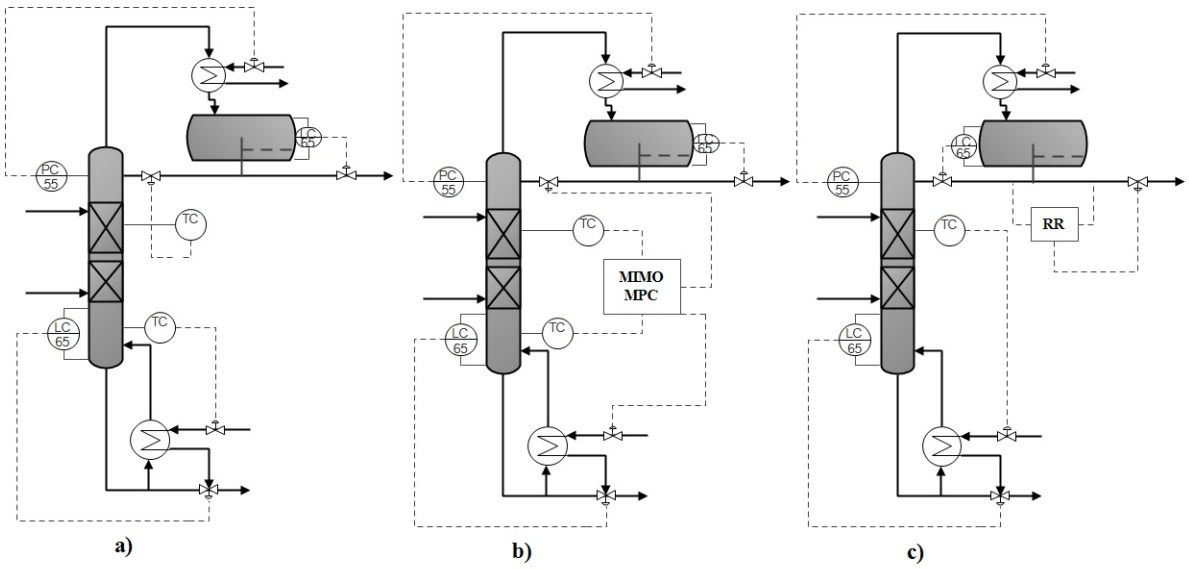

Figure 2-9: a) Two-point PI control configuration, b) MPC control configuration, c) Single-point PI control configuration Wahid and Putra [2018].

optimization in a real case was due to the non-linearities and the large set of differential-algebraic equations, making the approach computationally expensive.

In Zhang et al. [2019], the authors deal with the control and the annual total cost (TAC) optimization of a reactive-extractive distillation for the obtention of isopropyl acetate. The authors compared two control strategies based on cascade control; the kinetic and thermodynamic information was taken from the literature. There are no formal equations in the paper other than results and analysis for the different control strategies and the evaluation of the optimization function. The final results showed a significant reduction in the TAC without affecting operability. Instead, Haßkerl et al. [2018b,a] implemented and evaluated an integrated NMPC with economical optimization for a multiple reaction system in a reactive distillation column at a pilot-plant scale. The most interesting part of this work was the use of online software (python/c++ based software tool do-mpc), which allowed to solve the two layers of NMPC block coupled with the optimization problem, which reduces the computational time for real applications. Another interesting item is related to the use of an online spectrometer that allows to have online measurements of the concentration of the product and to estimate other variables. The authors used multiple shooting methods to solve the optimization problem and to reduce the computational time. The representation of the online connection with the advanced control strategy is presented in Figure **2-10**. Manipulating the catalyst charge, the reflux and distillate feed is controlled. With this, it is possible to extrapolate to an Economic RTO problem.

Haßkerl et al. [2018b] presented the same process system at the pilot-plant scale. They evaluated a variant of the EKF state estimation technique specifically adapted to handle models described by differential-algebraic equations (DAE) to estimate the full state vector of a reactive distillation process in a pilot plant. The state estimator was run online at the column using an OPC-DA as presented in Figure **2-10**. The authors evaluated the estimator performance, getting a good approximation to experimental evaluation.

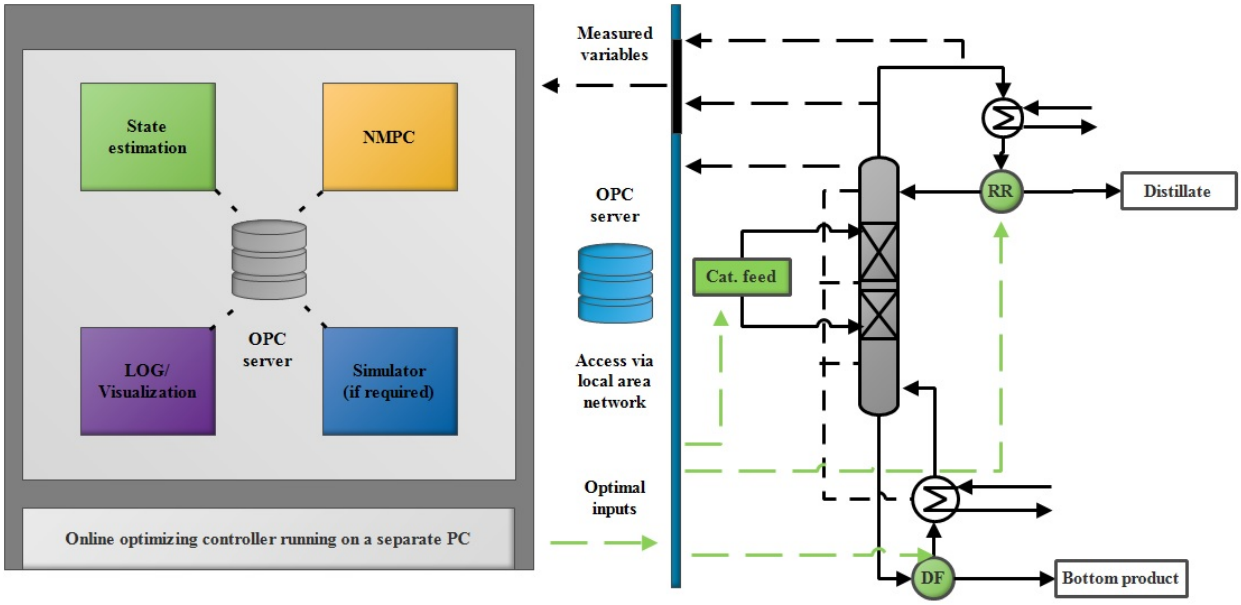

Figure 2-10: Local network and connections for advanced control in a RD column proposed by Haßkerl et al. [2018c].

Aqar et al. [2016] proposed a semi-batch reactive distillation column's optimal design and control operation to obtain methyl lactate. The authors presented a dynamic optimization problem for fulfilling constraints that include the end-product characteristics. The optimization problem was transformed into a nonlinear programming problem and was solved using Control Vector Parameterization (CVP) and Successive Quadratic Programming (SQP) technique in gPROMS.

Ahn et al. [2014] proposed a novel control technique, iterative learning control (ILC), to deal with errors in the modeling. The authors presented the production of methacrylic anhydride in a reactive distillation column. This study was simulated in ASPEN Plus and validated in a Samsung Cheil Industries Inc pilot-plant. The top temperature of the column was regulated at the boiling point of acetic acid by using a time-varying gains nonlinear PID controller, manipulating the reflux ratio.

Valluru and Patwardhan [2019] proposed an integrated frequent RTO and adaptive NMPC for finding the optimal operation cost of different process units. They used a dynamic model for parameters and unmeasured disturbances estimation by soft-sensors applications. The main objective was to eliminate the mismatch between the model used for steady-state operation and the control scheme. The results show a time reduction in the computational operation.

Finally, Griffith et al. [2018] proposed a new method for adaptively updating NMPC horizon lengths online via nonlinear programming (NLP) sensitivity calculation. The authors used the quasi-infinite horizon framework to reduce average computation time without much loss in performance and concerning the fixed-horizon NMPC. They evaluated their methodology in two case studies: a quad-tank and a reactive distillation. The mathematical description and demonstration are well described in different sections with a detailed math analysis. The results show a high reduction in the computational time for both case studies.

Some studies have demonstrated the effectiveness of NMPC for reactive distillation control. For example, in Kawathekar and Riggs [2007], the authors proposed an NMPC strategy for controlling the product purity of a reactive distillation column to produce methyl acetate. The proposed NMPC strategy outperformed PID control and LMPC regarding product purity and control performance.

As a result of this literature review, it can be concluded that it is necessary to implement process system engineering (PSE) techniques, such as design, real-time optimization, state estimation, dynamic modeling, and advanced control applied to a real operating system. In Tintavon and Kittisupakorn [2017], the authors presented an EKF estimator to predict the end-product composition in an RDC using a generic model controller (GMC) to control the temperature of a tray. With this information implemented in a GMC, data from temperature measurements might be used to reconstruct some of the main state variables in an RDC, including the product composition, reboiler, and condenser temperatures. As a result of all these scenarios, it can be concluded that it is necessary to implement process system engineering (PSE) techniques, such as design, real-time optimization, state estimation, dynamic modeling, and advanced control applied to a real operating system. In this case, a reactive distillation column is used to reach higher profitability while predicting final lactate properties and reducing computational time for real implementation Valluru et al. [2015b].

It is possible to generate new technologies and knowledge around the reactive distillation column topic applied to the green solvents production, being lactate esters, specifically n-butyl lactate, the most interesting one. A great opportunity exists at the Universidad Nacional de Colombia Chemical Engineering Laboratory in Bogotá. This laboratory has a pilot plant with a reactive distillation column, in which it is possible to simulate advanced control strate-

gies coupled with dynamic modeling and real-time optimization to increase the profitability of lactate production. For this purpose, long-chain alcohols like n-butanol could be used as raw material and, at the same time, generate new data (vapor-liquid equilibria) for the type of esterification reaction implemented.

The evaluation of the most critical factors involved in the process, such as; the obtention and characterization of the raw material, selection of the type of alcohol for esterification reaction and its thermodynamic and kinetic information, purification of the lactate ester obtained, application of the advanced control strategy and the optimization problem are topics that should be considered in this case.

It is important to attend to lactate production's technical and economic feasibility by reactive distillation column using the mentioned PSE techniques. In this sense, it offers many possible solutions to the green solvents obtention and implementation at industrial levels. Thus, fulfilling the goal of minimizing the environmental impact resulting from the use of solvents in chemical production can generate an industrial and economic interest focused on solving a feasibility problem Nelson [2009], Wypych [2014].

2.6. Final Remarks

This chapter showed several literature works proposing methodological strategies for obtaining VLE for the missing thermodynamic parameters and constructing reactive VLLE diagrams for the mixture of BuOH, LA, BuLac, and Water. Additionally, this chapter describes some advanced control strategies applied to RD processes, including LMPC, NMPC and the implementation of ANN in this type of process is well-studied in the literature.

However, there is still space in the literature for evaluating the production of BuLac in a reactive distillation column at the pilot-plant scale, especially generating thermodynamical binary interaction data and evaluating global optimization techniques to solve the Michelsen set of the non-linear equation to generate reactive VLLE quaternary diagram. Another interest for literature is the proposal of an advanced control strategy, LMPC or NMPC, integrated with state estimation techniques such as EKF or ANN to control the condenser and reboiler temperature profiles, manipulating the feed-ratio and boil-up-ratio, minimizing the reboiler duty while the end-product composition is guaranteed.

In the next chapter, the methodology used in this research work allows the obtention of thermodynamic binary interaction parameters and the construction of ternary and quaternary reactive VLLE diagrams. It is presented the methodology to model and validate the RD column at the pilot-plant scale, evaluating three different scenarios, and the improvement of the control system within a classical PID and an LMPC is exposed.

3 Methodology

This work deals with different methodologies (experimental, modeling, and control) to evaluate the production of n-butyl lactate at the pilot-plant scale. The experimental subsection presents a set of binary interaction parameters for the mixture of BuOH-BuLac at 5 and 10 kPa. Then, a methodology is proposed to obtain ternary and quaternary reactive and non-reactive phase diagrams. This methodology uses global optimization techniques to solve non-linear Michelsen equations. With the obtained thermodynamic information it is presented and evaluated a dynamic model for the RDC. The system is validated with three cases; the first one is with experimental information obtained in a previous run in the plant, the production of isoamyl acetate. The second one is based on the literature reports where the authors perform an experimental set against Aspen Plus simulations. Finally, the third case is the in silico BuLac production at the pilot-plant scale. The validated model is used to test and compare the performance of PID and LMPC to control the condenser and reboiler temperatures

The activities include the experimental and computational development of different routines to obtain the binary interaction parameters, the methodology to build the mentioned phase diagrams, the mathematical model and its validation for an RDC, and proposing advanced control strategies. This work aims to provide new thermodynamic information, phase diagrams, methodology construction, and tools for evaluating advanced control strategies to obtain BuLac at the pilot-plant scale.

As part of improving the performance of predictive controllers, this work studies the state estimation, ANN, of the main variables involved in the process and the application of LMPC or NMPC to obtain a final product with the desired quality while the reboiler duty is reduced.

3.1. Binary interaction Parameters: Experimental Section

In a conventional synthesis process, esterification is an equilibrium-limited reaction and usually does not reach completion. Consequently, the separation of the ester from the reactor must be carried out to improve performance. A more effective manufacturing path is process intensification by integrating reaction and separation processes Kumar and Mahajani [2007]. An accurate representation of the phase equilibria is required to enable an optimized design.

Peña-Tejedor et al. [2005a] have experimentally determined isobaric vapor-liquid equilibrium for esters and lactic acid mixtures, including the binary system butanol and butyl lactate at 101.325 kPa. The above-mentioned paper reported experimental data on the n-butanol and butyl lactate mixture density at 298.15 K. The excess molar volumes were calculated from densities and then correlated by the Redlich-Kister equation. No azeotrope was found in this binary system. Lomba et al. [2014] experimentally found the vapor pressures of butyl L-lactate. Regarding the system n-butanol-water, Iwakabe and Kosuge [2008] reported an experimental study for the VLE and VLLE at 101.325 kPa. VLE data for lactic acid-water were determined by Sanz et al. [2003] at 101.325 kPa. Liquid-liquid equilibrium data for water + lactic acid + butanol was studied experimentally at 298.2 K and 95kPa by Domingues et al. [2013]. However, there are no reports of phase equilibria at low pressures in the open literature that enable the design of separation systems working at low temperatures to reduce operating expenditures. For this reason, this work developed an experimental study of the isobaric vapor-liquid equilibrium for the n-butanol- butyl L-lactate system at 1 kPa and 5 kPa. These values were correlated with activity models that will allow further studies on synthesis processes.

To validate the quality of the experimental data, thermodynamic consistency tests based on the generalized Gibbs-Duhem equation have been developed over the past years Sánchez et al. [2017], Smith, J. Van Ness, H. Abbott [2009]. In this work, the Van Ness and Fredenslund tests Marcilla et al. [2013], Zumalacarregui [2018] were used as approving criteria, together with the evaluation and regression utilities implemented in Matlab®and Aspen Properties®9.0.

3.1.1. Materials

The reactive butyl L-lactate and 1-butanol were supplied by Sigma-Aldrich. The specifications of the samples are presented in Table **3-1**.

Table 3-1: Samples identification

Component	CAS reg. no.	Mass Fraction	Analysis Method
Butyl L-Lactate	34451-19-9	$\geq$ 0,9980	Gas chromatography
1-butanol	71-36-3	$\geq$ 0,995	Gas chromatography

3.1.2. Apparatus and Procedure

Figure **3-1** presents the experimental equilibrium Fischer Labodest VLE 602 equipment. It has a value of uncertainty of temperature and pressure of ± 0.1 K and 0.01 kPa, respectively. The less volatile component was added inside the mixer chamber to start the procedure. Then, mixtures by weight were added to keep the mixture in the mass fraction range of 0 to 1 of butyl L-lactate. Gas chromatography was carried out with butyl L-lactate and 1-butanol as external standards to perform the quantitative analysis. The equilibrium points were taken at conditions of pressure fixed and total reflux ratio. About the heating power, the condensed flux was 1-2 drops per second Sánchez et al. [2017], Manivannan et al. [2019].

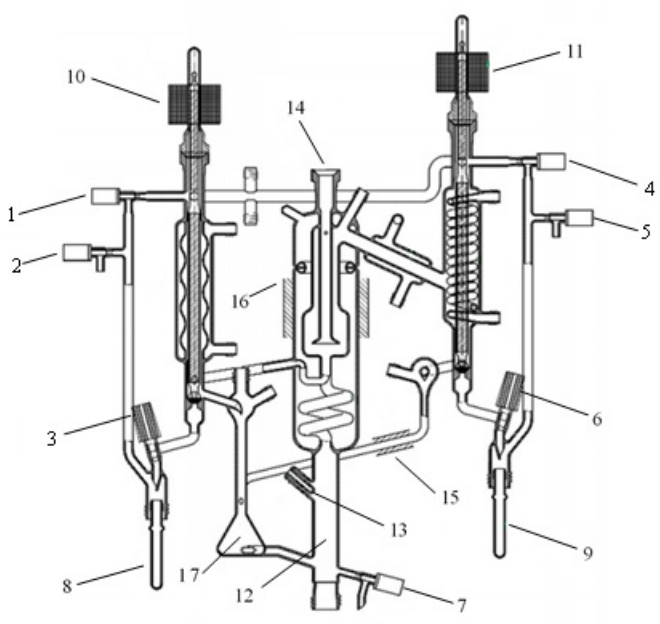

Figure 3-1: Schematic diagram of the Fischer Labodest VLE 602 apparatus: (1) valve of pressure equilibrium to liquid phase sample; (2,5) ventilation valve; (3) outlet valve for the liquid sample; (4) valve of pressure equilibrium to vapor phase sample; (6) outlet valve for the vapor sample; (7) discharge valve; (8) sample tube liquid phase; (9) sample tube vapor phase; (10) solenoid: liquid sample, flow controller; (11) solenoid: vapor sample, flow controller; (12) electrical immersion heater; (13) liquid temperature sensor; (14) vapor temperature sensor; (15) temperature control of heated tube, condensed vapor reflux; (16) temperature control of heated isolation jacket; (17) mixing chamber with stirrer bar 16.

Pressure, vapor, and liquid temperatures were considered to ensure the system's thermodynamic state. During the analysis period (30 min), the standard uncertainty was used as a

stability criterion. The above was intended to obtain a value of uncertainty less than 0.01kPa, 0.01K, and 0.05K for pressure, vapor, and liquid temperatures, respectively. The time required to set stability criteria was 3-4 hours. Finally, liquid and condensed vapor samples were analyzed when the equilibrium condition was reached.

3.1.3. Analysis

Gas chromatography analyzed all samples using a Shimadzu 2010plus GC with an automatic injector SGE column (BP20, 30 m x 0.32 mm) and a flame ionization detector (FID). The carrier gas was helium at 99.999 % of purity. The injector and detectors were at 523.15 K, and the oven was operated at a programmed temperature of 323.15K for 2 min; later, it increased at a heating rate of 20 K / min to 463.15 K and remained at 463.15 K for 1 min. The uncertainty in the concentration measurements was determined by analyzing solutions with specified compositions. The average error in the concentrations of the samples was 0.001 molar fraction for each component.

3.2. Reactive and non-reactive residue curve maps

This section presents a methodology based on the literature information for constructing reactive and non-reactive residue curve maps for the mixture of LA + BuOH + BuLac + Water. For this purpose, the characterization of the associated phase equilibrium models is improved, i.e., those models that include the quaternary system involved in the associated process for the synthesis of BuLac. In this sense, the present work starts from the basis of the fluid phase equilibria reported in the literature. Subsequently, it constructs and analyzes the non-reactive and reactive residue curve maps based on the Michelsen stability material balance and the transformed molar fractions Ung and Doherty [1995]. It also includes the required numerical methods, the kinetic validation of the respective esterification reaction, the reactive and non-reactive azeotropes found, and the topological thermodynamic consistency of the associated systems Okasinski and Doherty [1997].

3.2.1. Thermodynamic aspects

Regarding phase equilibria, different sources of information have been found in the literature. However, they are still insufficient to support a synthesis process of Butyl Lactate and Water from the esterification of Lactic Acid with n-butanol. Lomba et al. [2014] experimentally determined the vapor pressure of Butyl Lactate for a temperature range between 303.15 and

378.15 K at atmospheric pressure. Peña-Tejedor et al. [2005a] also experimentally determined the vapor-liquid equilibrium for the mixture n-butanol and Butyl Lactate at 101.325 kPa without finding azeotropes.

The activity coefficients of the system were based on the binary parameters reported in the literature (Table **3-2**). The binary parameters for Butyl Lactate - 1-Butanol were experimentally determined in this work Garcia et al. [2021]. Here, the binary coefficients for the NRTL model are calculated based on experimental data at 1 kPa and 5 kPa, and on data reported by Peña-Tejedor et al. [2005a] at 101.325 kPa, using built-in regression tools in Aspen Plus®V9.

Table 3-2: Binary interaction parameters for the NRTL activity-based model in the Butyl Lactate esterification system

Component i	**Component j**	**Source**	A_{ij}	A_{ji}	B_{ij}	B_{ji}	$\propto$
BuOH	W	1	0.00	0.00	-274.66	1442.40	0.20
BuOH	BuLac	2	0.79	-0.73	-158.78	134.43	0.30
BuOH	LA	1	0.00	0.00	1537.60	-654.60	0.20
W	LA	1	0.00	0.00	-128.98	-148.07	0.20
BuLac	LA	3	0.00	0.00	-130.30	327.59	0.30

1: Domingues et al. [2013],**2:** This work, **3:** UNIFAC

The binary parameters for n-butanol-Water, Lactic Acid-Water, and Lactic Acid-n-butanol were determined by Domingues et al. [2013]. They presented a liquid-liquid equilibrium data for Water + Lactic Acid + n-butanol at T = 298.2 K and P = 95 kPa. The binary parameters obtained by regression based on the NRTL model predict with a good agreement the behavior of the VLE for n-butanol and Lactic Acid. The same researchers presented binodal curves for the system n-butanol + Lactic Acid + Water based on experimental data.

UNIFAC estimated the binary parameters for Butyl Lactate-Lactic Acid. The binary parameters for Butyl Lactate-Water were omitted because there is no report in the literature regarding this binary pair. The estimation made by UNIFAC generates errors in the tests of thermodynamic topology. Obtaining thermodynamic equilibrium data for this mixture is very complex at the laboratory scale due to the highly polar nature of the substances. Hence the experimental measurement equipment presents overestimations.

To validate the parameters selected for the system, regressions of the binary and ternary equilibria reported experimentally were performed with the Aspen Plus®V9 tool. Figure

3-2 depicts the experimental data and the curve estimated from the regression performed in this study according to the NRTL model

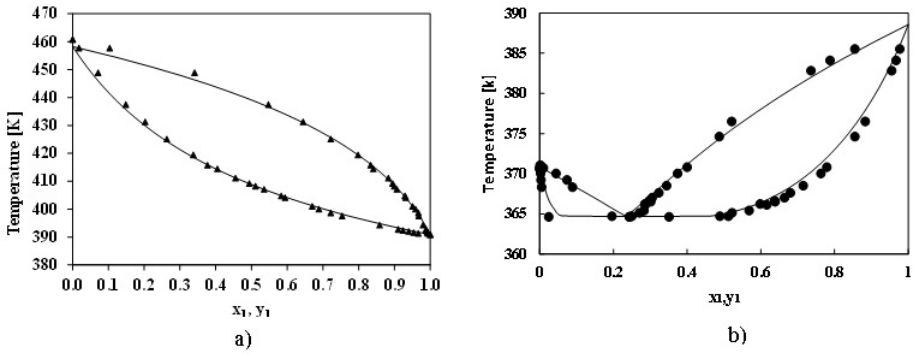

Figure 3-2: (a) Vapor-Liquid equilibrium (VLE) 1-Butanol (1) - Butyl Lactate (2) model regression (NRTL [This work] (-)), (▲) experimental data presented by Peña-Tejedor et al. Peña-Tejedor et al. [2005a] at 101.325 kPa. (b) VLE 1-Butanol (1) - Water (2) model regression (NRTL this work (-)), (●) experimental data presented by Iwakabe et al. Iwakabe and Kosuge [2001] at 93.3kPa.

Figure **3-3** shows the experimental information and the values calculated with the binary interaction parameters based on the NRTL model. The validation parameters for the system, 1-Butanol-Lactic Acid-Water, were constrained to forming the liquid-liquid region. In general, the differences are very small; It might be concluded that the parameters by Domingues et al. [2013] can be used in the NRTL prediction model.

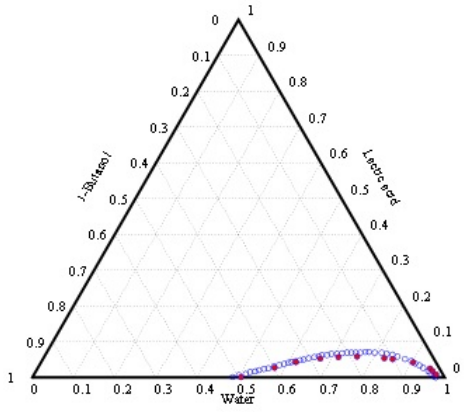

Figure 3-3: Ternary validation of the mixture 1-Butanol-Lactic Acid-Water Kiva et al. [2003]. (●) experimental data presented by Domingues et al. Domingues et al. [2013]. (○) This work.

The values for the different parameters of binary interaction in the system are presented in Table **3-2**. The ideal vapor phase was assumed due to pressure conditions (101.325 and 5 kPa). Besides, Kumar and Mahajani [2007] evaluated the same system at 101.325 kPa in a reactive distillation column assuming ideal behavior in the vapor phase.

3.2.2. Data analysis and phase equilibrium modeling

A methodology was developed based on the information spread in the open literature, including all the steps and equations required to determine the residue curve maps of these reacting systems. Then, a sequence of steps and related calculations were summarized in Figure **3-4**. This sequence works well for obtaining both reactive and non-reactive VLLE curve maps. An advantage of this methodology is that it includes the Michelsen material stability method, which is solved using a global optimization technique to assure convergence. The iterative calculation of flash VLE and VLLE with the numeric integration allows evaluating stability to generate residue curves.

The methodology can be extended to other similar reactive systems (esterification reactions) by giving the corresponding thermodynamic information, such as binary interaction parameters, vapor pressures (Antoine constants), and kinetic information, such as reaction rates. As mentioned above, the proposed methodology has the advantage of receiving input data for constructing reactive and non-reactive VL and VLL maps.

This section describes the equations for non-reactive and reactive residue curves and presents the Michelsen methodology of the material stability technique. Besides, it presents the global optimization algorithm and the isothermal flash approach. Finally, the pseudo homogeneous concentration-based kinetic model validation is described.

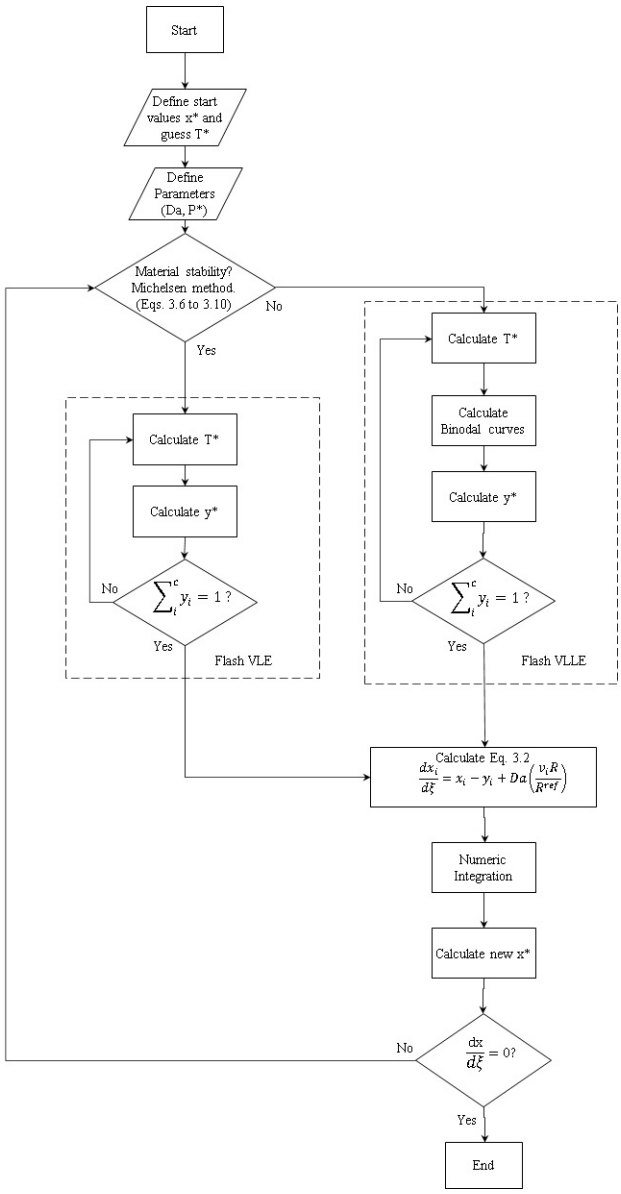

Figure 3-4: Flow-diagram for the methodology presented in this work.

3.2.3. Non-Reactive and Reactive Residue Curves Maps equations

A Non-Reactive Residue Curve Map (RCM) is the composition profile of a perfectly mixed residual liquid in a simple distillation, considering the system's constant pressure and equilibrium conditions. The mathematical model is represented by the differential equation (Eq. 3-1) of n components, where i = 1,2... n.

$$\frac{dx_i}{d\zeta} = X_i - Y_i \tag{3-1}$$

The terms X_i and Y_i are the mole fractions of component i at phase equilibrium in the liquid and vapor phases, respectively. The variable ζ is a dimensional time variable. In the case of reactive distillation, the Reactive Residue Curves Maps (RRCM) are constructed. The chemical reaction that takes place in the liquid phase is included. The differential equations (Eq. 3-2 and 3-3) represents the mathematical expression Venimadhavan et al. [1994], Barbosa and Doherty [1988], Londoño et al. [2006], Martínez et al. [2020a].

$$\frac{dx_i}{d\zeta} = X_i - Y_i + Da\left(\frac{v_i R}{R^{ref}}\right) \tag{3-2}$$

$$Da = \frac{L}{V} R^{ref} \tag{3-3}$$

where v_i is the stoichiometric coefficient of component i in reaction, R is the reaction rate at the bubble point, and R^{ref} is the reaction rate in a reference condition (T^{ref}, X^{ref}). Da is the Damkühler number, V is the molar flow rate of vapor, and L is the total number of moles in the liquid phase.

The ratio L/V indicates the amount of residual liquid concerning the vapor flow, leaving the differential. Small numbers of Da imply operations driven by distillation, large values of Da are kinetically controlled processes, and $Da = 0$ are non-reactive processes Martínez et al. [2020b].

The RCM and RRCM were performed by solving Eq. 3-1 and 3-2 in Matlab from a known random mixture in composition and pressure. The Matlab tool ode15s (for stiff equations) and the Euler method were used as integration methods. The first is for the curves vapor-liquid (VL) sections, and the second is for the vapor-liquid-liquid (VLL) sections. The number of equations can be high for equilibrium systems with multiple components and phases. Due to its simplicity, the Euler method can be computationally more efficient than more precise and complicated methods. Since Michelsen balances are inherently iterative, the Euler method, which is also iterative, fits well with this approach [Michelsen, 1992, Sánchez et al., 2020, Velandia et al., 2021].

The calculation of the RCM and RRCM can be divided into three zones. Firstly, once the random mixture has been defined, the material stability analysis of the mixture (Michelsen Method) is performed. Secondly, the isothermal flash of the mixture with VLE or VLLE is carried out depending on the nature of the mixture. Lastly, the integration method of the differential equations is carried out appropriately.

The RRCM diagrams are formulated using transformed composition diagrams to facilitate their interpretation Venimadhavan et al. [1994], Londoño et al. [2006]. For this purpose, Eq. 3-4 and 3-5 were defined, where the reference component is Butyl Lactate. These equations present the transformed compositions for Lactic Acid and n-butanol, respectively.

$$X_{LA} = x_{LA} + x_{BuLac} \tag{3-4}$$

$$X_{BuOH} = x_{BuOH} + x_{BuLac} \tag{3-5}$$

3.2.4. Michelsen Method (material stability)

Determining the vapor-liquid-liquid equilibrium zone (VLLE) is critical in heterogeneous distillation processes. For this purpose, it is required to know if a mixture with known temperature, pressure, and composition will spontaneously separate into more phases. The tool that allows knowing this behavior is the material stability analysis.

Regarding activity coefficients, the Gibbs free energy for liquid mixtures at low or moderate pressures can be modeled. Thus, the Gibbs tangent plane distance (TPD) for a mixture with c number of components at specified temperature T and pressure P is given in Eq. 3-6 Mollerup and Michelsen [2004].

$$TPD(w) = \sum_{i}^{c} y_i(\mu_i(y) - \mu_i(z)) \tag{3-6}$$

z is the mixture of known composition, temperature, and pressure, c is the number of components, and y is the composition of the test mixture. The stability of the mixture occurs when the steady states comply with $TPD(w) \leq \hat{a}0$.

The equations of state calculations are expressed in terms of fugacity coefficients, thus obtaining Eq. 3-7 .

$$TPD(w) = \sum_{i}^{c} y_i(Lny_i + Ln\hat{\varphi}_i(y) - Lnz_i - Ln\hat{\varphi}_i(z)) \tag{3-7}$$

Where

$$K = Lny_i + Ln\hat{\varphi}_i(y) - Lnz_i - Ln\hat{\varphi}_i(z) \tag{3-8}$$

By rearranging the equation, the stationary points of $TPD(y)$ can be obtained by solving the following set of algebraic nonlinear equations, subject to the mass balance restriction:

$$0 = Ln[y_i exp(-K)] + Ln\hat{\varphi}_i(y) - Lnz_i - Ln\hat{\varphi}_i(z) \tag{3-9}$$

and introducing the variable proposed by Michelsen $Y_i = y_i exp(-K)$ Michelsen [1982]:

$$0 = Ln(Y_i) + Ln\hat{\varphi}_i(y) - Lnz_i - Ln\hat{\varphi}_i(z) \tag{3-10}$$

The stationary points are located as solutions to Eq. 3-10. The solution was proposed using GlobalSearch Matlab Toolbox, and the composition in the mixture y as a decision variable. Stability was provided in all the stationary points corresponding to $\sum_i^c Y_i \leq 1$, and it is unstable if there is any solution where $\sum_i^c Y_i > 1$ Michelsen [1982].

Depending on the initial estimates, different convergence cases are presented: (i) the trivial solution ($y = z$); (ii) the non-trivial solution with $\sum_i^c Y_i > 1$, indicating material instability; and (iii) a non-trivial solution with $\sum_i^c Y_i \leq 1$, indicating material stability of the mixture z.

The mixture is unstable, dividing the original phase into two phases that decrease the total Gibbs Energy. After the material stability analysis, rigorous isothermal flash calculations are performed for the mixture to calculate the compositions of the phases into which the original mixture is divided.

3.2.5. Global optimization as a continuation method

A global optimization technique was implemented to assess the problem of mathematical convergence for the material stability (Michelsen method) due to the presence of a miscibility region for the system VLLE. This technique combines an indirect method with a homotopic approach Shen et al. [2015].

The GlobalSearch Matlab toolbox was used for solving the set of non-linear equations. It works using the scatter search and local Non-Linear Programming (NLP) solver Ugray et al. [2007]. The algorithm of GlobalSearch starts a local solver such as fmincon with a sequential quadratic programming (SQP) algorithm from multiple start points. Then, the algorithms

use multiple start points to sample multiple basins of attraction Mathworks.

Figure **3-5** presents an overview of the GlobalSearch algorithm. It uses a scatter-search mechanism to generate start points, then analyzes them and rejects those points unlikely to improve the best local minimum found. Afterward, it applies a local solver, such as fmincon with the SQP method, to evaluate the constraints. Finally, it gives a vector with the optimal solution Glover [1998].

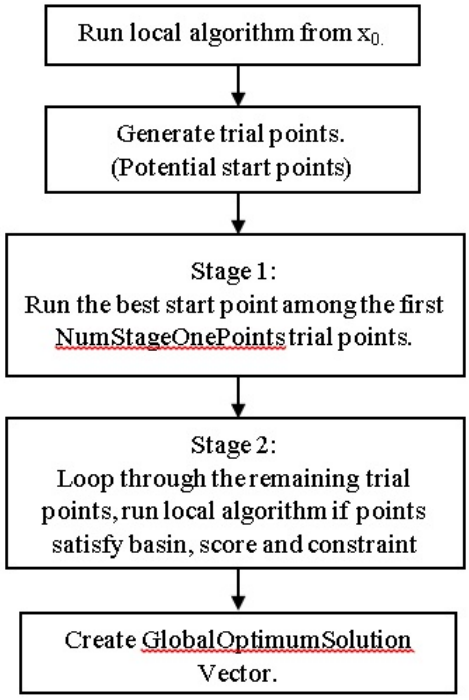

Figure 3-5: GlobalSearch algorithm Mathworks.

The GlobalSearch algorithm transforms the non-linear problem into an optimization problem in a general form, as shown in Eq. 3-11 to 3-14. The Eq. 3-11 is the objective function that contains vector decision variables such as liquid and vapor phase compositions, and it represents the Michelsen material stability equation.

$$Minimize f(x, y) \tag{3-11}$$

subject to the nonlinear constraints,

$$gl \leq G(x, y) \leq gu, \tag{3-12}$$

and to the linear constraints,

$$l \leq A_1 x + A_2 y \leq u, \tag{3-13}$$

$$x \in S, y \in Y, \tag{3-14}$$

where x is an n-dimensional vector of continuous decision variables, and y is a p-dimensional of discrete decision variables. The vectors gl, gu, l and u contain upper and lower bounds for the linear and nonlinear constraints. The matrices A_1 and A_2 contain the coefficients of any linear constraints. Finally, the set S is defined by simple bounds on x, the set Y is assumed to be finite, and it is often the set of all p-dimensional binary or integer vectors y that satisfy finite bounds Ugray et al. [2007]. Eq. 3-12 to 3-14 represent the non-linear and linear constraints that appear in the solution method of the Michelsen equation, such as optimality and conservation functions.

3.2.6. Isothermal flash

The isothermal flash calculation was performed in two ways: first, for a system with two-phase separation (VL) and, second, for a system with three-phase separation (VLL).

In both cases, the NRTL thermodynamic model was used for modeling the liquid phase, while the vapor phase was represented under the modified Raoult's law. An ideal vapor phase is assumed due to the mixtures' pressure conditions and nature.

3.2.7. Vapor-liquid equilibrium (VLE)

When the mixture is stable in the material stability analysis, a vapor-liquid equilibrium occurs in the system, thus resulting in the calculation of the VLE flash. If the system is in equilibrium, the fugacity of component i in the liquid phase is the same as in the vapor phase (Eq. 3-15) Smith, J. Van Ness, H. Abbott [2009].

$$f_{i,vapor} = f_{i,liquid}, \tag{3-15}$$

The relationship is expressed in Eq.3-16, assuming an ideal vapor phase Smith, J. Van Ness, H. Abbott [2009].

$$Py_i = P_i^{sat}\gamma_i x_i, \tag{3-16}$$

where P is total pressure, x_i and y_i are the mole fraction of component i in liquid and vapor phases, respectively, γ_i is the liquid phase activity coefficient of component i calculated with the thermodynamic model, and P_i^{sat} is the saturated vapor pressure of component i.

The flash was solved using the Newton-Raphson method using the mass balance of the vapor phase (Eq. 3-17) and the equilibrium temperature as the response variable. In this way, it is possible to obtain the temperature and composition of the vapor phase in equilibrium with the liquid phase at the pressure of the system.

$$0 = \sum_{i}^{c} y_i - 1, \tag{3-17}$$

3.2.8. Vapor-Liquid-Liquid Equilibrium (VLLE)

If the mixture is unstable in the material stability analysis, it separates into two liquid phases, thus resulting in the VLLE flash calculation. In the case of the VLLE, the fugacity of component i in the vapor phase is the same in both the first and the second liquid phases (Eq. 3-18) Smith, J. Van Ness, H. Abbott [2009].

$$f_{i,vapor} = f_{i,liquid1} = f_{i,liquid2}, \tag{3-18}$$

The composition of the mixture, known as a random liquid mixture, is considered the global composition of the liquid phases. For this reason, it is necessary to add Eq 3-19 - 3-24 to the liquid-liquid-vapor equilibrium to determine the compositions and distribution of the two liquid phases into which the overall mixture is divided Smith, J. Van Ness, H. Abbott [2009], Nann et al. [2013], Iwakabe and Kosuge [2008].

$$\gamma_i^{L1} x_i^{L1} = \gamma_i^{L2} x_i^{L2} = \frac{Py_i}{P_i^{sat}} \tag{3-19}$$

Where x_i is the mole fraction of component i in the liquid phase, $\hat{I}^3{}_i$ is the liquid phase activity coefficient of component $i$calculated with the thermodynamic model, superscripts $L1$, and $L2$ denote the phase number, P is the total pressure, y_i are the mole fraction of

component $i$in the vapor phase, and P_i^{Sat} is the saturated vapor pressure of component i.

$$X_i = x_i^{L1} L_1 + x_i^{L2} L_2 \tag{3-20}$$

Where X_i is the global mole fraction of component $i$in liquid phases, and $L1$ and $L2$ are the fractions of liquid 1 and liquid 2, respectively.

$$\sum_i^c x_i^{L1} = 1 \tag{3-21}$$

$$\sum_i^c x_i^{L2} = 1 \tag{3-22}$$

$$\sum_i^2 L_i = 1 \tag{3-23}$$

$$\sum_i^c y_i = 1 \tag{3-24}$$

The previously described equations were solved using the Matlab tool lsqnonlin, where the Eq. 3-2 is the objective function. It was solved using the trust-region-reflective algorithm. The results obtained are the composition and distribution of the two liquid phases, equilibrium temperature, and compositions of the vapor phase in equilibrium.

3.2.9. Kinetic Validation

For the kinetic evaluation, Eq. 2-1 was implemented. This expression was validated by Kumar and Mahajani [2007] for the esterification of Lactic Acid with n-butanol. The experimental temperatures were below 369.15 K, and LA compositions were below 30 %wt. For this reason, the oligomerization reactions were neglected. The kinetic expression was used as a complement of Eq. 3-2 to determine the reactive curve maps.

The parameters estimated by Kumar and Mahajani [2007] present a slight deviation from the experimental set at 369.15 K, 363.15 K, 333.15 K, and 318.15 K. Due to this deviation, the re-estimation of the four parameters was improved by minimizing the following

objective function (Eq. 3-25). For this purpose, the sum of the square of weighted residuals (SSWR) was used and solved with the hybrid method of simulated-annealing and interior point calculation. This algorithm was implemented because it combines non-deterministic and deterministic search methods to ensure good parameter estimation convergence.

$$SSWR = \sum_{i=1}^{n}\sum_{j=1}^{m}\left(\frac{\triangle_{ij}}{W_j^2}\right)^2 \tag{3-25}$$

where 'n' and 'm' are the total number of experimental data points presented by Kumar and Mahajani [2007] and the total number of variables, respectively, W_j is a standard data normalization factor for each variable, and $\triangle_{ij}$ is the difference between the predicted values and the experimental data ($y_{model} - y_{exp}$).

The obtained parameters are presented in Table **3-3**, as well as the comparison of the values of each parameter with those presented by Kumar and Mahajani [2007]

Table 3-3: Comparison of the estimated kinetic parameter based on the pseudo homogeneous activity-based model for the Confidence Interval of 95 %.

Parameter	**Kumar et al.**	**This Work**
$E_a(kj/mol)$	53.40±1,86	52.55±0,04
$E_b(kj/mol)$	52.24±6,01	51.28±0,06
$Ln(K_{f0})(mol/kgh)$	25.26±1,98	25.24±0,001
$Ln(K_{b0})(mol/kgh)$	23.34±0,63	23.38±0,001
Objective Function	0.003	9.63×10^{-4}

Table **3-3** shows that the parameters estimated in this work present a better fitting based on the value of the objective function: $9{,}63 \times 10^{-4}$ against 0.003 presented by Kumar and Mahajani [2007]. However, the differences with the parameters presented by Kumar and Mahajani [2007] are below 2 %. This agrees with Figure **3-6**, which represents the conversion percentage at four different temperatures.

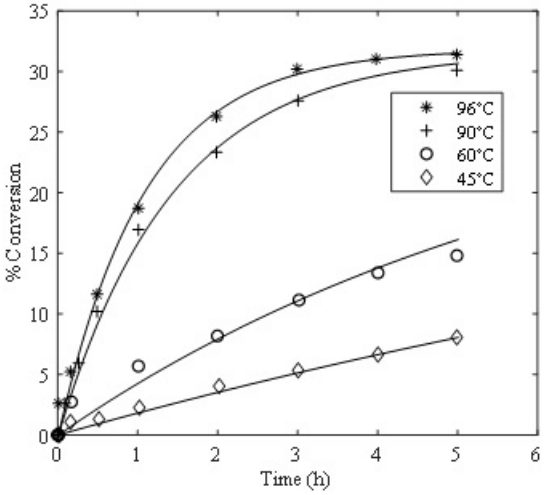

Figure 3-6: Kinetic validation with data from Kumar et al.Kumar and Mahajani [2007].

3.3. Modeling

This section develops a rigorous, dynamic, phenomenological-based model of Butyl lactate production in a reactive distillation column at the pilot-plant scale. First, some model assumptions and balance equations for reactive and non-reactive stages are presented in Section 3.3. Then, in Section 3.4, the reactive distillation column model is validated using three cases. In the first case, experimental data obtained during the production of isoamyl acetate in an RDC pilot-plant scale (located at Universidad Nacional de Colombia) were used (Case 1). The second case uses experimental results on the production of butyl lactate, reported by Kumar and Mahajani [2007] (Case 2). The production of butyl lactate was studied in silico at the pilot-plant scale. The third case is a simulation comparison between Aspen Plus v11 and Matlab R2020b (Case 3). Finally, a sensitivity study was carried out to analyze the system's behavior under changes in the operating variables.

Figure **3-7**a shows a picture of the batch reactive distillation column at Universidad Nacional de Colombia. Figure **3-7**b shows a general representation of the RDC, which is assumed to be divided into N theoretical equilibrium stages for modeling purposes. Stage 1 is the decanter, stage 2 is the condenser, and stage N is the reboiler (Figure **3-7**b). Figure **3-8** represents a general reactive stage.

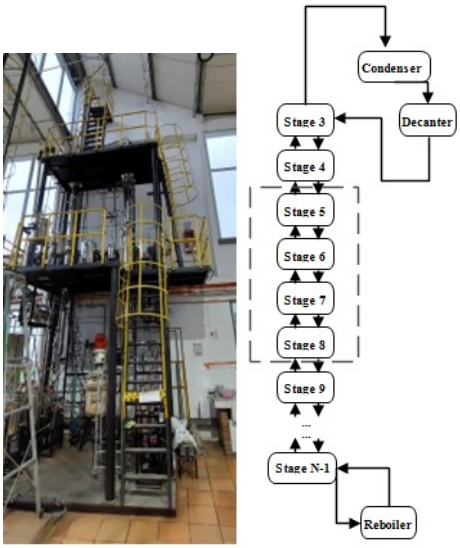

(a) (b)

Figure 3-7: (a) pilot-plant reactive distillation column, and (b) Stage-representation of a reactive distillation column b).

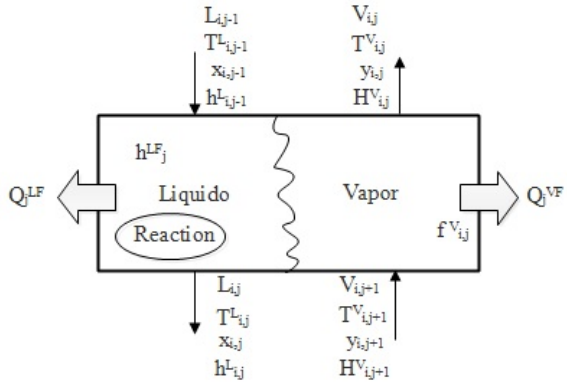

Figure 3-8: Representation of a general reactive stage.

3.3.1. Model Assumptions

To perform the modeling of the reactive distillation column, some assumptions must be made:

- For modeling the liquid phase, the NRTL model is used.
- There is no resistance to internal and external diffusive transport over the catalyst, and there is no resistance to transport over the fluid phases. Therefore, phase equilibrium is achieved homogeneously.

- A pseudo-homogeneous kinetic model is assumed.
- In the Decanter, the NRTL model is used for predicting liquid-phases behavior, and the k-value method is utilized to determine compositions in extracted and refined flows.
- The presence of oligomers is neglected.
- Reboiler and condenser are modeled as equilibrium stages.
- Variations in kinetic and potential energy are neglected.
- Equilibrium is assumed to be controlled by kinetics.
- Physical properties are constant.
- There is no heat loss from the column.
- Is considered a linear pressure drop along the column.
- Two phases (vapor-liquid) and a reaction in the liquid phase are considered.

3.3.2. Balance equations

This section presents the generalized mass and energy balances for reactive and non-reactive stages (Eq 3-26 to 3-28). For the three additional stages (decanter, condenser, and reboiler), the set of mass and energy equations are presented from Eq. 3-29 to 3-37.

3.3.3. Reactive and non-reactive stages

Based on the equilibrium stage model (Figure **3-8**), the mass and energy equations represent the dynamic behavior for the thermodynamic and kinetic transformation. F_i represents the feed flow of LA and BuOH; $R_{n,i}$, the reaction rate; $X_{F,I}$, the molar fraction of LA and BuOH in the feed;$Q_{r,I}$, the heat of reaction and $q_{F,i}$, the liquid fraction on the feed.

Total material balance:

$$\frac{dM_j}{dt} = L_{j-1} - Lj - V_j + F_j \tag{3-26}$$

Molar balance per component:

$$\frac{dx_{i,j}}{dt} = \frac{\left(x_{i,j-1}L_{j-1} + y_{i,j+1}V_{j+1} - x_{i,j}L_j - y_{i,j}V_j + x_{F,i,j}q_{F,j}F_j \; + R_{i,j} - x_{i,j}\frac{dM_j}{dt}\right)}{M_j} \tag{3-27}$$

Energy balance:

$$\frac{dT_j}{dt} = \frac{h_{j-1}L_{j-1} + H_{j+1}V_{j+1} - h_jL_i - H_jV_j + (h_{F,j}q_{F,j} + H_{F,j}(1-q_{F,j}))F_j + Q_{r,j} - h_j\frac{dM_j}{dt}}{M_jC_{pmix,j}} \tag{3-28}$$

3.3.4. Reboiler Stage

Equations 3-29 to 3-31 represent the dynamic behavior in the reboiler stage. B_{BuLac} represents the output flow of the BuLac product, V_B is the vapor flow as a function of the boil-up ratio, and Q_B, is the heat duty in the reboiler.

Total mass balance:

$$\frac{dM_B}{dt} = L_N - B_{BuLac} - V_B \tag{3-29}$$

Molar balance per component:

$$\frac{dx_{i,B}}{dt} = \frac{x_{i,N}L_N - x_{i,B}B_{BuLac} - y_{i,B}V_B - x_{i,B}\frac{dM_B}{dt}}{M_B} \tag{3-30}$$

Energy balance:

$$\frac{dT_B}{dt} = \frac{h_NL_N - h_BB_{BuLac} - H_BV_B + Q_B - h_B\frac{dM_B}{dt}}{M_B * C_{pmix,B}} \tag{3-31}$$

3.3.5. Condenser Stage

The set of equations 3-32 to 3-33 represents the dynamic behavior in the condenser stage. D_c is the condensed flow rate, and Q_c is the heat duty in the condenser.

Total mass balance:

$$\frac{dM_c}{dt} = D_c - F_o - F_A \tag{3-32}$$

Molar balance per component:

$$\frac{dx_{i,c}}{dt} = \frac{y_{i,1}V_1 - x_{i,c}D_c - x_{i,c}\frac{dM_c}{dt}}{M_{i,c}} \tag{3-33}$$

Enery balance:

$$\frac{dT_c}{dt} = \frac{H_1V_1 - Q_c - h_cD_c - h_c\frac{dM_c}{dt}}{M_cC_{pmix,c}} \tag{3-34}$$

3.3.6. Decanter Stage

The set of Equations 3-35 to 3-37 represents the dynamic behavior in the decanter stage. F_o and F_A represent the output flow of organic and aqueous phases, respectively. In contrast, $x_{i,o}$ and $x_{i,A}$ represent the mass fraction of each component i in the organic and aqueous phases, respectively.

Total mass balance:

$$\frac{dM_d}{dt} = D_c - F_o - F_A \tag{3-35}$$

Molar balance per component:

$$\frac{dx_{i,d}}{dt} = \frac{x_{i,c}D_c - x_{i,o}F_o - x_{i,A}F_A - x_{i,d}\frac{dM_d}{dt}}{M_d} \tag{3-36}$$

Energy balance:

$$\frac{dT_d}{dt} = \frac{h_c D_c - h_o F_o - h_A F_A - h_N \frac{dM_d}{dt}}{M_c C_{pmix,d}} \tag{3-37}$$

3.4. Model Application

As mentioned, model validation is performed in three scenarios, denoted here as case 1 to case 3. The set of Equations 3-26-3-37 can generally be used for modeling a RD column. However, the three cases used for validation are different, and therefore, the thermodynamic and kinetic models differ.

3.4.1. Case 1: Isoamyl acetate production

In this section, the production of isoamyl acetate (IAc) from acetic acid (AA) and isoamyl alcohol (IA) at the pilot-plant scale is evaluated. First, the thermodynamic and kinetic models are presented. Then, the column specifications for modeling and simulation are given.

Thermodynamic model

The γ-ϕ formulation is used without considering the pointing factor for the phase equilibrium calculations Smith, J. Van Ness, H. Abbott [2009].

$$y_i \ \varphi_i \ P = x_i \ \gamma_i {\varphi_i}^{sat} {P_i}^{sat} \tag{3-38}$$

Saturation pressures are calculated using the Extended Antoine Equation [Walpot, 2011] with parameters retrieved from Aspen Plus (Table **3-4**).

Table 3-4: Antoine Equation parameters retrieved from Aspen Plus.

Component	C1	C2	C3	C4	C5	C6	C7	Units
AA	46.3622	-6304.5	0	0	-4.2985	8.8865e-18	6	K, kPa
W	46.3622	-7258.2	0	0	-7.3037	4.1653e-06	2	K, kPa
IA	110.162	-10743	0	0	-13.165	1.1670e-17	6	K, kPa
IAc	92.6502	-8876.8	0	0	-11.075	2.4723e-17	6	K, kPa

AA: Acetic acid, **W:** Water, **IA:** Isoamyl alcohol and **IAc**: Isoamyl acetate

$$lnP_i = C_{1i} + \frac{C_{2i}}{T + C_{3i}} + C_{4i}T + C_{5i}lnT + C_{6i}T^{C_{7i}} \tag{3-39}$$

Based on the results of Correa Sanchez [2015], the activity and fugacity coefficients are determined using the Non-Random Two Liquids Model (NRTL) and the Hayden O'Connell Equation. The NRTL parameters are temperature dependent and are listed in Table **3-5**.

$$\tau_{ij} = A_{ij} + \frac{B_{ij}}{T} \tag{3-40}$$

$$G_{ij} = exp(-\alpha_{ij}\ \tau_{ij}) \tag{3-41}$$

$$ln(\gamma_i) = \frac{\sum_j x_j \tau_{ij} G_{ij}}{\sum_k\ x_k x_k G_{ki}} + \sum_j \frac{x_j G_{ij}}{\sum_k x_k G_{ki}} \left(\tau_{ij} - \frac{\sum_m x_m \tau_{mj} G_{mj}}{\sum_k x_k G_{kj}} \right) \tag{3-42}$$

Table 3-5: Binary Interaction parameters for the NRTL model and the quaternary system: acetic acid, isoamyl alcohol, isoamyl acetate, and water Correa Sanchez [2015].

Component i	**Component j**	A_{ij}	A_{ji}	B_{ij}	B_{ji}	α_{ij}
AA	W	-1.9763	3.3293	609.889	-723.888	0.3
IA	W	-2.2557	4.6762	1203.49	-93.3626	0.4
IAc	W	-0.2871	7.9245	754.013	-906.009	0.32
AA	IA	0.9632	-1.614	-214.477	469.04	0.47
AA	IA	-0.817	-0.2909	525.257	238.964	0.47
IA	IA	0	0	700.27	-379.459	0.3

AA: Acetic acid, **W:** Water, **IA:** Isoamyl alcohol and **IAc**: Isoamyl acetate

Finally, the non-idealities of the vapor phase are determined through fugacity coefficients with the formulation [Sánchez et al., 2019, 2020].

$$\varphi_i = exp\left(\frac{B_{ii}(P - P_i^{sat}) + \frac{1}{2}P\sum_j\sum_k x_k G_{kj}(2\delta_{ji} - \delta_{jk})}{RT}\right) \tag{3-43}$$

where,

$$\delta_{ji} = 2B_{ji} - B_{jj} - B_{ii} \tag{3-44}$$

$$\delta_{jk} = 2B_{jk} - B_{jj} - B_{kk} \tag{3-45}$$

B_{ij} [T] is the second virial coefficient that characterizes the binary interaction between i and j and it is calculated based on the HOC formulation.A complete formulation, including calculating the second virial coefficient, is published in George Hayden and O'Connell [1975], the interaction parameters can be determined from P-V-T data and statistical thermodynamic formulations. A complete formulation is published in Walpot [2011].

The solvation and association parameters for the HOC equation are presented in Table **3-6** Sánchez et al. [2020].

Table 3-6: Parameters of HOC equation for the system: acetic acid, isoamyl alcohol, water, and isoamyl acetate retrieved from Sánchez et al. Sánchez et al. [2020].

	AA	**W**	**IA**	**IAc**
AA	4.5	2.5	2.5	1.3
W	2.5	1.7	2.5	0.53
IA	2.5	2.5	2.2	2
IAc	1.3	0.53	2	0.53

AA: Acetic acid, **W:** Water, **IA:** Isoamyl alcohol and **IAc**: Isoamyl acetate

As it is shown in Figure **3-9**, the set of parameters employed can properly represent the two binary azeotropes and one ternary azeotrope of the system: isoamyl alcohol - acetic acid, isoamyl alcohol - isoamyl acetate, and acetic acid - isoamyl alcohol - isoamyl acetate, respectively, as also presented by Sánchez et al. [2019].

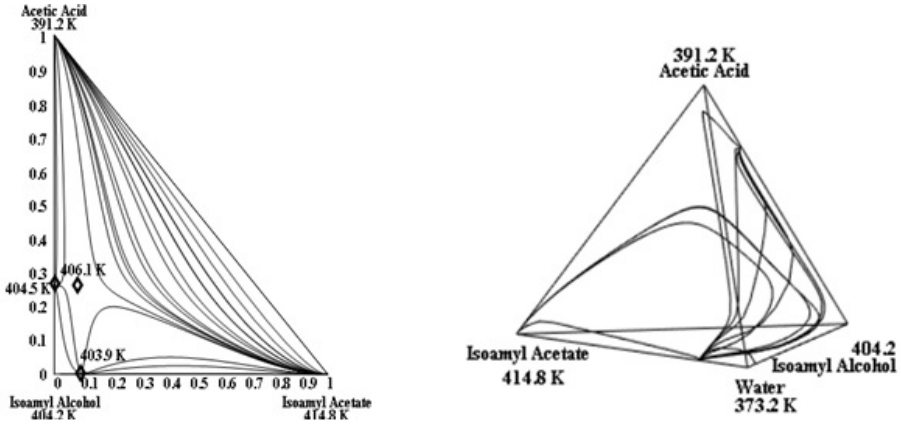

(a) (b)

Figure 3-9: Reactive distillation column scheme to produce isoamyl acetate in a batch process: ternary diagram a) and quaternary diagram b).

Kinetic model

Isoamyl acetate is produced by a reversible reaction between acetic acid and isoamyl alcohol in which water is the secondary product (Eq. 3-46).

$$AA + IA \leftrightarrow IAc + W(5{,}5kJ/mol) \tag{3-46}$$

Authors in Sánchez et al. [2019] determined experimentally the parameters to describe the esterification reaction in presence of the cation exchange resin Amberlyst 70. The experiments were conducted over a wide range of temperatures (353-383 °C), catalyst loadings (0.5-5 %wt), and molar ratios of acetic acid: isoamyl alcohol (0.5 - 2.0) to generate kinetic data under different conditions. Kinetic parameters are estimated using a pseudo-homogeneous model. The mass balance for the reaction corresponds to Eq. 3-47, where v_i is the is the stoichiometric coefficient of species i in the balanced chemical reaction, m_{cat} refers to the mass of the catalyst used in the reaction and n refers to the reaction rate.

$$\frac{(dn_i)}{dt} = v_i m_c atn\hat{I}^3 \rightarrow \frac{1}{(w_c atMW_i)}\frac{(dw_i)}{dt} = v_i n\hat{I}^3 \tag{3-47}$$

Where the reaction rate (Gamma) is expressed as a power law (Eq. 3-48 and 3-49).

$$\gamma_i(T,x) = k_{d,i}(x_A Acx_i AOH - \frac{x_w x_i AmAc}{k_{eq}}) \tag{3-48}$$

$$k_{d,1} = k_{d0} exp\left(\frac{-Ea}{R_g}\left(\frac{1}{T} - \frac{1}{T_0}\right)\right), T_0 = 378{,}15K \tag{3-49}$$

Figure **3-10** presents the kinetic validation of the model against the experimental data obtained by Sanchez Correa Sanchez [2015]. They present the experimental data, and Table **3-7** lists the kinetic parameters.

Table 3-7: Estimated kinetic parameters based on the pseudo homogeneous model Sánchez et al. [2019].

Parameters	**Sánchez et al. [2020]**
$\mathrm{kd}_0[kmol/kg\,h]$	2.9820
k_{eq}	4.5662
$\mathrm{E}_a[kJ/mol]$	44.2793×10^{-3}

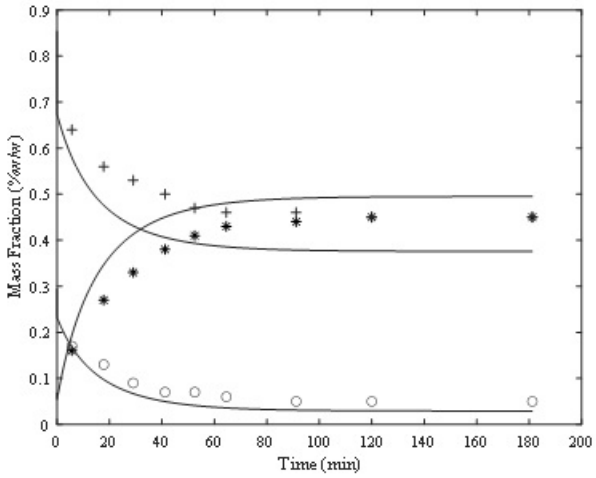

Figure 3-10: Kinetic validation for isoamyl acetate reaction at 383.15 K, (-) model prediction, (∘) acetic acid, (+) isoamyl alcohol, and (*) isoamyl acetate.

Column specifications

The experiments were performed in a reactive distillation column operating at atmospheric pressure. The column has a reactive section packed with Amberlyst 70, an acidic catalyst, and two non-reactive sections (stripping and rectifying zones) packed with Nutter Ring number 07, as well as one condenser and one reboiler as shown in Figure **3-11**. Simulation values are taken from the Sánchez et al. [2019] job in a batch process. Figure **3-11** shows the results of this simulation to obtain a background composition of Isoamyl acetate of 0.9982. Further column design specifications are presented in Table **3-8** [Bastidas Jiménez, 2014]. Table **3-8** presents the most approximate values of the reactive distillation column in the pilot plant, including internal characteristics of the same.

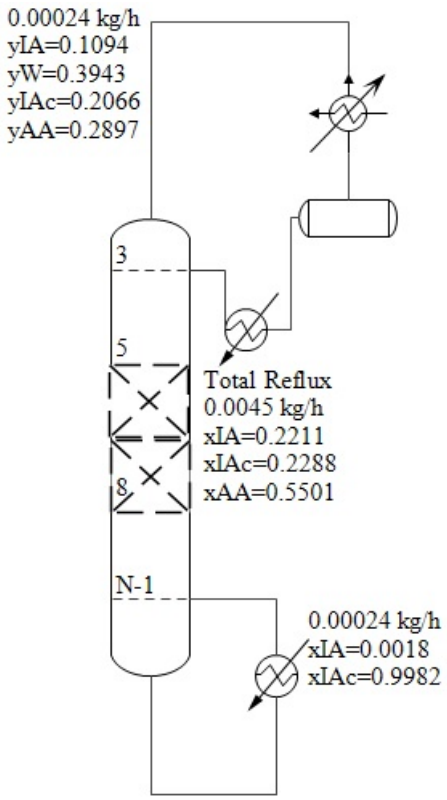

Figure 3-11: Reactive distillation column scheme to produce isoamyl acetate in batch process.

Table 3-8: Reactive distillation column internal specifications. Bastidas Jiménez [2014]

Parameters	**Value**
Diameter [m]	0.0762
Catalyst density per volume of the module [kg/m^3]	76
Number of reactive stages (3-6)	4
Stripping zone length per stage [m]	1.1
Rectifying zone length per stage [m]	1
Non-reactive section package height [m]	Stages 1-2: 1, Stages 7-11: 1.1
Reactive section package height [m]	1.1
Packaging	Nutter Ring No. 07

3.4.2. Case 2: Butyl lactate production reported by Kumar et al.

This section presents the production of butyl lactate from lactic acid and n-butanol for the case presented by Kumar and Mahajani [2007]. First, the thermodynamic and kinetic models used are described. Then, the column specifications for modeling and simulation are given.

Thermodynamic model

The VLE can be calculated by the gamma-phi model (Eq. 3-38). Due to the similar nature of the substances, the Poynting factor is assumed as 1, and the vapor phase is considered ideal. The VLE is expressed as the modified Raoult's law (Eq. 3-50):

$$y_i P = x_i \gamma_i P_i^{sat} \tag{3-50}$$

Saturation pressures are calculated using Antoine Equation and Extended Antoine equation (Eq. 3-51 and 3-52) with parameters retrieved from Aspen Plus.

Table 3-9: Antoine parameters for the butyl lactate system (BuOH e BuLac) this work and (LA, W) Aspen Plus database.

Component	C1	C2	C3	C4	C5	C6	C7	Units
LA[1]	7.5111	-1965.70	-91.021	-	-	-	-	K, kPa
W[2]	73.649	-7258.2	0	0	-7.3037	4.1653e-06	2	K, kPa
BuOH[2]	99.3822	-9866.4	0	0	-11.655	1.08e-17	6	K, kPa
BuLac[1]	7.142	-2160.134	235.46	-	-	-	-	K, kPa

$$^{1}logp_i^{*l} = C_{1i} + \frac{C_{2i}}{(T + C_{3i})} \tag{3-51}$$

$$^{2}Lnp_i^{*l} = C_{1i} + \frac{C_{2i}}{(T + C_{3i})} + C_{5i} LnT + C_{6i} T^{C_{7i}} \tag{3-52}$$

The NRTL activity model and their equations representing the thermodynamic model were described in Section 3.4. Table **3-10** lists the set of binary parameters related to the NRTL model. For the regression of the parameters, the complete set of experimental data was used, giving more weight in the optimization to the values of 5 and 1 kPa. It was implemented Aspen Plus V11 using Maximum-likelihood as the objective function, Deming as

the initialization function, and Weighted least squares as the optimization algorithm with a convergence tolerance of 1 $\times 10^{-6}$. The results show a good fit considering the three pressure ranges evaluated (101.33, 5, and 1 kPa). The values show a root mean square percentage error of 0.22 % and an average deviation of 0.25 K.

Table 3-10: NRTL parameters for the butyl lactate system [This work].

Component i	**Component j**	A_{ij}	A_{ji}	B_{ij}	B_{ji}	α_{ij}
BuOH	W	11.86	32.03	-4690.40	-10000.00	0.20
BuOH	BuLac	0.79	-0.73	-158.78	134.43	0.30
BuOH	LA	0.00	0.00	1537.60	-654.60	0.20
W	LA	0.00	0.00	407.70	-454.30	0.30
BuLac	LA	0.00	0.00	-130.30	327.59	0.30

Kinetic model

In this case, the pseudo-homogeneous activity model and the table with the kinetic values are presented in Section 3.2.9. It should be noted that the values of parameters presented in the mentioned section and Table **3-11** are similar. Still, values in Table **3-11** present a good fitting.

Table 3-11: Kinetic parameters from the pseudo homogeneous activity-based model.

Parameters	**Value**
$E_a[kJ/mol]$	52.55±0,04
$E_b[kJ/mol]$	51.28±0,06
Ln $k_{f0}[mol/kg\,h]$	25.24±0,01
Ln $k_{b0}[mol/kg\,h]$	23.38±0,01

Column specifications

Kumar and Mahajani [2007] evaluated the process in the laboratory scale reactive distillation column with the operating conditions presented in Figure **3-12**. The authors used

a glass column with a 55 mm diameter and 2.7 m height. The reactive zone was packed with KATAPAK-S filled with ion-exchange Amberlyst 15. Non-reactive zones (rectifying and stripping) were packed with a wire mesh supplied by Evergreen India Ltd. A Dean-Stark apparatus was located at the top of the column to remove the aqueous phase and recycle the organic phase from the azeotropic mixture of n-butanol and water. Lactic acid and butanol were continuously fed to the top and bottom of the reactive section, respectively. Water was continuously removed at the top of the column. More column design specifications are presented in Table **3-12**.

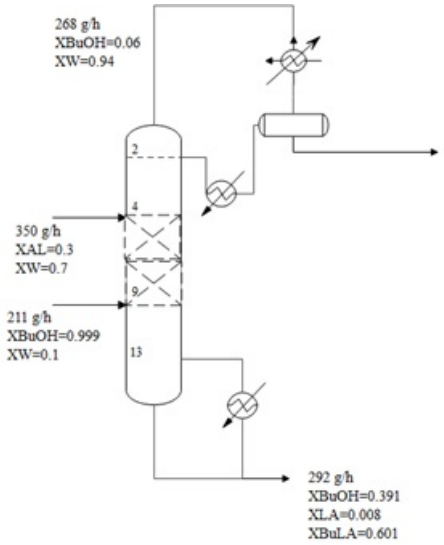

Figure 3-12: Reactive distillation column scheme to produce butyl lactate in a continuous process [Kumar and Mahajani, 2007]..

Table 3-12: Internal specifications of the reactive distillation column.[Kumar and Mahajani, 2007]

Parameters	Value
Diameter [mm]	55
Number of reactive stages (5-8)	3
Number of non-reactive stages (2-4, 9-13)	8
Reactive section diameter (Cm)	7.5
Non-reactive section diameter (Cm)	6.65
Catalyst loading per stage [g]	30
Catalyst (Katapak-S)	Amberlyst 15
Operating pressure [kPa]	101.325

3.4.3. Case 3: In silico Butyl lactate production at pilot-plant scale

In this section, the production of butyl lactate at pilot-plant conditions is tested in silico. All the thermodynamic (Tables **3-8** and **3-9** and Equations 3-40 to 3-42) and kinetic (Table **3-10** and **3-11** and Equations 2-1, 3-51 and 3-52) information are presented in Sections 3.4.1 and 3.4.2. Figure **3-13** present the plant's operational conditions to be reproduced in silico. The presented operational conditions are based on the actual operability at the pilot-plant scale. It contains the physical restrictions that can be observed in reality, such as the maximum flow rate of the feed pumps, minimum operating pressure (50 kPa), and oversizing of the reboiler. The bottom flow rate was fixed to obtain the higher product while the hydrodynamic restrictions were fulfilled. The Aspen Plus simulator and Matlab/Simulink evaluated and compared this scenario.

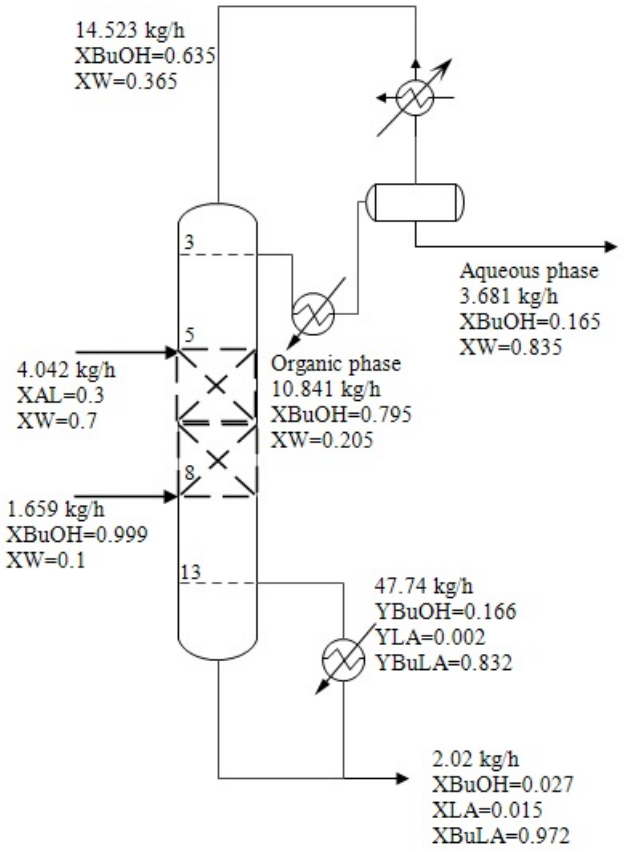

Figure 3-13: Operating conditions of a RDC at pilot-plants scale to produce butyl lactate.

3.5. Advanced Control Strategy

This section presents the advanced control proposal, NMPC, compared against a multivariable strategy, PID, and LMPC control. In the same way, the set of equations for estimating unmeasured disturbances and states by an artificial neural network (ANN) is presented. Finally, the control performance analysis for an LMPC system is shown using ANN as a parameter and state estimator.

3.5.1. MIMO PID

The Proportional-Integral-Derivative (PID) controller is a fundamental component of control engineering, providing a simple yet effective method to regulate systems based on error feedback. The PID controller calculates the control variable, $u(t)$, as follows:

$$u(t) = K_p e(t) + K_i \int e(t)dt + K_d \frac{de(t)}{dt} \tag{3-53}$$

where K_p, K_i, and K_d are the proportional, integral, and derivative gains, respectively, and $e(t)$ is the difference between the desired and actual output, known as the error [Sigurd and Ian, 1979]. Chien, Hrones, and Reswick (CHR) method was used to tune the parameters of the PID controller [Cohen and Coon, 1952]. Table **3-13** shows the calculation equations of the parameters Kp, τ_i and τ_d.

Table 3-13: CHR Tunning Parameters.

Controller	**Kp**	τ_i	τ_d
P	$\frac{0,3\tau}{KL}$	∞	0
PI	$\frac{0,35\tau}{KL}$	1.2τ	0
PID	$\frac{0,6\tau}{KL}$	τ	0.5L

where The open-loop method involves the identification of key process parameters:

- K: The steady-state process gain, which is the ratio of the output change to a change in input.
- L: The process dead-time or delay time. It signifies the time taken for the process output to initiate a change after an input change.
- τ: The process time constant. Post the delay L, the output changes and the time it takes for the output to achieve about 63.2 % of its total change is represented by τ.

The values of the proportional, integral, and derivative constants can be calculated as $Kp = \frac{0,3\tau}{KL}$, $K_i = \frac{Kp}{\tau_i}$, and $K_d = \frac{Kp}{\tau_d}$.

However, PID controllers, initially conceptualized for Single-Input Single-Output (SISO) systems, face challenges when expanded to Multi-Input Multi-Output (MIMO) systems due to potential interactions between various inputs and outputs. The Singular Value Decomposition (SVD) and the Relative Gain Array (RGA) are invaluable in designing and tuning PID controllers in MIMO systems.

SVD provides a way to transform a complex MIMO system into a set of simpler, decoupled Single-Input Single-Output (SISO) systems. Given a matrix A of the system, SVD decomposes it as:

$$A = U\Sigma V^T \tag{3-54}$$

Here, U and V are unitary matrices comprising left and right singular vectors of A. Σ is a diagonal matrix with singular values of A. In a control context, singular values indicate the system's gain along different directions.

On the other hand, the RGA assists in pairing inputs and outputs in MIMO systems for decentralized control, calculated as follows:

$$\Lambda = G \times (G^{-1})^T \tag{3-55}$$

Each element of the RGA is given by, where G_{ij} represents the plant/gain matrix for a set of input parameters that control a set of output parameters:

$$\Lambda_{ij} = \frac{G_{ij}}{G_{i.}} \times \frac{G_{.j}}{G_{..}} \tag{3-56}$$

where, Λ_{ij} represents an individual element of the RGA. The indices i and j denote the specific row and column in the RGA matrix, corresponding to a particular input-output pairing in a multivariable control system. G_{ij} denotes the element of the plant or system gain matrix at the i^{th} row and j^{th} column. It represents how the j^{th} input affects the i^{th} output. $G_{i.}$ represents the sum of the gains in the i^{th} row of the gain matrix, measuring how all inputs combined affect the i^{th} output. $G_{.j}$ indicates the sum of the gains in the j^{th} column of the gain matrix, showing the overall effect of the j^{th} input on all outputs. $G_{..}$ represents the sum of all elements in the gain matrix, indicating the total interactive effect of all inputs on all outputs in the system. The RGA provides a measure of interaction between various input-output pairs.

Thus, through the combined use of SVD and RGA, a comprehensive picture of system interactions can be formed, paving the way for effective design and tuning of PID controllers in complex MIMO systems [Sigurd and Ian, 1979, Luyben and Luyben, 1997]. The SVD and RGA are powerful tools in designing PID controllers for MIMO systems. SVD is applied to the system's gain matrix, G, decomposing it into unitary matrices U and V^T, and a diagonal matrix Σ containing singular values. This decomposition aids in identifying the system's directional gains and potential control challenges. The RGA, calculated as $\Lambda = G \times (G^{-1})^T$, assesses the degree of interaction between control loops. It helps pair inputs and outputs and understand each control loop's relative influence. Combined, SVD and RGA inform the design of PID controllers by providing insights into the system's dynamics, which is crucial

for achieving desired control objectives in MIMO systems.

Based on SVD and RGA analyses, a 2×2 system will be evaluated where the objective is to control the temperature of the condenser and reboiler (T_2 and T_{14} respectively), manipulating Feed Ratio and Boilup Ratio (FR and BR respectively). Section 4.4 will demonstrate the reason for pairing these variables.

The system's gain matrix G is analyzed using SVD. SVD decomposes G into three matrices: U, Σ, and V^T. Here, U and V are unitary matrices, and Σ is a diagonal matrix consisting of the singular values. This decomposition helps in understanding the directional gains and the coupling effects in the system.

The RGA is computed using the formula $\Lambda = G \times (G^{-1})^T$. The RGA provides insights into the interaction between different control loops in the system. It is crucial for determining the most effective pairing of inputs and outputs, which is a critical aspect in the design of a MIMO PID controller.

Based on the insights gained from SVD and RGA, the PID controllers can be designed for each input-output pair. The singular values guide the controller's tuning, highlighting the dominant dynamics and coupling effects. Conversely, the RGA assists in assigning the PID controllers to the most appropriate pairs, ensuring effective control with minimal interaction.

In Equation 3-58, the transfer function matrix $\mathbf{G}(s)$ represents a 2-input 2-output for a centralized system where all the four elements of the matrix are presented.

$$\mathbf{G}(s) = \begin{bmatrix} G_{11}(s) & G_{12}(s) \\ G_{21}(s) & G_{22}(s) \end{bmatrix} \tag{3-57}$$

$$\mathbf{G}(s) = \begin{bmatrix} \frac{a_{11}s+b_{11}}{s^2+c_1s+d_1} & \frac{a_{12}s+b_{12}}{s^2+c_2s+d_2} \\ \frac{a_{21}s+b_{21}}{s^2+c_3s+d_3} & \frac{a_{22}s+b_{22}}{s^2+c_4s+d_4} \end{bmatrix} \tag{3-58}$$

To parametrize this system with a single vector, we can use:

$$\theta = \begin{bmatrix} a_{11} & b_{11} & a_{12} & b_{12} & a_{21} & b_{21} & a_{22} & b_{22} \end{bmatrix}^T \tag{3-59}$$

The relative gain array (RGA) gives a measure of interaction between input-output pairs:

$$\text{RGA} = \begin{bmatrix} \frac{G_{11}}{G_{11}+G_{21}} & \frac{G_{12}}{G_{12}+G_{22}} \\ \frac{G_{21}}{G_{11}+G_{21}} & \frac{G_{22}}{G_{12}+G_{22}} \end{bmatrix} \tag{3-60}$$

The RGA helps determine suitable pairings of inputs and outputs for decentralized PID controllers. The PID controllers are then tuned on the individual SISO loops.

In this sense, the single vector parametrization allows the MIMO system to be identified from data. The RGA then helps design appropriate decentralized PID controllers, which can be tuned for the individual input-output pairings [Luyben and Luyben, 1997].

3.5.2. Model predictive controller (MPC)

Model Predictive Control (MPC), encompassing both LMPC and NMPC, is an advanced control strategy well-suited for systems with multivariable interactions, constraints, and modeling uncertainties. These qualities make MPC suitable for controlling complex processes such as a pilot-scale reactive distillation column.

In the case of LMPC, a linear predictive model is employed, providing advantages in terms of computational simplicity and a rich theoretical basis [Camacho and Bordons, 2004, Maciejowski, 2002]. Contrarily, NMPC utilizes a nonlinear predictive model, catering to systems with severe nonlinearity, albeit with a higher computational demand [Mayne et al., 2000]. LMPC and NMPC formulations explicitly incorporate constraints within the optimization problem, a crucial feature for many process control applications.

Section 4.4 presented a unified formulation of the MPC strategy that serves both LMPC and NMPC applications. Equations 3-61-3-67 give the objective function and constraints of the MPC problem, serving as a formal mathematical representation of the control objectives:

$$\min_{\mathbf{u},\epsilon_\mathbf{k}} \left[\sum_{j=1}^{p} \|y(k+j|k) - w(k+j)\|^2_{\mathbf{Q}} + \sum_{j=1}^{m} \|\Delta u(k+j-1)\|^2_{\mathbf{W}} + \rho\epsilon_k^2 \right] \tag{3-61}$$

subject to

$$x(k+j) = f(x(k+j-1), u(k+j-1), \boldsymbol{\mu}), \tag{3-62}$$

$$g(y(k+j), x(k+j), u(k+j-1), \boldsymbol{\mu}) = \mathbf{0}, \tag{3-63}$$

$$x(k) = \hat{x}(k) \tag{3-64}$$

$$u_{min} \leq u(k+j-1) \leq u_{max}, \tag{3-65}$$

$$\Delta u_{min} \leq u(k+j-1) - u(k+j-2) \leq \Delta u_{max}, \tag{3-66}$$

$$y_{min} - \epsilon_k \leq y(k+j) \leq y_{max} + \epsilon_k, \tag{3-67}$$

In this formulation, $y(k+j|k)$ represents the output prediction j sampling periods ahead, while $w(k+j)$ is the reference trajectory, and $\Delta u(k) = u(k) - u(k-1)$ represents the control increment. $x(k+j)$ denotes the system's state vector. The slack variable ϵ_k is defined for

the entire control interval k, indicating that it is a single parameter used throughout the prediction horizon. The term $\|x\|_H^2$ defines the weighted Euclidean norm of $x \in \mathbb{R}^n$, given by $\|x\|_H^2 = x^T H x$, where $H \in \mathbb{R}^{n \times n}$ is a positive semi-definite matrix. Eqs. 3-62 to 3-63 describe the process model with $\boldsymbol{\mu}$ being the model parameter vector, while equation 3-64 represents the initial condition of the prediction horizon. The optimization problem constraints related to controlled, manipulated, and control action variations are presented in Eqs. 3-65 to 3-67. The tuning parameters include prediction horizon p, control horizon m, sampling period T_s, error weighting matrix of the controlled variables $\mathbf{Q}$, movement minimization weighting matrix $\mathbf{W}$, and penalty associated with violation of soft constraints ρ.
In the LMPC control, the Equations 3-62 and 3-63 are described by linear models, and the linear models were obtained by identification as follows:

$$G(s) = \begin{bmatrix} \frac{b_{11}s+b_{10}}{s^2+a_1s+a_0} & \frac{b_{12}s+b_{10}}{s^2+a_1s+a_0} \\ \frac{b_{21}s+b_{20}}{s^2+a_1s+a_0} & \frac{b_{22}s+b_{20}}{s^2+a_1s+a_0} \end{bmatrix} \tag{3-68}$$

where $G(s)$ is a 2x2 transfer function matrix relating the two inputs to the two outputs. A common denominator second-order transfer function model structure was chosen.

The prediction error method was used to estimate the unknown parameters b_{11}, b_{10} etc. in the transfer function matrix. The `tfest()` function in MATLAB was used to perform the estimation.

The identified model was validated by comparing its simulated output to measured test data from the physical system under previously unseen input conditions. The model was deemed acceptable based on good fit (% error ¡5 %).

The tuning of MPC systems presents challenges due to the numerous parameters involved, especially when dealing with multivariable processes. Giraldo et al. [2022] introduced a methodology, further formalized in Giraldo et al. [2022], known as Model Predictive Control Tuning (MPCT). The MPCT employs a hybrid optimization framework that combines both integer and real variables, encapsulated in the decision variable vector $\mathbf{x}_{dv}$. This vector includes elements such as prediction and control horizons and the diagonal weight matrices $\mathbf{Q}$ and $\mathbf{W}$. To address the ill-conditioned matrices in multivariable systems, the MPCT algorithm scales the internal model of the controller. In the LMPC context, an optimization problem is formulated to scale the system model by minimizing its condition number. The optimization procedure is conducted sequentially, initially employing the Goal Attainment Method (GAM) followed by the Variable Neighborhood Search (VNS). The GAM minimizes the square error between predefined reference trajectories and the actual closed-loop outputs, establishing the desired system behavior. VNS refines these results by adjusting the prediction and control

horizons to minimize the distance between the closed-loop responses and the initially calculated trajectories. An implementation of the MPCT methodology is available in MATLAB and can be accessed from the following GitHub repository: https://github.com/sergioacg/Model-Predictive-Control/tree/main/MPC-Tuninghttps://github.com/sergioacg/Model-Predictive-Control/tree/main/MPC-Tuning.

3.5.3. Non-linear model predictive controller (NMPC)

NMPC is a type of control strategy used to regulate dynamic processes with non-linear behavior, where the control action is computed by solving a dynamic optimization problem. In NMPC, a model of the system to be controlled is used to predict its future behavior based on the current and past states and inputs. Then, an optimization problem is formulated to minimize a cost function that includes the predicted states and inputs over a finite horizon. The optimal control action is obtained by solving this optimization problem subject to constraints on the system states, inputs, and outputs Lima et al. [2023].

The NMPC is transformed into NLP by parameterizing the states and controls for the direct approach. The goal is to implement NMPC for a 2-input, 2-output nonlinear system. The nonlinear plant is modeled as follows:

$$\dot{x} = f(x, u) \tag{3-69}$$

$$y = g(x, u) \tag{3-70}$$

where $x \in \mathbb{R}^n$ is the state vector, $u \in \mathbb{R}^2$ is the input vector, $y \in \mathbb{R}^2$ is the output vector, and $f(x, u)$ and $g(x, u)$ represent the nonlinear dynamics.

The control algorithm solves the finite horizon optimal control problem at each sample time:

$$\min_{u} \; l(x, u) + \int_{t_0}^{t_f} l(x(\tau), u(\tau)) d\tau \tag{3-71}$$

$$\text{s.t. } \dot{x} = f(x, u), \; x(t_0) = \hat{x}(t_0) \tag{3-72}$$

where $l(x, u)$ is the cost function and $\hat{x}(t_0)$ is the current state estimate. A single shooting transcription transforms this into a nonlinear programming (NLP) problem.

The NLP problem is solved using a sequential quadratic programming (SQP) solver from the MATLAB/Simulink Nonlinear Model Predictive Control Toolbox at each sample time. The plant model updates the numerical approximations of the Hessian and Jacobian at each iteration.

The NMPC controller was implemented in MATLAB using the Model Predictive Control Toolbox. The SQP solver allows efficient solutions to the nonlinear optimization problem online. Stability constraints were included to ensure closed-loop stability. The NMPC controller performance was validated on the physical system.

3.5.4. State Estimator

State estimators act in the set of Eq. 3-62 as state observers to predict x_0 from noisy measurements and models with uncertainty. The difference and observation models are reformulated in the set of Eq. 3-73 and 3-74, respectively, where the model parameters and perturbations can also be estimated. However, they do not change during the evolution of the model (i.e., $\theta_{k+1} = \theta_k$) Lima et al. [2023].

$$\begin{aligned} x'(k+1) &= \begin{bmatrix} x(k+1) \\ \theta(k+1) \end{bmatrix} = f'(x(k), u(k), \theta(k)) + w'(k) \\ f'(x(k), u(k), \theta(k)) &= \begin{bmatrix} f(x(k), u(k), \theta(k)) + w(k) \\ \theta(k) + w_\theta(k) \end{bmatrix} \end{aligned} \tag{3-73}$$

$$y(k) = \begin{bmatrix} h(x(k), u(k)) & 0 \end{bmatrix} \begin{bmatrix} x(k) \\ \theta(k) \end{bmatrix} + v(k) \tag{3-74}$$

Artificial Neural Network (ANN)

An Artificial Neural Network (ANN) is a computational framework influenced by the structure and operations of biological neural systems. Its principal applications include regression analysis, classification, and data processing Hippert et al. [2001].

The fundamental constituent of an ANN is the neuron. This neuron accepts several inputs X, processes them, and produces an output Y. Initially, the inputs X are blended linearly using weights and a constant bias b. The resulting value is then deployed as the argument for the transfer function. The transfer function possesses two key features: it is differentiable and non-decreasing. Commonly used transfer functions include the sigmoid and linear functions. A diagram representing a neuron with four inputs is provided in Figure **3-14** Ahmad et al. [2019].

The ANN parameters are ascertained (or the ANN is trained) by minimizing a loss function. This study's optimization approach is the scaled conjugate gradient backpropagation. This

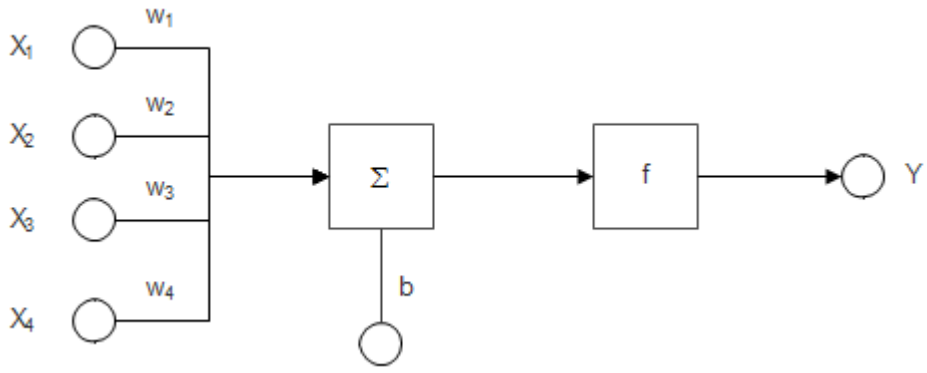

Figure 3-14: ANN configuration

technique displays linear or superlinear convergence and is aptly suited for addressing large-scale problems Ahmad et al. [2019].
Figure **4-36** presents the structure of the proposed ANN, which was developed to estimate process states and disturbances in the reactive distillation column. The network has 16 input neurons, 20 hidden neurons, 4 outer layer neurons, and 4 output neurons. The 16 inputs were selected based on available measurements from the column - temperatures at various stages, FR, BR, and BuLa composition in the bottom. These variables are expected to contain information about the process states and disturbances. This network structure was estimated based on several comparative analyses of different networks considering metrics such as R^2 and performance during training.

The disturbance to be estimated is the LA composition in the feed, which impacts separation performance. Training data was generated by simulating the validated column model at the pilot scale under different feed compositions, ranging $\pm$ 30 % of the nominal LA value.

A feedforward network structure was created with hyperbolic tangent activation functions in the hidden layer and linear activations in the outer layer. The tangent function allows the modeling of nonlinear relationships between the inputs and outputs.

The network was trained using Levenberg-Marquardt backpropagation to minimize errors between network outputs and training targets. Performance was validated on an unseen test dataset. The ANN was trained with a target value of 1200 epochs, gradient value of 1 $\times 10^{-7}$, and the error function was the mean squared error (MSE).

The regressor, a vector with measured signals, was built with two-time temperature delays, manipulated variables, composition, and disturbance. In the output layer are the filtered signal of condenser and reboiler temperatures, the prediction of n-butyl lactate composition, and the disturbance prediction were considered. It consists of the following input variables:

$[T_1(t-1), T_1(t-2), T_2(t-1), T_5(t-1), T_5(t-2), T_7(t-1), T_7(t-2), T_{12}(t-1), T_{12}(t-2), T_{14}(t-1), BR(t-1), BR(t-2), FR(t-1), FR(t-2), xBuLa(t-1), xLA_f(t-1)]$.

where T_1 to T_{14} are the measured temperatures, BR, and FR are the boil-up and feed ratio, respectively, $xBuLa$ is the n-butyl lactate composition in the bottom of the column, and xLA is the composition in the feeding, which normally is considered as an unmeasured disturbance.

In silico data were obtained for building the ANN predictions; the total number of data analyzed was 10348, and 70 % of those data were used for training, and the remaining data were used for validating and testing the ANN (15 % and 15 % respectively). It is important to note that all the data were normalized between 0-1.

The artificial neural network has four output neurons, each representing an estimated parameter:

- Output 1: Condenser temperature (T_2).
- Output 2: Re-boiler temperature (T_{14}).
- Output 3: BuLa composition in the bottom ($xBuLa$).
- Output 4: Disturbance, LA composition in the feed (xLA_f).

The first three outputs represent important internal states of the separation column that indicate its current performance.

The fourth output estimates the composition of LA in the feed, which is treated as an unknown disturbance to the column. Feed composition changes impact product purity, so estimating this disturbance is useful for control and optimization.

These four parameters were selected as outputs because they are difficult or impossible to measure directly. The trained neural network uses the 16 available measurements at its input to infer these important unmeasured states and disturbances.

A was mentioned, a script code was developed, and the Matlab Toolbox â€œnewfftâ€ was used for building a feed-forward back propagation neural network. Neurons in the inner and outer layers use a hyperbolic tangent (tansig) activation function. The output neuron uses a linear activation function (purelin). The Levenberg-Marquardt backpropagation (using the â€˜trainmlâ€™) and the Gradient descent with momentum weight and bias (using the â€˜learngdmâ€™) methods were used for training and learning functions, respectively. Finally, the MSE was used as a performance index.

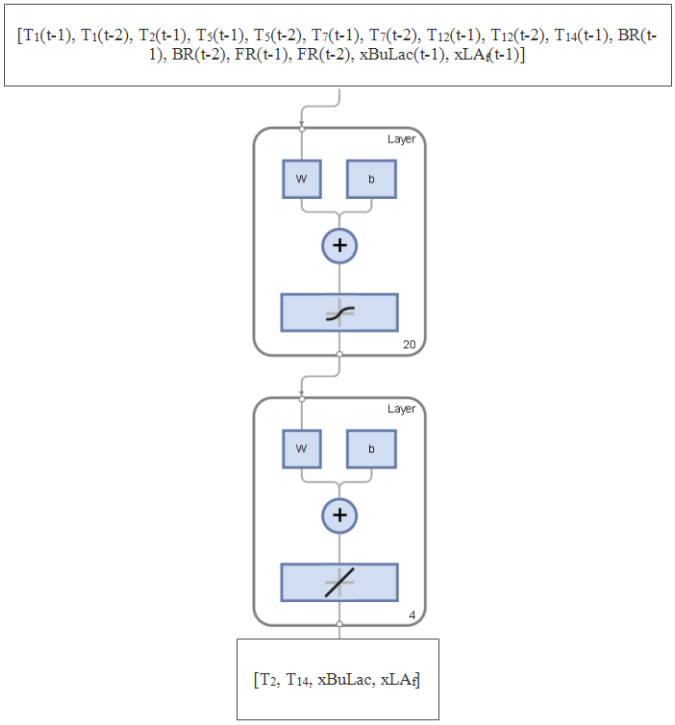

Figure 3-15: ANN configuration

3.5.5. Control proposal

Figure **3-16** represents the control strategy in the reboiler and condenser to control the temperatures in the aforementioned equipment by manipulating the boil up-ratio and feed ratio, respectively. The RGA and SVD were applied to the linearized process model to guide input-output pairings. The FR exhibits strong dynamic coupling with T2, while BR is strongly coupled to T14.

The condenser and reboiler temperatures are critical variables impacting product purity. The FR and BR effectively manipulate these temperatures, thereby controlling the separation performance.

FR adjusts the column feed rate and split between lactic acid and n-butanol, directly influencing the overhead condenser duty. BR regulates the reboiler heat input to the column bottoms. Together, these mass and energy flows enable control of the distillate and bottom composition.

The selected input-output pairings diagonalize the system interactions to avoid instability from loop interactions. The RGA and SVD analysis, therefore, justifies the selection of these manipulated and controlled variables.

Figure **3-17** shows the proposed LMPC, and NMPC control considering disturbance and noise. Similarly, the state estimation and perturbation proposal is presented using ANN to filter noise from measured variables, estimate the unmeasured disturbance (LA composition in the feed), and estimate the composition of BuLa as a bottom product of the column. For the disturbance, with the estimation by ANN, the objective is to pass from an unmeasured disturbance (UD) to a measured disturbance (MD). Therefore, based on the model, it is possible to identify a linear model of the disturbance and use it within the structure of the MPC control.

Performance indices will be used to compare control strategies such as 'The Integral Time Absolute Error' (ITAE), which is defined as:

$$ITAE = \int_0^\infty t \cdot |e(t)|\, dt \tag{3-75}$$

where $e(t)$ is the error signal at time t, which is the difference between the desired and actual outputs.

And 'The Integral Time Squared Error' (ITSE) is another performance index, defined as:

$$ITSE = \int_0^\infty t \cdot e(t)^2\, dt \tag{3-76}$$

The ITSE emphasizes reducing large errors that persist for a long time because the error is squared. This chapter shows the methodology associated with the control proposal (*in silico*) and status estimation for the reactive distillation system at the pilot plant scale. Based on the information provided, it is hoped that the advanced control strategy, together with the estimate, will generate an appropriate proposal for the above system.

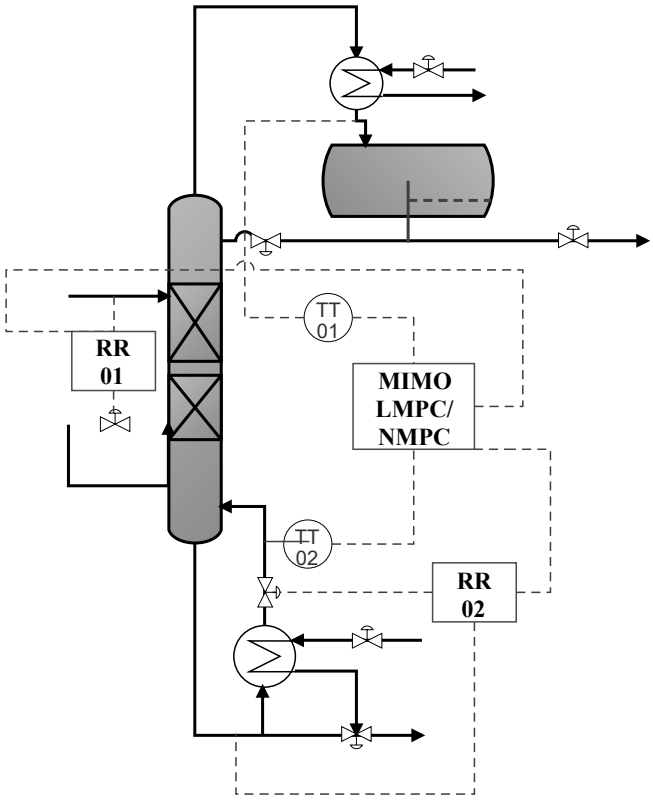

Figure 3-16: Advanced control proposal to produce n-butyl lactate at pilot plant scale, comparison between LMPC and NMPC.

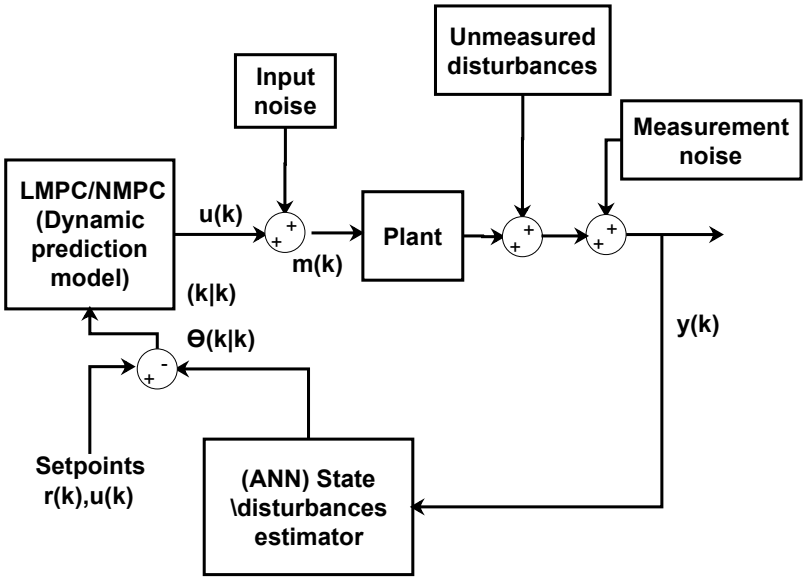

Figure 3-17: Scheme of the advanced control proposal to produce n-butyl lactate using a model of an RDC at pilot-plant scale.

4 Results and Discussion

4.1. Isobaric Vapor-Liquid Equilibrium for the Binary Mixture of 1-butyl lactate + 1-butanol at 1 and 5 kPa

Tables **4-1** and **4-2** present the composition of the liquid and vapor phases, experimental temperature, and pressure at 1-5 kPa. The Raoult extended equation (Equation 3-50) was used to calculate the activity coefficients, and, considering the low pressure (1-5 kPa), an ideal behavior in the vapor phase was assumed. The mixture of alcohol + ester presents no azeotrope. Finally, this section is organized as follows: first, the obtained experimental values are presented; second, the thermodynamic consistency of the experimental data was performed; and third, it is presented a model parameter regression with the obtained experimental data.

4.1.1. VLE Experimental Data

The experimental data (T, x, y) (Table **4-1** and Table **4-2**) were correlated using the non-linear regression method available in Aspen Plus® V9. NRTL and UNIQUAC activity models were used to adjust the binary parameters. The objective function was the maximum likelihood with the initialization method of weighted least squares, and the convergence algorithm was the Deming algorithm with a tolerance of 1×10^{-6}.

Table 4-1: 1-butyl lactate (1) + 1-butanol (2) at 1 kPa

$T^b[K]$	x_1^c	y_1^d	γ_1^e	γ_2^f
300.080	0.000	0.000	0.000	0.970
301.330	0.084	0.018	2.348	0.953
301.480	0.082	0.017	2.310	0.941
302.240	0.112	0.023	2.154	0.918
302.400	0.117	0.022	1.949	0.913
302.580	0.152	0.027	1.825	0.934
302.460	0.193	0.033	1.633	0.919
303.910	0.262	0.038	1.370	0.968
304.290	0.266	0.036	1.220	0.951
305.720	0.355	0.049	1.140	0.968
306.080	0.380	0.048	1.011	0.985
307.210	0.430	0.052	0.898	0.989
308.760	0.493	0.069	0.935	0.984
310.900	0.585	0.079	0.788	1.034
311.750	0.620	0.096	0.852	1.050
313.190	0.654	0.105	0.798	1.043
314.390	0.691	0.117	0.782	1.066
338.130	0.988	0.878	0.992	1.009
338.470	0.991	0.890	0.984	1.203
341.420	1.000	1.000	0.933	0.000

[a]Standard uncertainties u of p, T, x and y are $u(p) = 0{,}01$ kPa, $u(T) = 0{,}01$ K, and $u(x) = u(y) = 0{,}001$. [b]Equilibrium temperature. [c]Liquid-phase mole fraction of 1-butyl lactate. [d]Vapor-phase mole fraction of 1-butyl lactate. [e]Activity coeï¬¬$ciento f 1 - butyllactate$. [f]Activity coeï¬¬$ciento f 1 - butanol$.

Table 4-2: 1-butyl lactate (1) + 1-butanol (2) at 5 kPa

$T^b[K]$	x_1^c	y_1^d	γ_1^e	γ_2^f
373.490	1.000	1.000	0.977	0.000
357.020	0.901	0.392	0.911	1.172
354.460	0.879	0.332	0.899	1.182
342.890	0.703	0.131	0.804	1.097
341.790	0.687	0.117	0.780	1.119
336.740	0.556	0.073	0.796	1.074
336.700	0.553	0.075	0.814	1.067
333.840	0.462	0.053	0.809	1.058
333.340	0.456	0.051	0.812	1.076
331.260	0.359	0.038	0.863	1.037
330.850	0.352	0.038	0.902	1.049
327.110	0.118	0.016	1.396	0.972
326.910	0.118	0.017	1.520	0.982
324.440	0.000	0.000	0.000	1.016

[a]Standard uncertainties u of p, T, x and y are $u(p) = 0{,}01$ kPa, $u(T) = 0{,}01$ K, and $u(x) = u(y) = 0{,}001$. [b]Equilibrium temperature. [c]Liquid-phase mole fraction of 1-butyl lactate. [d]Vapor-phase mole fraction of 1-butyl lactate. [e]Activity coefficient of 1-butanol. [f]Activity coefficient of butyl L-lactate.

Using the γ-ϕ model (Equation 3-50), the activity coefficients may be calculated for the VLE data [Smith, 1950]. Due to low pressure (1 and 5 kPa) and the similar nature of the substances, the Poynting factor is assumed as 1, and the vapor phase is ideal. The Antoine constants for obtaining the n-butanol and n-butyl lactate vapor pressures were taken from literature and the Aspen plus V9 database. The Antoine equation parameters are reported in Table **3-4**.

The VLE data was obtained for the binary system of n-butyl lactate (1) + n-butanol () at two pressures - 1 kPa and 5 kPa. The measurements included bubble point temperature, liquid phase composition, vapor phase composition, and activity coefficients.

Examination of the data shows expected trends for a low relative volatility system. Significant changes in liquid composition are required at both pressures to see appreciable changes in vapor composition and temperature. This indicates azeotrope formation is likely [Michelsen, 1992].

The activity coefficient data indicates moderately non-ideal behavior, with the highest deviations from ideality occurring in the center of the composition range. This suggests the presence of maxima in the Gibbs excess energy and supports the likelihood of azeotrope formation at higher pressures.

Comparison of the 1 kPa and 5 kPa data shows the impact of pressure on relative volatility and ideality. The activity coefficients show lower deviations at the higher 5 kPa pressure. Additionally, the 5 kPa isotherms have a more pronounced composition range with $\frac{d(y_1)}{d(x_1)} > 1$, indicating improved relative volatility.

4.1.2. NRTL and UNIQUAC Parameters Regression

The default Equations (3-40 to 3-42) were used in Aspen PlusÂ® V9 with the relation for the NRTL model with regression parameters. Three α values were evaluated, which generated three NRTL models (NRTL1, NRTL2, and NRTL3). The α values were selected based on reports for esterification mixtures [Smith J. Van Ness and H. Abbott, 2009]. For this case, the best results (Table **4-3**) were for the model NRTL2 with $\alpha = 0{,}3$, representing the degree of interaction between the two liquids in a binary mixture.

Table **4-3** reports the binary interaction parameters A_{12}, A_{21}, B_{12} and B_{21} of the models obtained from the correlation of experimental VLE data for the system n-butanol (1) â€“ n-butyl L-lactate (2) with NRTL and UNIQUAC activity models, considering the set of studied pressures (1, 5 and 101.325 kPa). Different values of the α_{12} parameter were estimated in the NRTL equation. The root-mean-square deviations (rmsds) of the temperature (T), vapor-phase mole fraction (y_1), and the regressed parameters are listed in Table **4-3**, where the lowest rmsds is for NRTL2 (α=0.3). The rmsds are expressed in Equations. 4-1 and 4-2.

$$rmsd(T) = \left(\sum_{i=1}^{N} \frac{(T_i^{Calc} - T_i^{Exp})^2}{N} \right)^{0,5} \tag{4-1}$$

$$rmsd(T) = \left(\sum_{i=1}^{N} \frac{(y_i^{Calc} - y_i^{Exp})^2}{N} \right)^{0,5} \tag{4-2}$$

Table 4-3: Binary interaction parameters for the System n-butanol (1) + n-butyl L-lactate (2) obtained with data sets presented in this work at 1, 5 kPa

Model	**Parameters**					**rmsds**			
	$\mathbf{A}_{12}$	$\mathbf{A}_{21}$	$\mathbf{B}_{12}[K]$	$\mathbf{B}_{21}[K]$	α	**1 kPa**		**5 kPa**	
						T [K]	**y2**	**T [K]**	**y2**
NRTL1	-0.476	0.409	-20.483	37.68	0.1	0.93	0.002	0.97	0.005
NRTL2	-0.726	0.792	134.427	-158.781	0.3	0.94	0.002	0.99	0.005
NRTL3	-0.273	0.189	10.499	13.292	0.47	0.94	0.002	0.98	0.005
UNIQUAC	-0.93	0.735	190.054	-150.661	—	0.96	0.002	0.99	0.005

Figure **4-1** and Figure **4-2** present the T-x-y diagram obtained for the system under consideration. Both figures evidence a good agreement between experimental data using the NRTL model.

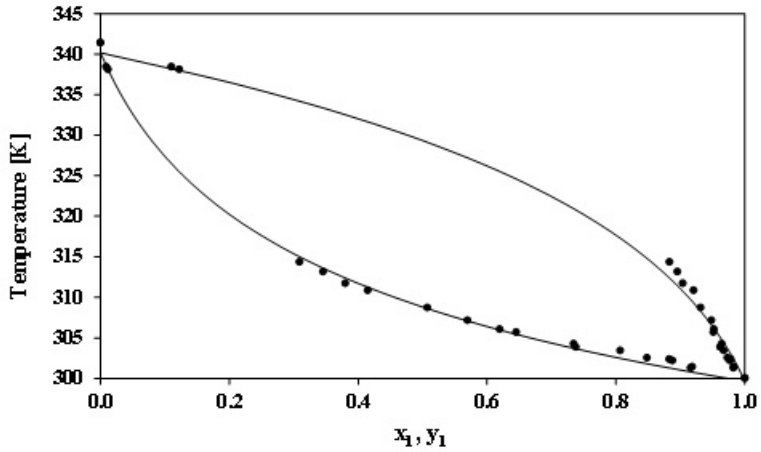

Figure 4-1: T-x-y diagram for the system 1-butanol (1) + butyl L-lactate (2) at 1.0 kPa. (•) experimental data and (-) NRTL2 calculations made in this work (α=0.3).

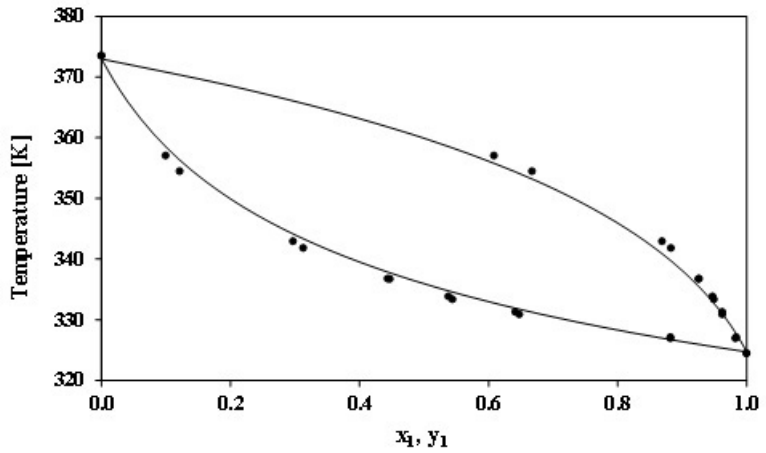

Figure 4-2: T-x-y diagram for the system 1-butanol (1) + butyl L-lactate (2) at 5.0 kPa. (•) experimental data and (-) NRTL2 calculations made in this work (α=0.3).

Figure **4-3** compares the performance of the parameters obtained in this work with the experimental data of VLE reported by Peña-Tejedor et al. [2005a] at 101.325 kPa.

Figure **4-3** allows concluding that the obtained parameters present a good fitting at the three different pressures (101.325, 5, and 1 kPa), which means that a wide pressure interval can be predicted for this mixture. The mentioned prediction could be used in reactive distillation studies and process design to avoid the oligomerization conditions in the system due to high temperatures, as discussed previously.

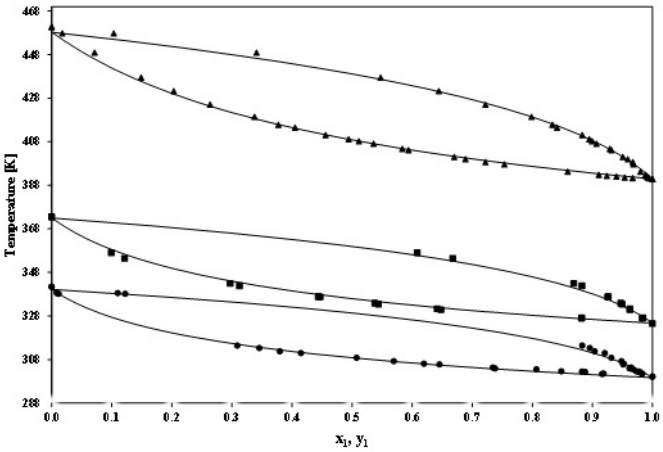

Figure 4-3: T-x-y diagram for the system 1-butanol (1) + butyl L-lactate (2). (-) NRTL2 calculations made in this work (α=0.3), at (•) 1.0 kPa (this work), (■) 5.0 kPa (this work) and (▲) 101.325 kPa Peña-Tejedor et al. [2005a].

In Figure **4-4**, the residuals of the equilibrium temperature (T) and vapor-phase mole fraction (y_2) are plotted for the NRTL model. The deviations are uniformly distributed around zero and less than 2.0 and 0.01 for temperature and vapor-phase mole fraction, respectively.

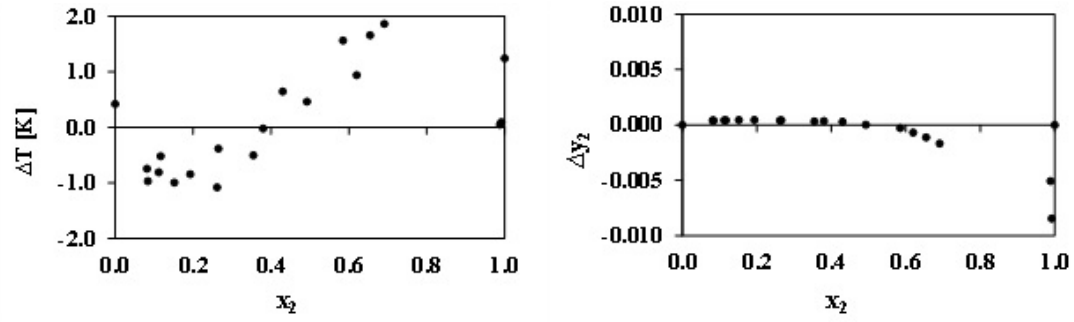

Figure 4-4: Residuals of equilibrium temperature (T) and vapor-phase mole fraction (y_2) calculated by the NRTL2 (α=0.3) model at 1 kPa.

Figure **4-5** shows the percentage differences between butyl L-lactate K-values from the model and data plotted against the liquid mole fraction of butyl L-lactate at different pressure conditions. The error was compared against the model and experimental data reported by Peña-Tejedor et al. [2005a] at 101.325 kPa. The obtained percentage error shows a 55 % deviation at 1 kPa in the lowest liquid mole fraction region due to the small deviation in the liquid phase in the prediction model. However, this result agrees with the results presented by Peña-Tejedor et al. [2005a], where the percentage error decreases. The results in Table **4-3** and Figure **4-4** show that the model allows predicting temperature and vapor mole fraction with a low rmsd.

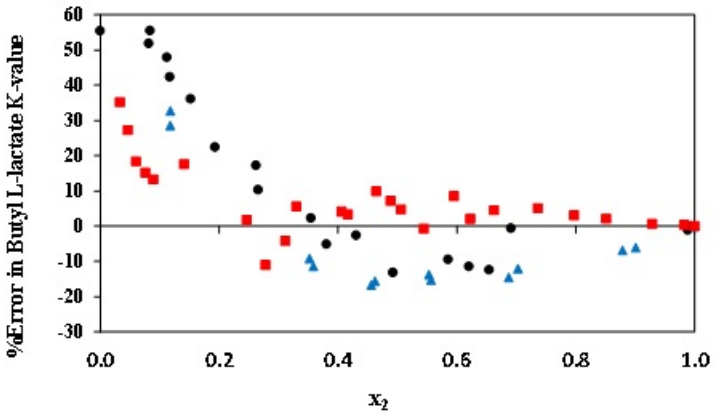

Figure 4-5: Percentage errors of model K-values of butyl L-lactate at (●) 1.0 kPa (this work), (▲) 5.0 kPa (this work) and (■) 101.325 kPa [9].

4.1.3. Thermodynamic Consistency

According to the components' nature and the system's ideal behavior, Van Ness and Fredenslund's methods Marcilla et al. [2013], Zumalacarregui [2018] were chosen for thermodynamic consistency. As a result of the research by Xu et al. [2020], Eqs. 4-3 and 4-4 represent the Van Ness point-by-point test, referring to the mean percentual relative and absolute deviation between experimental data and calculated values for pressure and composition, respectively.

$$\triangle P_1 = \frac{1}{N}\sum_{i=1}^{N} 100 \left| \frac{P_{1,i}^{exp} - P_{1,i}^{calc}}{P_{1,i}^{exp}} \right| \tag{4-3}$$

$$\triangle y_1 = \frac{1}{N}\sum_{i=1}^{N} 100 \left| y_{i,1}^{exp} - y_{i,1}^{calc} \right| \tag{4-4}$$

The term N represents the number of experimental data, $y_{1,i}^{exp}$ and $P_{1,i}^{exp}$ the vapor fraction and pressure, respectively, and $y_{1,i}^{calc}$ and $P_{1,i}^{calc}$ are the calculated vapor fraction and pressure, respectively. To achieve consistency, the values of $\triangle y_1$ and $\triangle P_1$ must be less than 1. Table **4-4** presents the Van Ness consistency test for NRTL and UNIQUAC models, and all of the samples $\triangle y_1$ and $\triangle P_1$ had values less than 1, which means the VLE data passed the test.

The Fredenslund test requires evaluating the Legendre orthogonal polynomials Marcilla et al. [2013] (Eq 4-5).

$$g^E = \frac{\triangle G^E}{RT} = x_1 x_2 \sum_{k=1}^{n} a_k L_k(x_1) \tag{4-5}$$

The term a_k refers to the coefficients of order k, and $L_k(x_1)$ represents the Legendre polynomials where $L_0(x_1) = 1$ e $L_1(x_1) = x_1$. (Eq. 4-6):

$$L_k(x_1) = \frac{1}{k}\left[(2k-1)(2x_1-1)L_{k-1}(x_1) - (k-1)L_{k-2}(x_1)\right] \tag{4-6}$$

Eq. 4-7 describes the condition to pass the test:

$$\sum_{i=1}^{n} \frac{|y_i^{calc} - y_i^{exp}|}{n} \leq 0{,}01 \tag{4-7}$$

Finally, the value of the Fredenslund test was 0.00097 for 1 kPa and 0.0034 for 5 kPa, and both met the constraint of Eq 4-7. Tables **4-4** and **4-5** present the calculated values of Van Ness and Fredenslund tests for a pressure system of 1 kPa and 5 kPa, which allow concluding that the obtained data was reliable.

Table 4-4: Van Ness Test for Thermodynamic Consistency

Preassure	**Model**	$\triangle P_1$	$\triangle y_1$	**Results**
1 kPa	NRTL1($\alpha = 0{,}1$)	0.12	0.111	Passed
	NRTL2($\alpha = 0{,}3$)	0.12	0.108	Passed
	NRTL3($\alpha = 0{,}47$)	0.12	0.104	Passed
	UNIQUAC	0.12	0.097	Passed
5 kPa	NRTL1($\alpha = 0{,}1$)	0.16	0.233	Passed
	NRTL2($\alpha = 0{,}3$)	0.16	0.220	Passed
	NRTL3($\alpha = 0{,}47$)	0.16	0.225	Passed
	UNIQUAC	0.16	0.218	Passed

Table 4-5: Fredenslund Test for Thermodynamic Consistency

Preassure	**Method**	$\triangle y_1$	**Resulst**
1 kPa	Fredenslund	0.00097	passed
5 kPa	Fredenslund	0.0034	passed

4.1.4. Conclusions of the section

New isobaric experimental data of the liquid-vapor equilibrium were obtained for the n-butanol + butyl L-lactate system at 1 and 5 kPa. The experimental data presented thermodynamic consistency according to the Van Ness and Fredenslund tests. Nonlinear regression was performed to find the binary interaction parameters for the UNIQUAC and NRTL activity models. These data provide new thermodynamic information for further studies related to the process synthesis of the analyzed system. This new set of parameters makes predicting VLE for the n-butanol + butyl L-lactate system at a wide range of pressures possible. Besides, these data can be used for future studies in which the oligomerization reaction of lactic acid and lactate must be avoided by operating at low pressures.

4.2. Reactive and non-reactive residue curve maps analysis to produce Butyl Lactate by catalytic distillation

This section presents the RCM and RRCM resulting from integrating the models explained in Section 3.2 for the butyl lactate synthesis system. The studied system is a mixture of four components (1-butanol - lactic acid - butyl lactate - water) that gives rise to a reversible liquid phase reaction catalyzed by an ion exchange resin. Section 4.2.1 presents the RCM for the ternary and quaternary systems and the topology consistency analysis. Section 4.2.2 presents the RRCM for the quaternary system, evaluating different values of the Damhköler number.

4.2.1. Analysis of the non-reactive curve maps

RCM is obtained by solving Eq. 3-1 for various starting liquid compositions. The resulting RCM are shown in ternary and quaternary diagrams.

VLLE Ternary residue curve diagrams

Figure **4-6** presents the RCM in ternary diagrams for the system at 101.325 kPa. In these diagrams, each vertex is a pure component of the system. The system exhibits one region of partial miscibility and two binary azeotropes at 101.325 kPa: A heterogeneous butanol-water azeotrope ($x_{BuOH} = 0.236$, $x_w = 0.765$, T= 366.7 K) and a homogeneous lactic acid - butyl lactate azeotrope (x_{BuLA}= 0.114, x_{La}= 0.886, T= 447.7 K). The butanol-water azeotrope Iwakabe and Kosuge [2001], Venimadhavan et al. [1994] is known in the literature, but the lactic acid-butyl lactate azeotrope has not yet been determined experimentally. The system contains two stable nodes (pure components butyl lactate and lactic acid): One unstable node (binary butanol-water azeotrope) and three saddle nodes (pure components butanol, water, and the binary azeotrope butyl lactate - lactic acid).

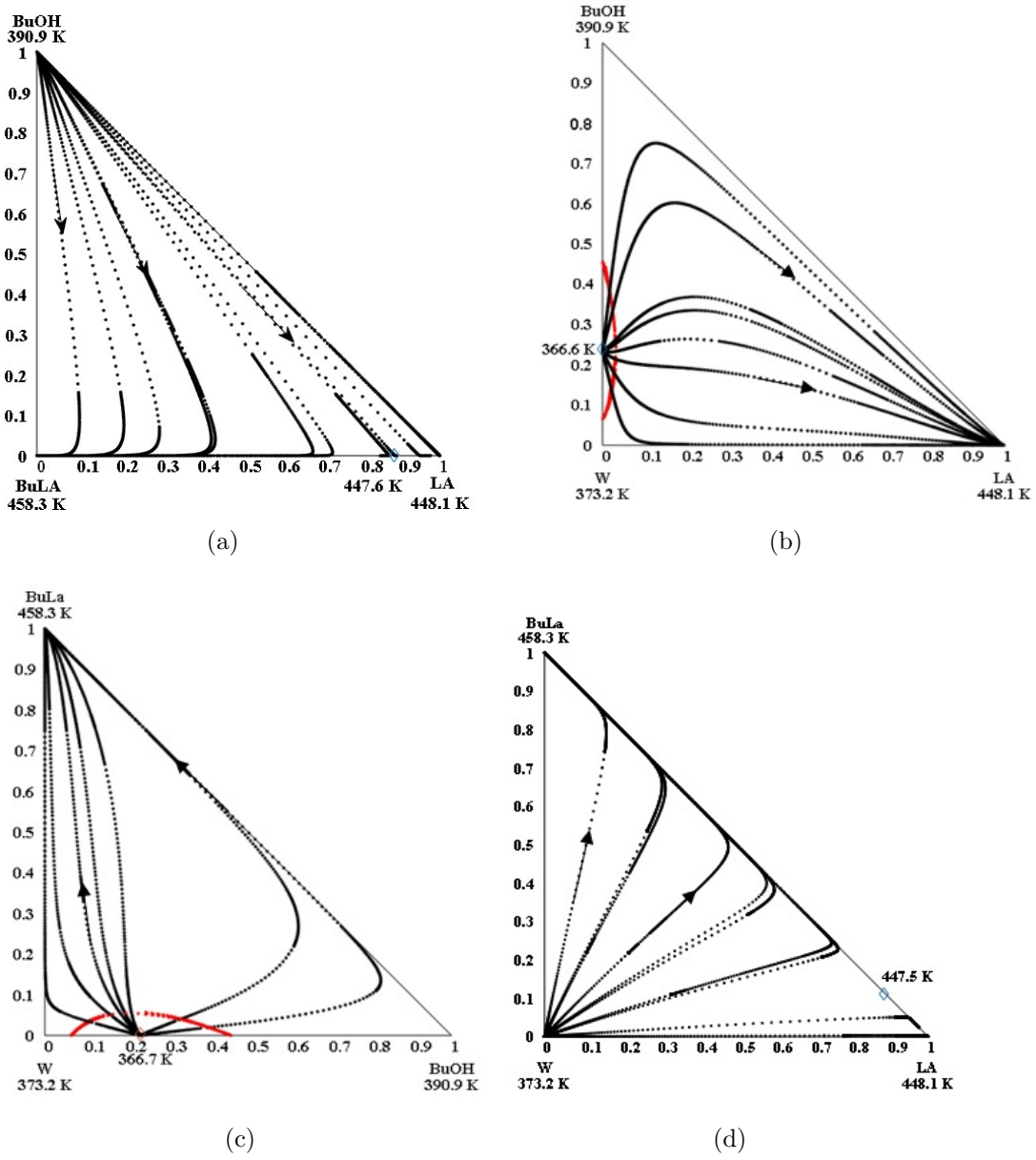

Figure 4-6: Ternary residue curve maps (non-reactive VLLE at 101.325 kPa) (• • •) Binodal curve.: (a)n-butanol, lactic acid, n-butyl lactate; (b) n-butanol, lactic acid, water; (c) n-butanol, n-butyl lactate, water, and (d) lactic acid, n-butyl lactate, water.

Due to the autocatalytic secondary reaction (Lactic Acid oligomerization) favored by temperature, this reaction must be carried out at low pressures to avoid high temperatures that decrease the selectivity of the process Asthana et al. [2006]. For this reason, RCM at low pressure (5 kPa) was evaluated.

Figure **4-7** depicts the RCM in ternary diagrams for the system at 5 kPa, exhibiting a binary azeotrope and one region of partial miscibility, as at 101.325 kPa. This mixture has a heterogeneous n-butanol-Water binary azeotrope (x_{BuOH}= 0.153, x_w= 0.848, T=303.0 K). The system contains one stable node (Lactic Acid), one unstable node (binary n-butanol-Water azeotrope), and three saddle nodes (pure components n-butanol, Water, and Lactic Acid).

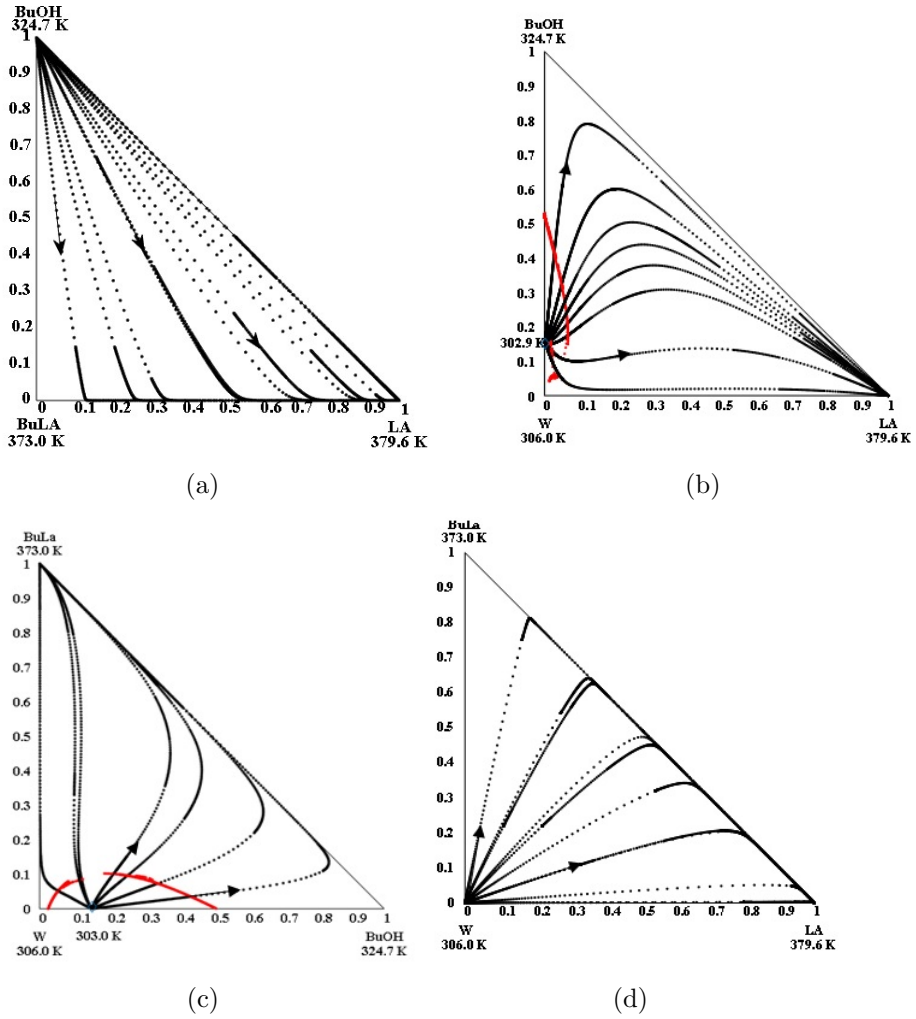

Figure 4-7: Ternary residue curve maps (non-reactive VLLE at 5 kPa). (●●●) Binodal curve. (a)n-butanol, lactic acid, n-butyl lactate; (b) n-butanol, lactic acid, water; (c) n-butanol, n-butyl lactate, water; and (d) lactic acid, n-butyl lactate, water.

In the synthesis of Butyl Lactate, a high conversion of Lactic Acid is expected; therefore, the Butyl Lactate - Water - n- butanol subsystem makes it possible to identify the nodes present in operation (Figures **4-6**c and **4-7**c). A stable node (Butyl Lactate) and an unstable node (n-butanol-Water binary azeotrope) are observed. For the distillation operation, these nodes imply that the bottom stream will be mostly Butyl Lactate, and the top vapor of the column will present a composition close to the heterogeneous azeotrope.

VLLE quaternary residue curve diagrams

Figure **4-8** presents the RCM in quaternary diagrams at two different pressures. The bottom product can be Butyl Lactate or Lactic Acid at the pressure condition of 101.325 kPa (two distillation zones) and Lactic Acid at 5 kPa. The top product will be the heterogeneous azeotrope at 101.325 kPa and 5 kPa. Butyl Lactate can be obtained as a bottom product considering these differences, the expected high conversion of Lactic Acid in the process and an excess of alcohol to favor the conversion.

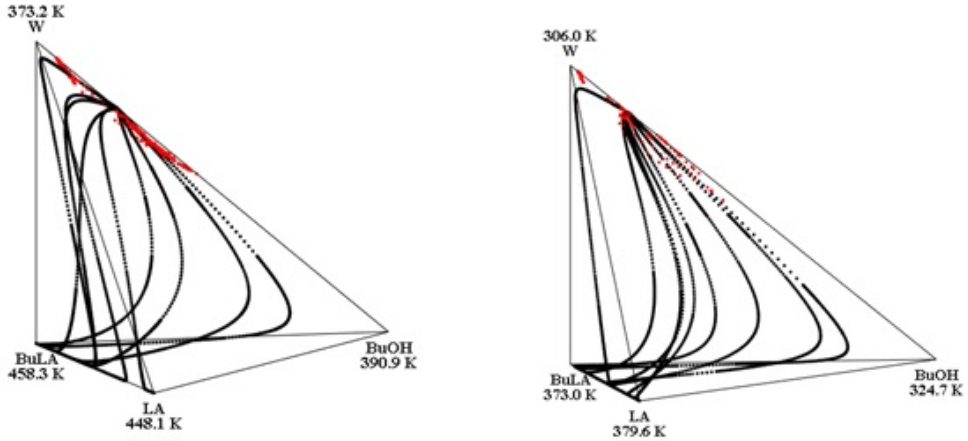

(a) (b)

Figure 4-8: Quaternary Residue curve maps (non-reactive VLLE) at (a) 101.325 and (b) 5 kPa. (• • •) Binodal curve.

Validation of topological structure of the calculated nonreactive maps

The topological consistency analysis by Kiva et al. [2003] was performed for the residue curve maps. The general expression of this rule for n components is presented in Eq. 4-8.

$$\sum_{K=1}^{n} 2^K \left(N_K^+ + S_K^+ - N_K^- + S_K^-\right) = 1 + (-1)^{n-1} \tag{4-8}$$

where N_K is the number of nodes that contain k number of components, S_K is the number of saddle nodes that contain k numbers of components, and n is the number of components. The corresponding positive and negative indices are explained by Kiva et al. [2003] and are based on the location of the node and the direction of increase of boiling temperature of each node. It depends on the direction in which the curve approaches and departs from the saddle point or the direction of the curve at the stable or unstable node point.

The topological consistency for ternary systems was evaluated by simplifying the azeotropic ruleMartínez et al. [2020a] (Eq.4-9). The different node indices identified in the ternary mixtures are listed in Tables **4-6**, **4-7**, **4-8**, and **4-9**.

$$2N_3 + N_2 + N_1 = 2S_3 + S_2 + 2 \tag{4-9}$$

Table 4-6: Topological consistency for the ternary system 1-butanol, butyl lactate, water.

Preassure	**101.325 kPa**		**5 kPa**	
Singular Point	**Type**	**Nomination**	**Type**	**Nomination**
Pure components				
1-Butanol	Saddle	S_1	Saddle	S_1
Butyl Lactate	Stable node	N_1	Stable node	N_1
Water	Saddle	S_1	Saddle	S_1
Binary azeotropes				
1-Butanol-Water	Unstable node	N_2	Unstable node	N_2
Azeotropic rule				
$2N_3 + N_2 + N_1$		2		2
$2S_3 + S_2 + 2$		2		2

Table 4-7: Topological consistency for the ternary system lactic acid, butyl lactate, water.

Preassure	**101.325 kPa**		**5 kPa**	
Singular Point	**Type**	**Nomination**	**Type**	**Nomination**
Pure components				
Lactic Acid	Stable node	N_1	Stable node	N_1
Butyl Lactate	Stable node	N_1	Saddle	S_1
Water	Unstable node	N_1	Unstable node	N_1
Binary azeotropes				
Lactic Acid - Butyl Lactate	Saddle	S_2	NA	NA
Azeotropic rule				
$2N_3 + N_2 + N_1$		3		2
$2S_3 + S_2 + 2$		3		2

Table 4-8: Topological consistency for the ternary system lactic acid, 1-butanol, water.

Preassure	**101.325 kPa**		**5 kPa**	
Singular Point	**Type**	**Nomination**	**Type**	**Nomination**
Pure components				
Lactic Acid	Stable node	N_1	Stable node	N_1
1-Butanol	Saddle	S_1	Saddle	S_1
Water	Saddle	S_1	Saddle	S_1
Binary azeotropes				
1-Butanol - Water	Unstable node	N_2	Unstable node	N_2
Azeotropic rule				
$2N_3 + N_2 + N_1$		2		2
$2S_3 + S_2 + 2$		2		2

Table 4-9: Topological consistency for the ternary system lactic acid, 1-butanol, butyl lactate.

Preassure	**101.325 kPa**		**5 kPa**	
Singular Point	**Type**	**Nomination**	**Type**	**Nomination**
Pure components				
Lactic Acid	Stable node	N_1	Stable node	N_1
1-Butanol	Unstable node	N_1	Unstable node	N_1
Butyl Lactate	Stable node	N_1	Saddle	S_1
Binary azeotropes				
Lactic Acid - Butyl Lactate	Saddle	S_2	NA	NA
Azeotropic rule				
$2N_3 + N_2 + N_1$		3		2
$2S_3 + S_2 + 2$		3		2

The topological consistency for quaternary systems was evaluated using Eq. 4-10. The different node indices identified in the quaternary mixtures are listed in Table **4-10**.

$$8\left(N_3^+ + S_3^+ - N_3^- - S_3^-\right) + 4\left(N_2^+ + S_2^+ - N_2^- - S_2^-\right) + 2\left(N_1^+ + S_1^+ - N_1^- - S_1^-\right) = 0 \quad (4\text{-}10)$$

Table 4-10: Topological consistency for quaternary system.

Preassure	**101.325 kPa**			**5 kPa**		
Singular Point	**Type**	**TI**	**Nomination**	**Type**	**TI**	**Nomination**
Pure components						
1-Butanol	Saddle	-1	S_1-	Saddle	-1	S_1-
Water	Saddle	-1	S_1-	Saddle	-1	S_1-
Butyl Lactate	Stable node	-1	N_1-	Saddle	-1	S_1+
Lactid Acid	Stable node	-1	N_1-	Stable node	-1	N_1-
Binary azeotropes						
1-Butanol - Water	Unstable node	1	N_2+	Unstable node	1	N_2+
Lactic acid - Butyl Lactate	Saddle	1	S_2+	NA	NA	NA
Azeotropic rule						
$8\left(N_3^+ + S_3^+ - N_3^- - S_3^-\right)$		0			0	
$4\left(N_2^+ + S_2^+ - N_2^- - S_2^-\right)$		8			-4	
$2\left(N_1^+ + S_1^+ - N_1^- - S_1^-\right)$		-8			4	

Figure **4-9** is the unfolding of the ternary diagrams at 101.325 kPa that allows evaluating the nodes present in the system for the topological analysis. The azeotropic rule is fulfilled in all the studied cases, which evidences that the thermodynamic model is consistent and feasible.

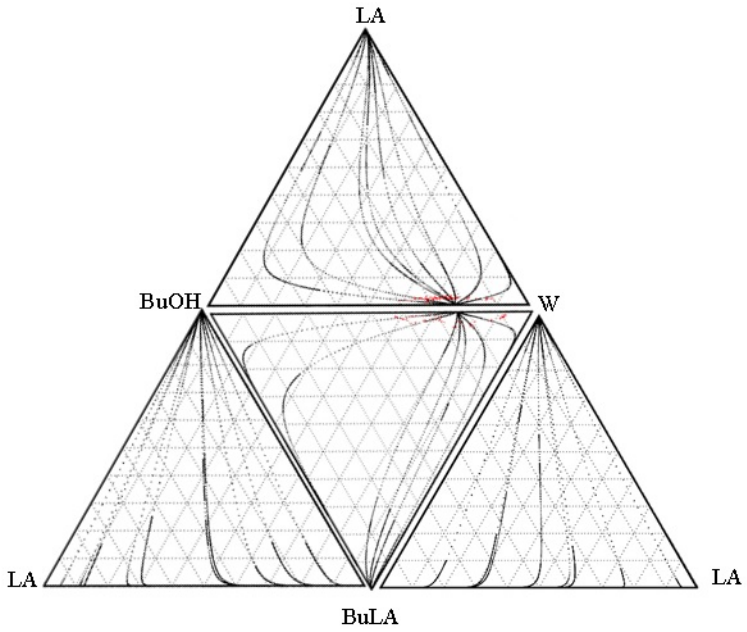

Figure 4-9: Non-reactive residue curves maps for the quaternary system lactic acid - 1-butanol - butyl lactate - water at 101.325 kPa. Unfold into the corresponding ternary diagrams.

4.2.2. Analysis of the reactive curve maps

This subsection presents the analysis of the residue reactive curve maps. The Damköhler number is used to evaluate the kinetically controlled model at different ratios of reaction rate and evaporation rate. The low values of Da mean a slow reaction rate compared with the evaporation rate, whereas high values of Da correspond to fast reaction rates Walpot [2011].

VLLE reactive curve maps at 101.325 kPa

A set of VLLE reactive curve maps at different Da values was constructed to determine the effect of the kinetic expression in the separation process. The Da values move from non-reactive conditions (i.e., Da=0) to kinetically controlled regimes ($i.eDa \rightarrow \infty$), based on the approximation performed by Cho et al. [2012], Martínez et al. [2020a]. Figure **4-10** presents the RRCM for the (a) quaternary system and (b) in transformed variables (i.e., Eqs. 3-2, 3-4 and 3-5), as obtained for $Da = 0$. The pure components are in the vertices of the two-dimensional and three-dimensional diagrams, which exhibit only one azeotrope at 366.7 K. The binary azeotrope n-butanol-water is an unstable node ($x_{BuOH} = 0.236$, $x_w = 0.765$).

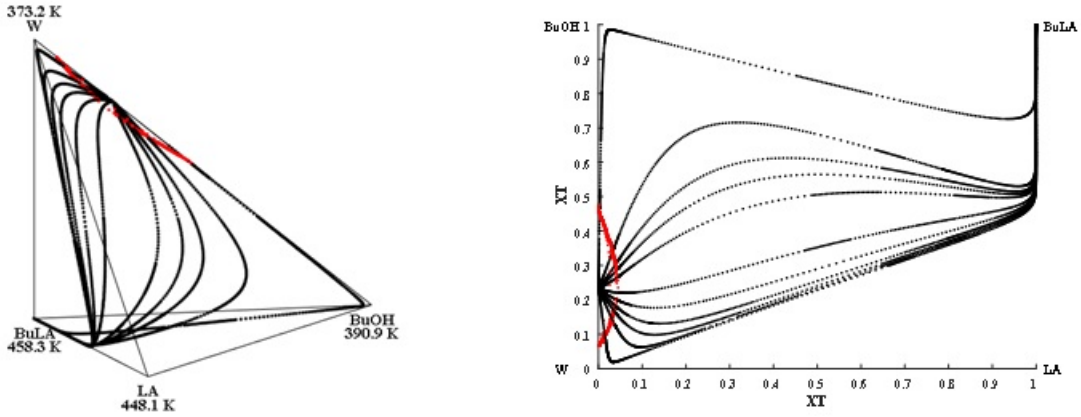

(a) (b)

Figure 4-10: VLLE reactive curve maps at 101.325 kPa and Da=0, a) quaternary system and b) transformed variables. (• • •) Binodal curve.

In Figure **4-11**, a similar approximation is presented but with Da=0.05. Figure **4-10** shows the same unstable and stable nodes. The residue curves change in the direction of increasing boiling temperature and are a function of the kinetic equilibria constant or Da number Okasinski and Doherty [1997].

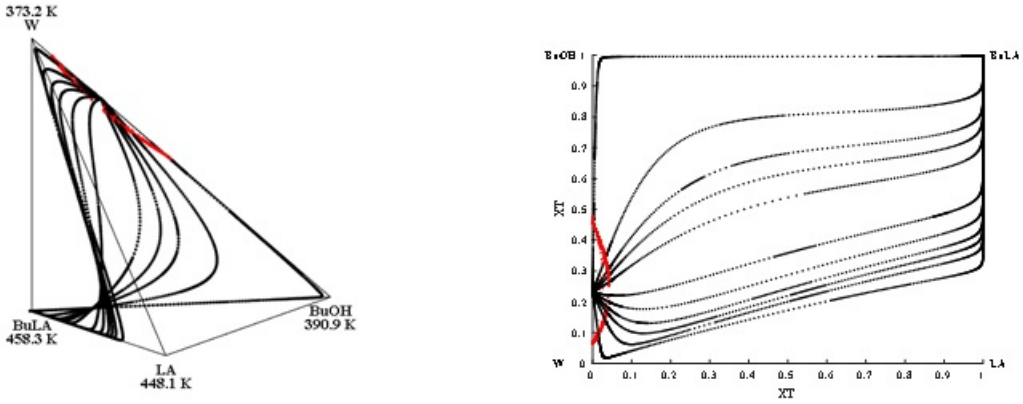

(a) (b)

Figure 4-11: VLLE reactive curve maps at 101.325 kPa and Da=0.05, a) quaternary system and b) transformed variables. (• • •) Binodal curve.

Figure **4-12** shows at Da=0.1 that the stable and unstable nodes are the same as in Figure **4-10** and Figure **4-11** (independently of the starting compositions).

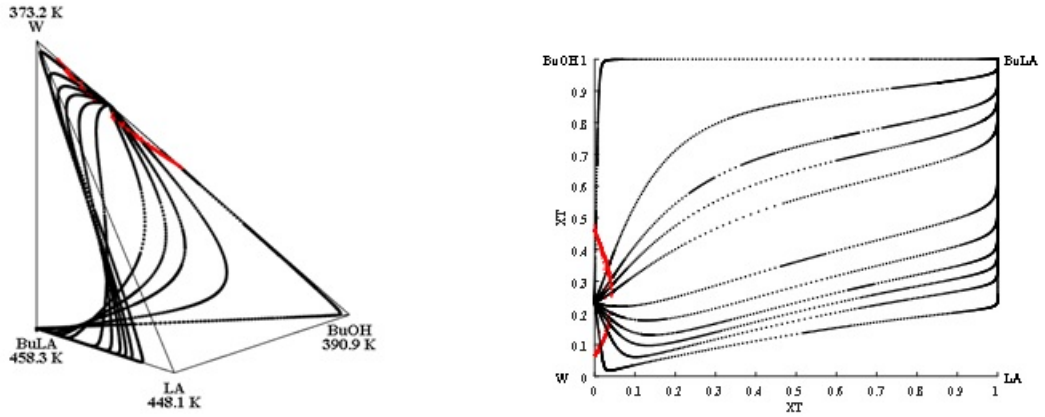

(a) (b)

Figure 4-12: VLLE reactive curve maps at 101.325 kPa and Da=0.1, (a) quaternary system and (b) transformed variables. (• • •) Binodal curve.

However, in Figure **4-13** with Da=2, the saddle-node 1-Butyl Lactate-Lactic Acid (X_{BuLAc}=0.114, X_{LA}=0.886, T=447.5 K) is observed obtaining two distillation regions. This means that operating a reactive distillation process, using a feed with a slight excess of 1-Butanol, could obtain an almost pure Butyl Lactate, as concluded in subsection 4.2.1.

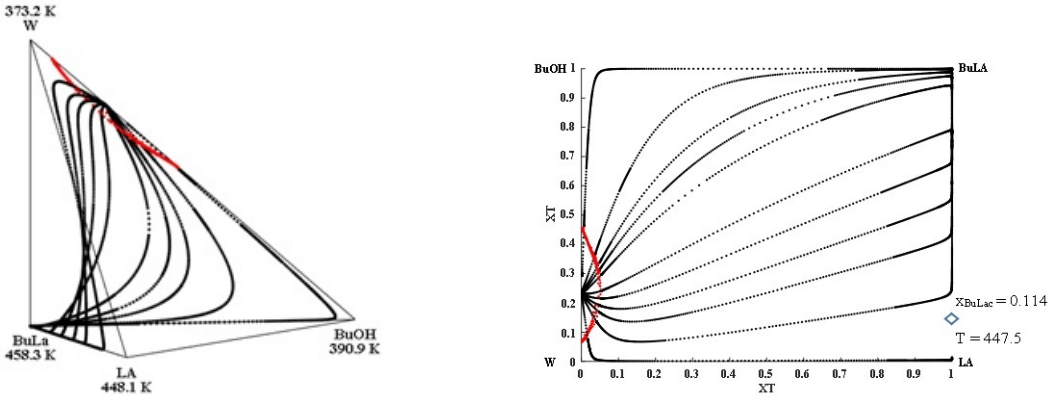

(a) (b)

Figure 4-13: VLLE reactive curve maps at 101.325 kPa and Da=2.0, a) quaternary system and b) transformed variables. (• • •) Binodal curve.

Values of $Da > 2$ produced no changes in the residue curves, and as can be observed, even no reactive azeotropes were formed. This means that with values of $Da \geq 2$, the system is controlled by the kinetic, which agrees with those observed in industrial reactive distillation columns Shah et al. [2012], Asthana et al. [2005].

4.2.3. Conceptual scheme of a preliminary reactive distillation column

The RRCM obtained at $Da = 2$ was used to conceptualize a reactive distillation column. This value was selected because, at this condition, the column operates under kinetically controlled regimes. In Figure **4-14**, the balance of the column is represented by a straight line connecting the stable node (bottom product) and the unstable node (top product). As observed, Butyl Lactate with high purity can be obtained as the bottom product (B), whereas the heterogeneous binary azeotrope is obtained as the top product (D). Indeed, the top product can be condensed and separated in a decanter to remove the aqueous phase and recycle the organic phase to the system, thus favoring the reaction towards the products.

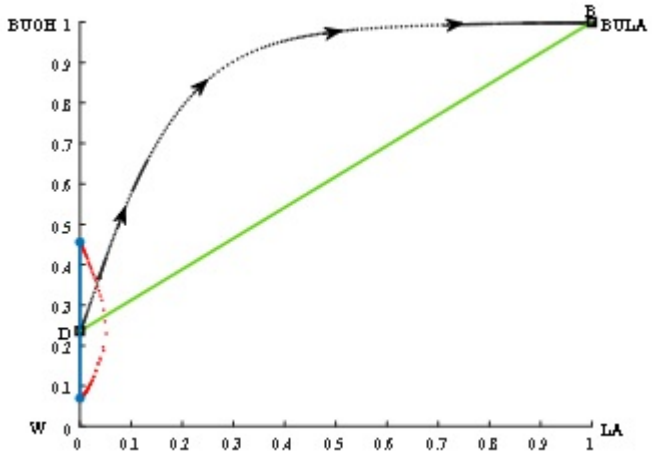

Figure 4-14: RRCM in transformed compositions for a $Da = 2$: Composition profiles. (−) reactive residue curve maps, (• • •) binodal curve, (−) RD material balance and (−) tie line of the distillate product.

The feed Lactic Acid composition was set below 30 %wt. At higher compositions, oligomerization reactions appear, and process design and the construction of reactive curve maps become more challenging Asthana et al. [2005], Dai et al. [2018]. A conceptual design of a reactive distillation column was presented with the specifications of Table **4-11**, where it can be observed that it is possible to obtain a bottom product with 98 % wt of Butyl Lactate.

Figure **4-15** presents the process flow diagram with the obtained design. Figure **4-16** shows the temperature and column composition profiles. The evaluated pressure (25 kPa) is reachable at an industrial scale, allowing obtaining the desired temperature profile along the column. The pressure operation condition leads to obtaining temperatures below 355.15 K in zones where Lactic Acid is in high concentration, while zones exceeding this temperature have low Lactic Acid composition. Hence the oligomer formation is minimized. Under these conditions, the simulation presented reaction rates for the oligomerizations with maximum values of 4×10^{-4} kmol/h, leading to ppm-level compositions. In the rectification section, 1-Butanol and Water are accumulated, obtaining the composition of the heterogeneous azeotrope. In the stripping zone, Butyl Lactate is concentrated to be obtained as the bottom product.

Table 4-11: Operating conditions of reactive distillation.

Design variable	Value
Total stages	13
Rectifying section	1 - 3
Reactive section	4 - 9
Stripping section	10 - 13
Feed molar ratio	BuOH:LA=1.4
Lactic Acid feed	4
Flow rate	4150 kg/h
Composition (wt fraction)	LA=0.3
	W=0.7
n-butanol feed	9
Flow rate	1416
Composition (wt fraction)	BuOH=0.999
	W=0.001
Condenser temperature	313.15
Bottom product	2026 kg/h
composition (wt fraction)	BuLac=0.987
	AL=0.006
	BuOH=0.007
Distillate product	Heterogeneous azeotrope BuOH-W
	7979 kg/h
Composition (wt fraction)	BuOH=0.449
	W=0.501
Aqueous phase product	3540 kg/h
composition (wt fraction)	BuOH=0.109
	W=0.891
Organic phase	4439 kg/h
composition (wt fraction)	BuOH=0.810
	W=0.190
Catalyst loading per stage	100 kg
Pressure	25 kPa

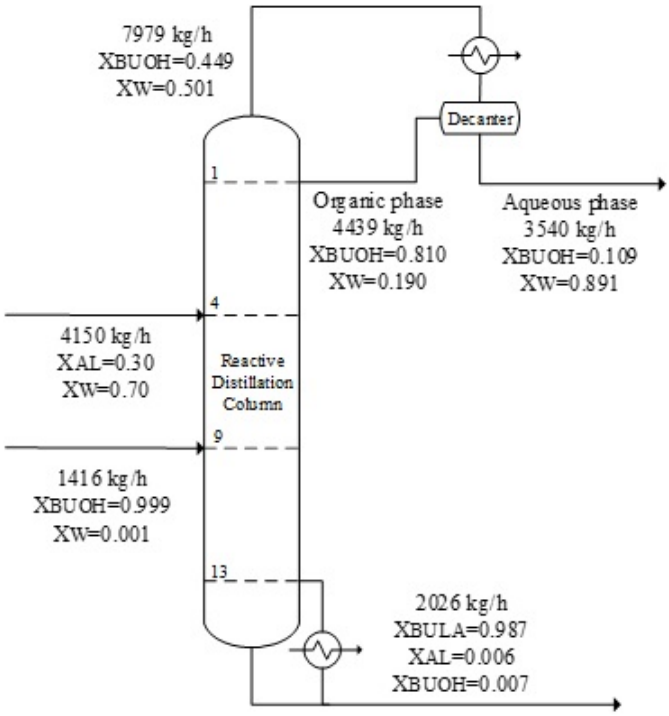

Figure 4-15: Reactive distillation column (%wt fraction).

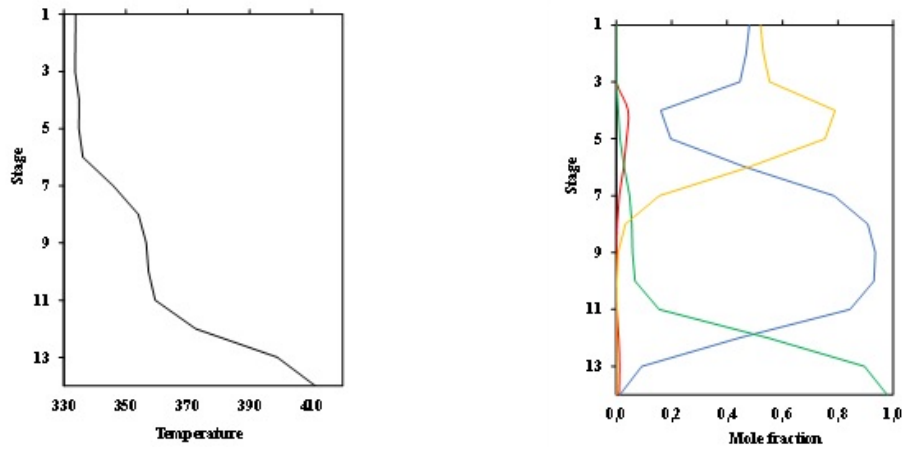

(a) (b)

Figure 4-16: Column (a) temperature and (b) composition profile (–) LA, (–) BuOH, (–) BuLac and (–) W.

4.2.4. Conclusions of the section

This section presented a thermodynamic approximation for studying the quaternary system: Lactic Acid, n-butanol, Butyl Lactate, and Water. Initially, the thermodynamic information, such as VLE and VLLE was reviewed, and the NRTL thermodynamic model was used

with a unique set of binary parameters. The quaternary system Lactic Acid-n-butanol-Butyl Lactate-Water was modeled accurately with a good prediction of the azeotrope reported in the literature (n-butanol-Water). A new azeotrope (Butyl Lactate-Lactic Acid) was identified, which had not been reported in the literature. Besides, this work involved a comprehensive revision and validation of the ternary n-butanol, Lactic Acid, and Water. LLE phase equilibrium data was used for validating the obtained thermodynamic information. An analysis of the model indicates no ternary and quaternary azeotropes. This agrees with the topological analysis, which is consistent based on considering the azeotropic rule.

The reactive residue curve maps for the quaternary system were calculated under chemical equilibrium conditions and represented in transformed coordinates. According to the results of the map analysis, reactive azeotropes were not found. Butyl lactate can be obtained as a bottom product, and the azeotrope n-butanol-Water can be obtained as the top product in a reactive distillation process.

The proposed methodology for constructing the residue curve maps studied in this work serves as a tool for conceptual studies with a complete description of the calculation and global optimization techniques. This methodology complements the information spread in the open literature for constructing reactive and non-reactive residue curve maps for VLL equilibria. This implies an advantage in its construction based on a global optimization technique. However, this methodology presents a disadvantage related to computational time due to the global optimization techniques that should be addressed.

The residue maps obtained were used to propose a preliminary reactive distillation column in a process intensification case. The resulting proposal allows obtaining a product with high purity of Butyl Lactate (98 % wt). For future work, the thermodynamic information can be completed with new experimental data for the mixture Butyl Lactate - water and validate the existence of the azeotrope Butyl Lactate-Lactic Acid.

4.3. Green solvents production in a pilot-plant reactive distillation column: modeling and experimental validation

4.3.1. Phenomenological Model Validation

This section presents the column simulation results for the three scenarios introduced in Section 3.4. Table **4-12** presents all the scenarios comparison. The first scenario addressed isoamyl acetate production in a reactive distillation column at the pilot-plant scale. The

thermodynamic and kinetic equations presented in Section 3.4.1 were validated against experimental data in Sánchez et al. [2017], Martínez et al. [2020a]. Figures **3-9** and **3-10** show the validation for the thermodynamic and kinetic models, respectively. These models correctly predict the experimental data set, which means that the set of equations could be used to represent the phenomena on the RDC.

$$MSE = \frac{1}{n}\sum_{1}^{n}\left(Y_i - \hat{Y}_i\right)^2 \tag{4-11}$$

Table 4-12: Phenomenological model validation in cases

Case	Thermodinamic Model	Kinetic Model	Operation Type
1. Isoamyl Acetate (Pilot Plant)	NRTL-HOC	Pseudo-homogeneus kinetic model	Batch process with experimental data
2. N-butyl lactate (Lab-scale-literature)	NRTL	Pseudo-homogeneus kinetic model	Continuous with experimental data
3. N-butyl lactate (Pilot Plant)	NRTL	Pseudo-homogeneus kinetic model	Continuous without experimental data

For Case 1, the experiments in the RDC at the pilot-plant scale were carried out at total reflux. The water produced is removed first, and the organic phase recirculates to the column's top stage. The column was modeled and simulated in Matlab R2020b according to the description in Section 3.3 and Figure **3-7** (b). To determine the fitting between experimental data and the model, the mean square error (MSE) index was used (Equation 4-11), where term n means the number of experimental data, y^{exp} is the experimental data, and y^{calc} is the corresponding model prediction. Figure **4-17** shows the model predictions for case 1 (at steady state). With the validated model for isoamyl acetate production by RD, it is possible to evaluate the production of n-butyl lactate since all the cases include the same mass and energy balance structure represented through the equilibrium stage model. The deviations in the model are because oligomerization reactions are not considered. The thermodynamic and kinetic models change according to the nature of the compounds. However, for the evaluated

cases, it is possible to implement the same kinetic and thermodynamic model for the liquid phase because esterification reactions with similar compounds occur in these systems.

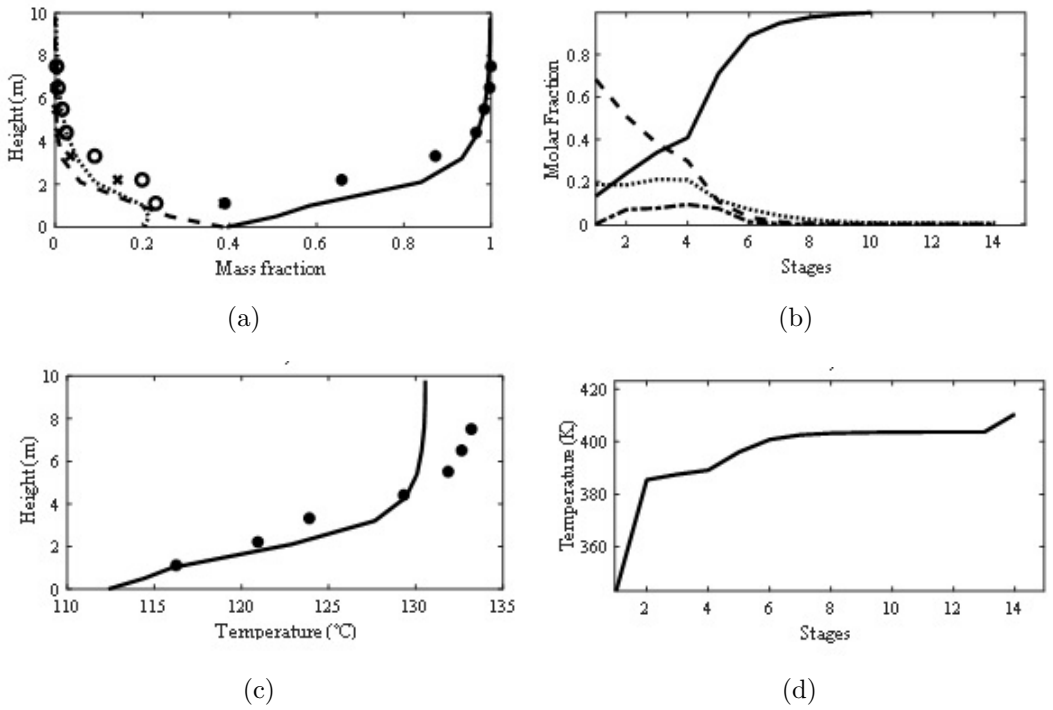

Figure 4-17: (a) Mass fraction profiles: experimental (•) IAc, (o) IA, (x) AA and model (-) IAc, (···) IA, (- - -) AA. (b) Temperature profile: experimental (•) and model (-). (c) Molar fraction profiles: model (-) IAc, (···) IA, (- - -) AA, (-•-) Water. (d) Temperature profile: model (-).

In Case 2 it was evaluated the production of butyl lactate based on the report of Kumar and Mahajani [2007]. The model developed in this work was compared with the model in Aspen V11 and experimental data presented by Kumar and Mahajani [2007]. Section 3.4.2 presented the thermodynamic and kinetic information (i.e., Tables **3-9** to **3-11**). The RD column for Case 2 is operated continuously, as is presented in Figure **3-12**. Figure **4-18** shows the temperature and mole fraction profiles for the Kumar and Mahajani [2007] experimental data and the comparison with Aspen V11 and Matlab R2020b simulations.

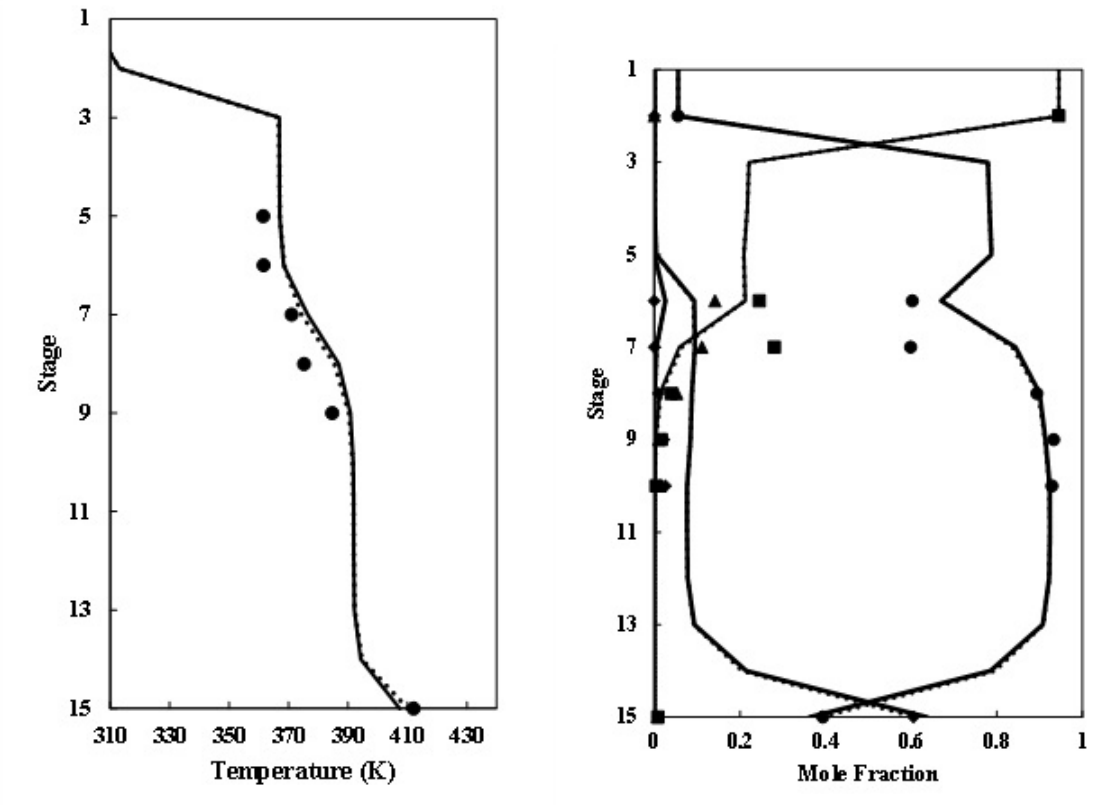

(a) (b)

Figure 4-18: (a) Temperature profile [10] (•), Aspen Plus V11 (-) and Matlab R2020b (—) W, (■) ButOH, (▲) LA, (♦) BuLac and Matlab R2020b (—) W, (-) ButOH, (-.-) LA, (· · ·) BuLac. (b) Composition profiles, Kumar et al. [16] (•) W, (■) ButOH, (▲) LA, (♦) BuLac, Aspen Plus V11 (-) and Matlab R2020b (—).

Although it can be observed that a good fitting was obtained for both simulators, the Matlab model showed a lower MSE value (see Table **4-13**). This is because authors in Kumar and Mahajani [2007] presented estimated thermodynamical information using the UNIFAC model for the missing parameters; meanwhile, this work used experimental calculated parameters. Furthermore, authors presented binary interaction parameters for the mixture butanol-water and butanol-butyl lactate using the UNIQUAC model; however, as was presented in Garcia et al. [2021], Velandia et al. [2021], there is a better representation for these mixtures using the NRTL model (i.e Tables **3-9** to **3-11**).

Table 4-13: MSE comparison between experimental data and simulation obtained in Aspen Plus V11 vs Matlab.

MSE	Temperature (K)	xBuLac(%W/W)
Matlab	38.37	0.003
Aspen V11	50.15	0.004

The Matlab model correctly represents the production of butyl lactate in RDC. This information can now be used to evaluate RD production at the pilot-plant scale.

In Case 3 it was evaluated the production of BuLac in a RDC at the pilot-plant scale, as was described in Section 3.4.3. Tables **3-9** to **3-11** present the thermodynamic and kinetic information, respectively, and Figure **3-13** represents the system model based on the RDC described in Section 3.4.1. The results were compared using Aspen plus V11 simulator and Matlab R2020b. In both cases, the results agree and present the same tendency.

Figure **4-19** a depicts composition profiles along the column. With the presented operation conditions, BuLac with a purity of 93 (mol %) is guaranteed, while the BuOH composition is maintained in excess along the column. Figure **4-19** b shows the temperature profile. There, it can be observed that the simulated model in Matlab is in good agreement with the results obtained in Aspen plus. The MSE obtained for the BuLac fitting was 0.0004, and the temperature was 11.12. In this case, a bottom product mass flow of 2.02 kg/h with a composition of 93 (mol %) BuLac. Inlet product conditions are established based on the operative restrictions in the RDC at the pilot-plant scale. With these conditions, a boil-up ratio of 27 is reached. Therefore, it is possible, at least in silico, to obtain butyl lactate in a RDC at pilot-plant scale with a composition of commercial interest (93-98 %w/w) Clark et al. [2015].

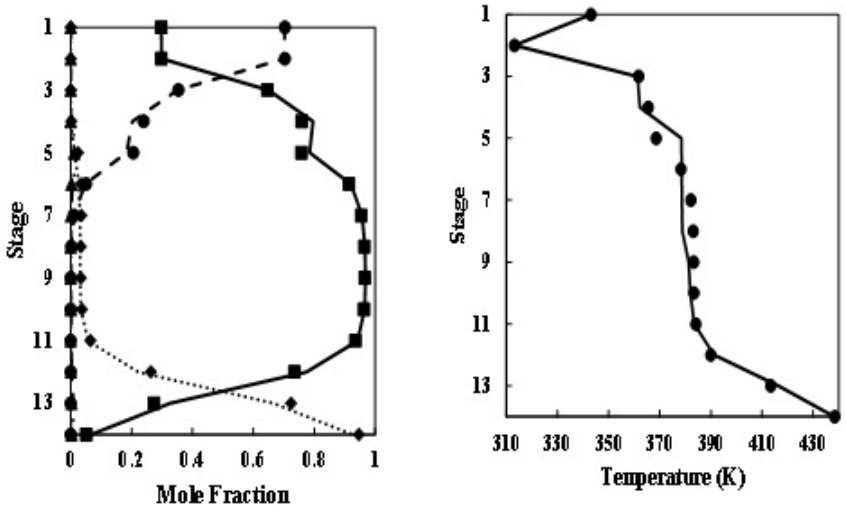

(a) (b)

Figure 4-19: (a) Mole fraction profiles: Aspen Plus V11 (•) W, (■) ButOH, (▲) LA, (♦) BuLac and Matlab R2020b (—) W, (-) ButOH, (-.-) LA, (...) BuLac. (b) Temperature profile: Aspen Plus V11 (•) and Matlab R2020b (-).

In Figure **4-20**, liquid and vapor flow rates along the column and the model results using Aspen Plus V11 and Matlab R2020b are compared. Few deviations with an MSE concerning the vapor flow rate of 0.014 are obtained due to the differences in the properties calculation. However, the Matlab model adequately represents the Aspen Plus V11 profiles. This means that the Matlab model fulfills the hydrodynamic restrictions obtained in Aspen Plus V11.

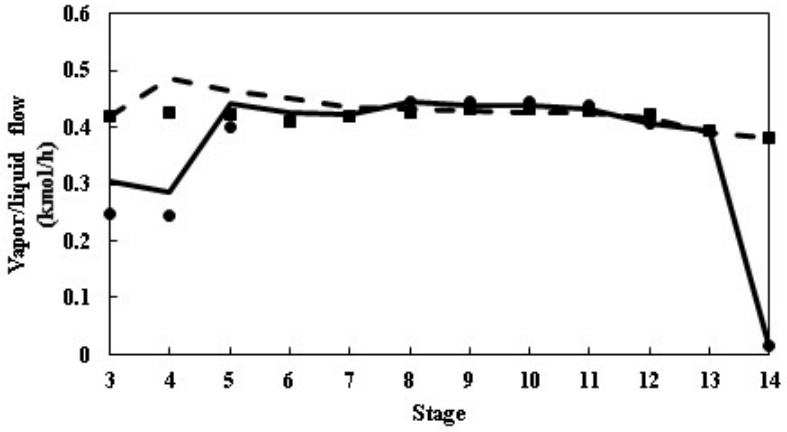

Figure 4-20: Aspen Plus V11 (•) Molar Liquid flow rate, (■) Molar Vapor flow rate and Matlab R2020b (-) Molar Liquid flow rate, (—) Molar Vapor flow rate.

The three validation cases prove the modeling methodology can accurately represent reacti-

ve distillation processes for various green solvent production systems. The model structure was flexible and predictive across different operating conditions. This establishes a robust platform for simulation, control, and optimization.

Figure **4-21** present the dynamic behavior in stage tray 2 for temperature a) and mole fraction of butyl lactate b). All variables reach a steady state behavior with a condenser temperature of around 313 K.

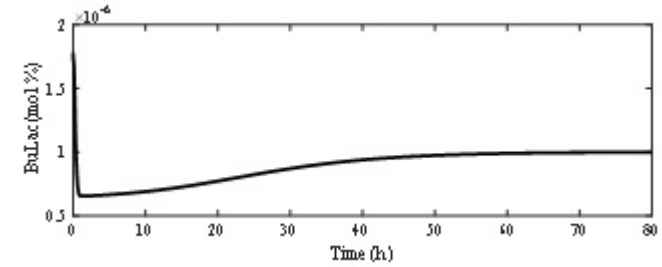

(a)

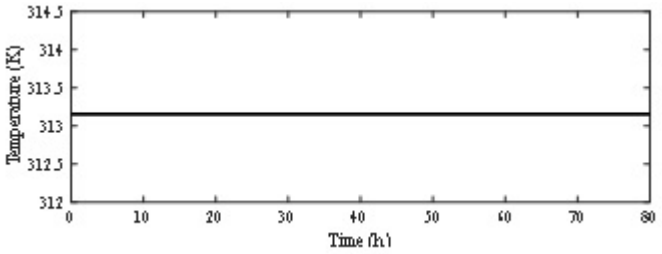

(b)

Figure 4-21: Dynamic profiles in stage tray 2 (a) Temperature and (b) Mole fraction of butyl lactate.

Figure **4-22** presents the dynamic behavior, as a inlet LA composition perturbation in the tray N tray where the temperature was stabilized around 438.5 K (Figure **4-22** a) and the final composition of BuLac was 93 (mol %) (Figure **4-22** b).

It is important to note that the modeled processes try to reproduce reality in the pilot plant. However, it is necessary to establish optimal operating conditions that help to reduce energy costs and retain the final composition of BuLac at desired values. By using the developed dynamic model, it is possible to determine the different stability regions to obtain operating conditions for applying optimal control strategies. It is also possible to evaluate the dynamic behavior of the main variables, such as compositions and temperatures.

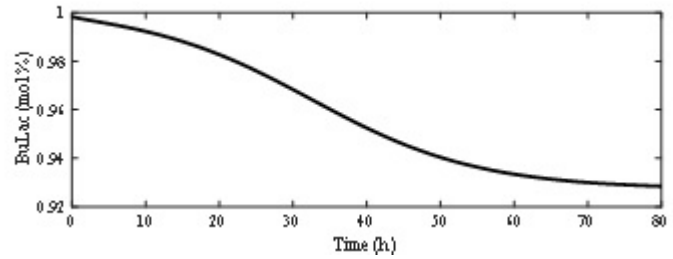

(a)

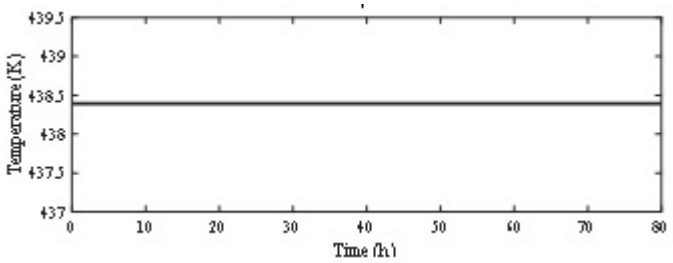

(b)

Figure 4-22: Dynamic profiles in stage tray 2 (a) Temperature and (b) Mole fraction of butyl lactate.

4.3.2. Sensitivity analysis

Further simulation studies for the esterification of lactic acid with butanol were carried out in Aspen Plus® v11. The RADFRAC module, which has a rigorous model based on calculating mass and heat transfer rates, was employed for this purpose. These simulations were mainly used to study the effect of operating parameters in the esterification process.

The reboiler was modeled as an equilibrium stage for the Aspen Plus simulation. The condenser was connected to a decanter to separate the two-phase mixture.

It is important to note that column internals in the hydraulic design correspond to Katapak SP-11 of Sulzer. However, the Aspen Plus Mellapack package is utilized for simulation purposes. Mellapak is approximately equivalent to Katapak catalyst modules [Sánchez et al., 2019].

The thermodynamic and kinetic models employed are mentioned in Section 3.4.2, respectively. Additionally, in the simulation, autocatalytic secondary reactions were included to evaluate the effect of the oligomer reaction in the process. These reactions occur due to lactic acid oligomerization, are favored by temperature, and appear at feed compositions of lactic acid superior to 30 % wt. For the formation of the oligomers, two additional reactions are considered (Equation 4-12 and 4-13) [Velandia et al., 2021].

$$2LA \rightleftarrows L_2 + W \tag{4-12}$$

$$LA + L_2 \rightleftarrows L_3 + W \tag{4-13}$$

$$k_a = k_{0,a} e^{-E_a/RT} \tag{4-14}$$

$$k_b = k_{0,b} e^{-E_b/RT} \tag{4-15}$$

where L_2 corresponds to lactic acid dimer and L_3 corresponds to lactic acid oligomers. These reactions describe lactic acid oligomer formation. Reaction parameters for a pseudo-homogeneous model to describe these reactions are presented in the same study and shown in Table **4-14**. The Eq. 4-14 and 4-15 represent the reaction rates for the oligomerization reactions Asthana et al. [2006].

Table 4-14: Kinetics of lactic acid oligomer formation.

Parameters	**Value**
$k_{0,a}[kgsol/kgcats]$	1.62x10^3
$k_{0,b}[kgsol/kgcats]$	6.67x10^3
$E_a[kJ/mol]$	52000
$E_b[kJ/mol]$	50800
K_1	5.0
K_2	5.0

The effect of the operating parameters has been studied using the simulation mentioned before. The simulation results in Table **4-15** and the process flow diagram in Figure **4-23** corresponds to the base case. The results of this simulation are used as a starting point for process sensitivity analysis. The flow of reactants, as well as the compositions obtained, allow to have a gap for the variables analyzed in the process.

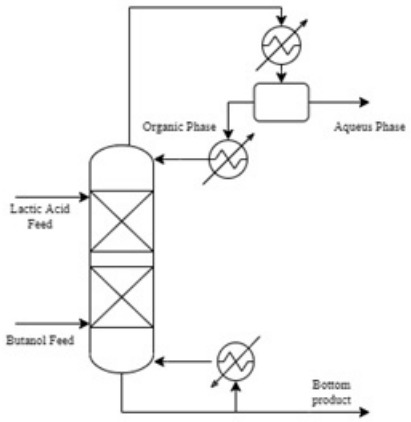

Figure 4-23: Proposed process flow diagram for esterification of lactic acid with butanol in Aspen Plus V11.

Table 4-15: Simulation results for the case base of the esterification process simulated in Aspen Plus V11.

Base Case Parameters	**Esterification**
Feed LA flow rate [kmol/h]	0.0135
Feed BuOH flow rate [kmol/h]	0.0225
Top product flow rate [kmol/h]	0.1722
Bottom product flow rate [kmol/h]	0.0209
Reflux composition (mole fraction)	
BuOH	0.4846
W	0.5154
BULA	2.636×10^{-9}
Bottom composition (mole fraction)	
BuOH	0.3549
W	0.0015
BULA	0.3435
LA	0.3000
Condensed duty [kW]	-3.849
Reboiler duty [kW]	3.669

Considering that the modeled reactive distillation column is constructed, the effect of distillate mass flow, molar feed ratio, and feed temperature of lactic acid are evaluated.

Effect of distillate mass flow

In Figure **4-24**, distillate mass flow at the top stream was varied from 3 to 13 kg/h to examine its effect on the conversion of lactic acid. Initially, conversion presents a slight increase with distillate mass flows below 8.9 kg/h, approximately. However, over this value, conversion increases to reach a stable state with high conversions, where it is important to evaluate other operating conditions. A higher condenser duty is necessary to enrich the vapor stream and reach the desired separation for a superior distillate mass flow. Additionally, higher mass flows at the column result in a higher reboiler duty, as shown in Figure **4-25**. It is worth highlighting hydraulic issues, such as oversizing and changing column diameters, were not perceived in the simulation for this range of distillate mass flows, according to the hydraulic design of the column. Figure **4-26** shows the response of the reboiler temperature concerning changes in the boil-up ratio; in the figure, it can be seen that the system presents multiple steady states to certain operating temperature conditions in the reboiler. This indicates that the operation of this system involves control challenges due to the non-linearities and the multiple steady states involved in the system.

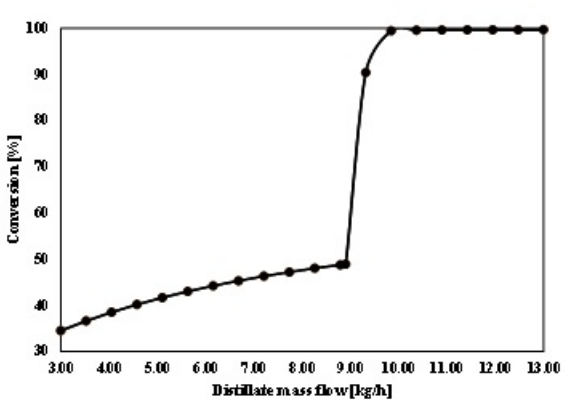

Figure 4-24: Effect of distillate mass flow on lactic acid conversion.

As mentioned before, in Figure **4-25**, the relationship between distillate mass flow and reboiler and condenser duties is evident. Condenser and reboiler duties augment with increases in the distillate mass flow since more energy must be removed and provided, respectively.

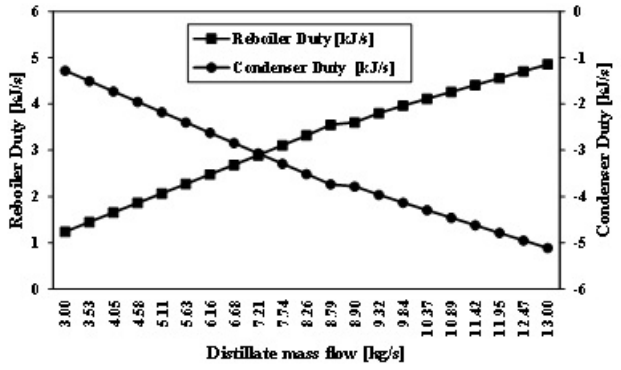

Figure 4-25: Effect of distillate mass flow on condenser -●- (Q_c) and reboiler -■- (Q_r) duties.

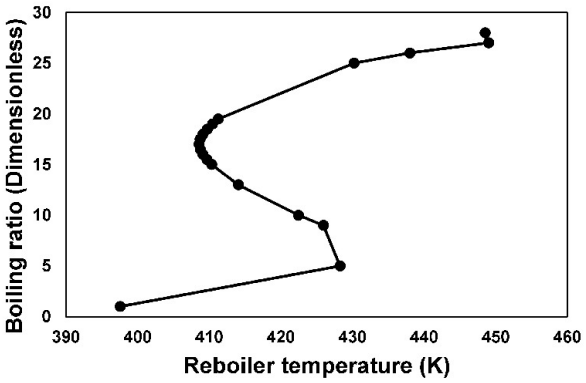

Figure 4-26: Multiplicity of stable states concerning boilup ratio variations and reboiler temperature.

Effect of molar feed ratio

The molar flow of butanol is varied from 0 to 110 kmol/h to evaluate different molar feeding ratios of lactic acid: butanol as shown in Figure **4-27**. A ratio of 1:4 to 1:8 generates a conversion between 56-58 %. This implies that for an LA composition of 30 % w/w, there is a fairly high addition of water, working within the equilibrium reaction's limit. Values higher than these ratios do not make sense due to the amount of water added to the systems as well as the low conversion difference that is obtained concerning the ratio of 1:8.

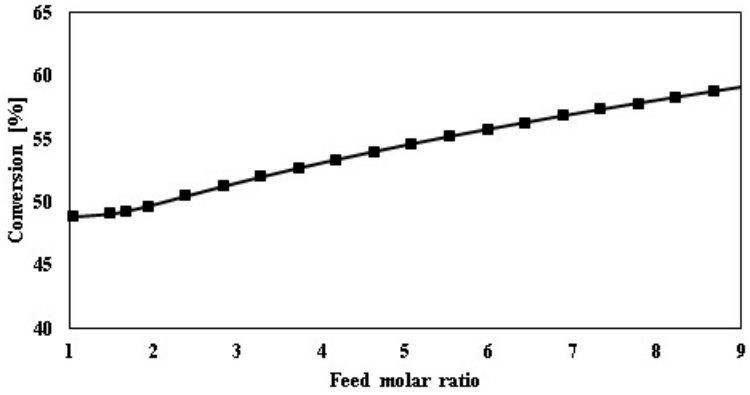

Figure 4-27: Effect of molar feed ratio on conversion.

Effect of feed temperature

The feed temperature of lactic acid is varied from 50 to 120 °C to evaluate its effect on conversion and reboiler and condenser duties. At temperatures from 50 to 90 approximately, conversion remains constant. However, it shows an increase at temperatures over 90 (Figure **4-28**) and the typical pattern of a possible bifurcation. Despite the increase in conversion, operating in temperatures over 90 is impossible since oligomerization occurs at these conditions, as can be observed in Figure **4-29** a). In contrast, Figure **4-29** b) shows the butanol and lactic acid molar composition on the product stream. It decreases as butyl lactate increases; however, oligomer concentration increases (Figure **4-29** a).

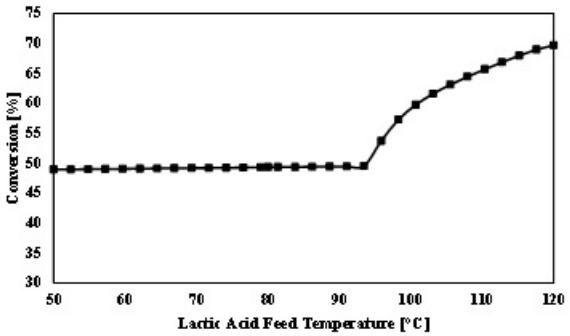

Figure 4-28: Effect of lactic acid feed temperature on conversion and butyl lactate molar flow in bottoms.

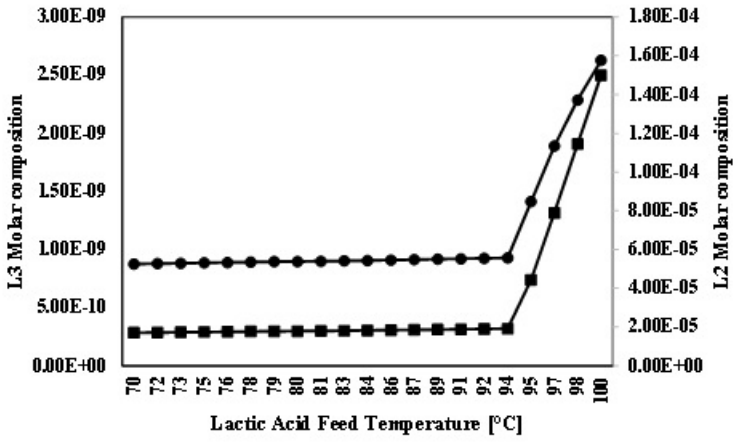

(a)

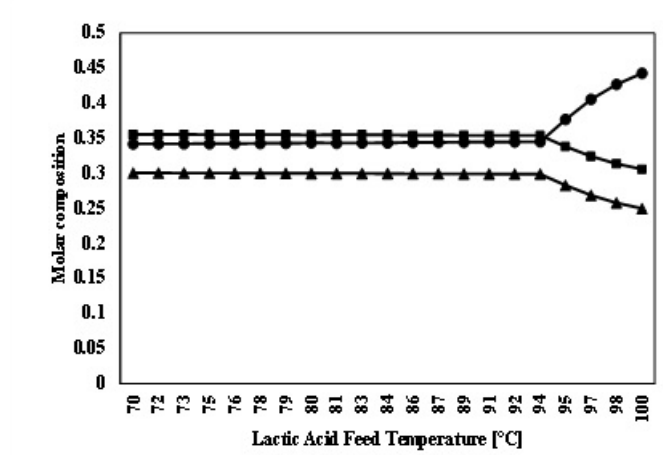

(b)

Figure 4-29: Effect of lactic acid feed temperature on product liquid composition. (a) Oligomers molar composition L2 -●- and L3 -■-. (b) Reactive and main product molar composition: butyl lactate liquid molar fraction -●-, butanol liquid molar fraction -■- and lactic acid liquid molar fraction -▲-.

The same occurs with condenser and reboiler duties, as heat duties have a reduction for feeding temperatures over 90°C, which is a condition that reduces selectivity (Figure **4-30**).

Effect of the catalyst loading

The catalyst loading was varied over 0.0225 and 1.05 kg (total amount of catalyst) to evaluate its effect on the conversion of LA (Figure **4-31**). The conversion increases while the catalyst loading increases; at a high catalyst loading (0.3249 kg), a quantitative conversion close to 100 % is achieved. According to Kumar and Mahajani [2007], with high catalyst loading, the reaction is no longer controlled by kinetic.

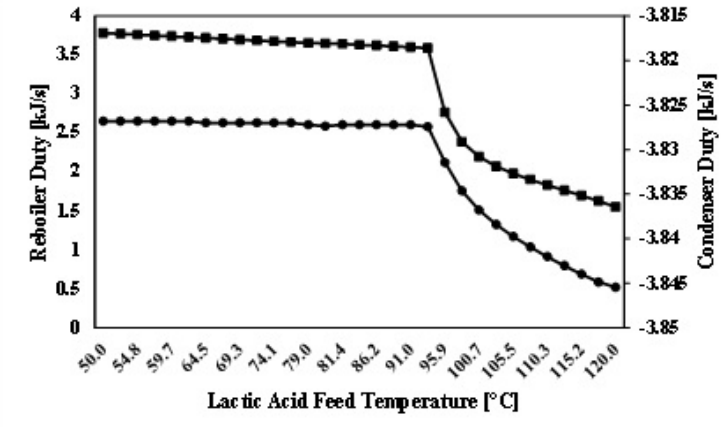

Figure 4-30: Effect of lactic acid feed temperature over reboiler -■- and condenser -●- duty.

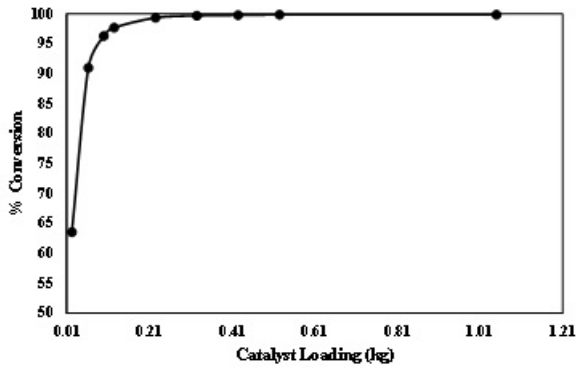

Figure 4-31: Effect of the catalyst loading on the conversion.

4.3.3. Conclusions of the section

The obtained results of isoamyl acetate production evaluation (Case 1) allow for establishing that mass and energy balances agree with experimental data. It means that the developed model can be extended to the production of butyl lactate at the evaluated scale. In Case 2, the comparison of the model implemented in Matlab against Aspen Plus V11 and experimental data support the robustness of the model and the possibility of evaluating, in silico, the production of butyl lactate at the pilot-plant scale. Furthermore, Case 3 indicates that it is possible to obtain butyl lactate in the RDC at the pilot-plant scale; however, validation in the real plant is required.

According to the sensitivity analysis results, reaching higher conversions with distillates mass flows over 8.9 kg/h, high molar feed ratios, and catalyst loading over 0.325kg is possible. However, it implicates higher condenser and reboiler duties since it is necessary to enrich the vapor phase and achieve the desired separation degree. In the same way, there is an increase in mass flow at the column, which can negatively impact its hydraulic behavior. The feed temperature of lactic acid impacts conversion as well. Over 90 °C the conversion increases, but the molar composition of oligomers starts to increase, reducing selectivity. Even though oligomer composition is low, it is important to evaluate other process variables, such as temperature and pressure to determine the feasibility of the operation conditions.

This work presented a model analysis and validation against different scenarios, allowing for comparing different operating conditions. The presented model is in a dynamic state and could be used to perform stability and control analysis to achieve a high conversion and optimal process operation.

4.4. Control Proposal

4.4.1. PID controller

SVD and RGA

For the design and development of the control system, a second-order model was initially identified that establishes the relationship between the manipulated and controlled variables of the system. This linear model was based on simulations of a validated pilot plant model (Chapter3.3), ensuring an accurate and realistic representation of system behavior under operational conditions. Different pairs of variables were analyzed, evaluating different control possibilities in the plant.

The transfer functions that describe this linear model for the 2x2 system are presented in Equation 4-16. These transfer functions capture the system dynamics and provide a useful mathematical description that can be used for controller design.

$$\mathbf{G}(s) = \left[\begin{array}{c|cc} & \text{FR} & \text{BR} \\ \hline T_2 & g_{11}(s) & g_{12}(s) \\ T_{14} & g_{21}(s) & g_{22}(s) \end{array}\right] \tag{4-16}$$

where:

$$g_{11}(s) = \frac{2.687 \times 10^{-5}s + 8.43 \times 10^{-9}}{s^2 + 0.0001108s + 2.271 \times 10^{-8}}$$
$$g_{12}(s) = \frac{-1.495 \times 10^{-5}s + 7.807 \times 10^{-9}}{s^2 + 0.0004505s + 7.777 \times 10^{-8}}$$
$$g_{21}(s) = \frac{0.0161s - 7.563 \times 10^{-6}}{s^2 + 0.0001978s + 1.688 \times 10^{-8}}$$
$$g_{22}(s) = \frac{2.591 \times 10^{-5}}{s + 2.531 \times 10^{-5}}$$

2.687 (4-17)

The term g_{11} has a positive zero because both terms of the numerator are positive, and the plant did not show an inverse response for this pair. In the transfer function g_{12}, the coefficient of the linear term in the numerator is negative (-1.495 x 10^{-5}). This indicates an inverse response between the manipulated variable (boilup ratio) and the process variable (condensate temperature). An increase in the boilup ratio will likely result in a slight decrease in condensate temperature and vice versa. This inverse response is small, and the system

recovers quickly.

An increase in BR can increase the light components sent to T_2. With more lightweight (more volatile) components to the top due to increased BR, these more volatile components can condense at lower temperatures. Therefore, an increase in the BR can cause a decrease in the temperature of the condensate.

Figure **4-32** presents a non-linearity between BR and conversion. For values between BR = 10 and BR = 14, the system enters in a high non-linear region, generating complexity in the operation process. This is part of a general analysis of non-linearity in the system whose information was used to complement the general data set and establish the appropriate operating regions for the simulation. The selection of the operating points was based on nonlinearity and operability analyses of the real plant, establishing that the ranges of the manipulated variables should be $13.39 \leq \text{BR} \leq 26.77$ and $0.1198 \leq \text{FR} \leq 0.1317$.

A 95 % adjustment criterion with a 100 s sampling period was used for identification, and Figure **4-33** a) present the model identification for BR - T_2 and Figure **4-33** b) present the model identification for BR - T_{14}. Figures **4-34** a) and b) present the model identification for FR-T_2 and FR-T_{14} respectively. In all cases, the adjustment criterion was achieved, representing a good quality of the adjustment model.

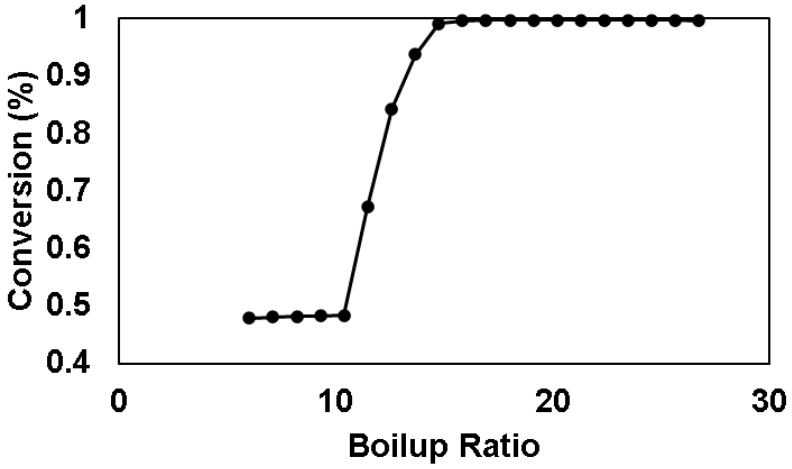

Figure 4-32: Non-linearity effect in Boilup-ratio vs Conversion.

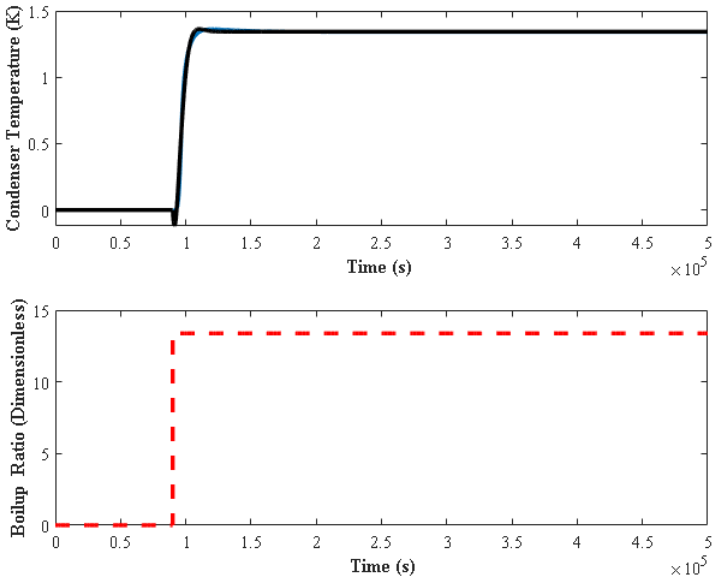

(a)

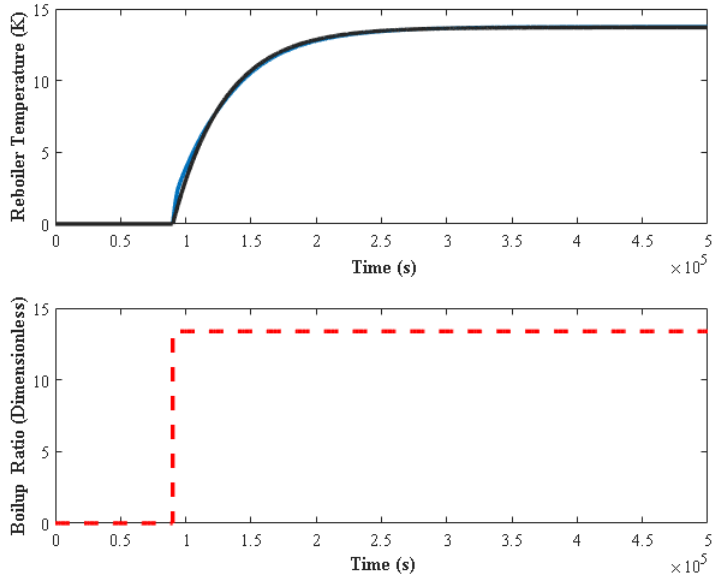

(b)

Figure 4-33: Identification for the pair a) BR - T_2, model(−), plant (−), disturbance (−−) and b) BR - T_{14}, model(−), plant (−), disturbance (−−).

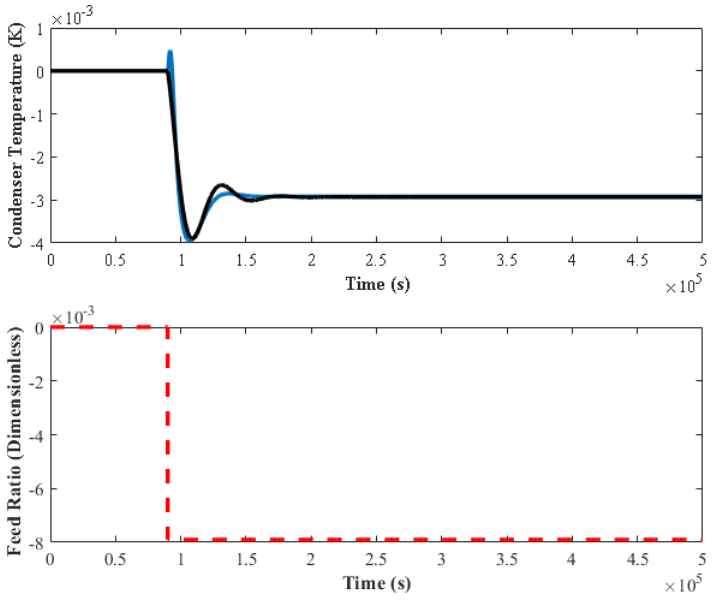

(a)

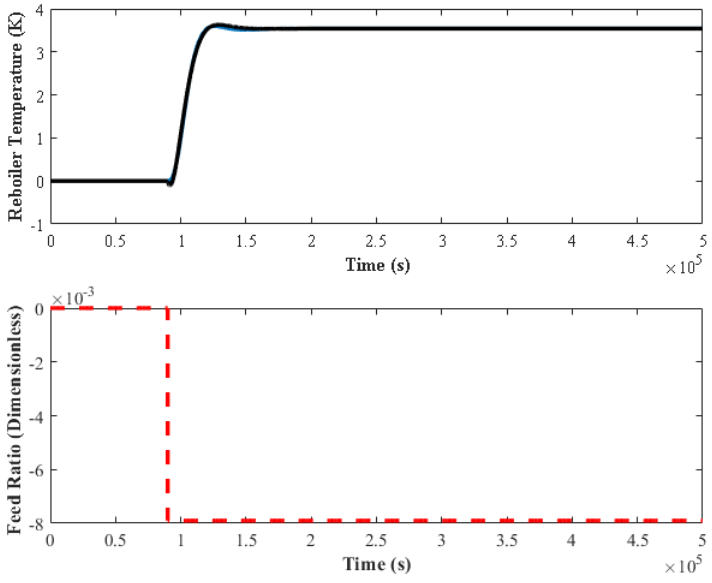

(b)

Figure 4-34: Identification for the pair a) FR - T_2, model(-), plant (-), disturbance (−−) and b) FR - T_{14}, model(-), plant (-), disturbance (−−).

This model identification-based control methodology has several advantages. Firstly, it allows for a deeper understanding of system dynamics, which is essential for designing an effective control system. Secondly, the identified linear model provides a basis for designing controllers that can be implemented and tested in simulation before implementation in the actual plant. Finally, the model also facilitates the sensitivity and robustness analysis of the control system, which is crucial for ensuring its performance in the presence of uncertainties and disturbances.

To determine the pairing controlled and manipulated variables, SVD and RGA analyses were performed, evaluating the possibilities in the distillation column in the pilot plant following the validated model. The SVD values indicate the significance of each input-output direction. The first singular value of 0.6044 is larger than the second value of 0.5034 (Table **4-16**).

This shows the first input-output pairing (Feed Ratio - T2) is more significant than the second pairing (Boilup Ratio - T14). With respect to the matrices U and V, a diagonal of 1 is presented. U vectors are orthogonal to each other and represent a base for the space of the rows of the original matrix. V-vectors are also orthogonal to each other and represent a base for the column space of the original matrix

Table 4-16: SVD obtained values

SVD values
0.6044
0.5034

In Table **4-17**, the optimal pairing appears to be Feed Ratio-T_2, where T_2 is the temperature in the condenser and Boilup Ratio-T_{14}, where T_{14} is the temperature in the reboiler (assuming T_2 and T_{14} are the controlled variables). This is because the diagonal elements (0.9916, 0.9916) are the closest to 1, and the off-diagonal elements (0.0084, 0.0084) are the farthest from 1.

This means that the effect of the Feed Ratio is felt more on T_2 and less on T_{14}, and similarly, the effect of the Boilup Ratio is felt more on T_{14} and less on T_2. This pairing would likely result in the least interaction between control loops if these pairs were controlled independently. The RGA and SVD analyses support the choice of Feed Ratio and Boilup Ratio as appropriate manipulated variables for controlling T2 and T14, respectively. The RGA shows

reasonable pairings, while the SVD confirms the relative importance of the two input-output directions. On the other hand, this shows that the MIMO PID control proposal is centralized.

Table 4-17: RGA Matrix

Manipulated variable	T_2	T_{14}
FR	0.9916	0.0084
BR	0.0084	0.9916

Tuning of the controller parameters

Based on the open-loop Chien, Hrones and Reswick methodology, the MIMO PID controller is a 2x2 system implemented using four SISO PID controllers that interlock each input with each output. The selected controlled variables, as was mentioned before, are the condenser temperature T_2 and reboiler temperature and T_{14}, and the manipulated variables are the (n-butanol/lactic acid feed ratio) and the boilup-ratio. Each PID is tuned using the open-loop CHR methodology for the SISO case. The values of the linear approximation of the first-order system with delay and oscillation are present in Table **4-18**. It should be noted that the identified plant model is not a dead time model. However, for the obtained model to tune the MIMO PID control is necessary to determine the dead time, and as seen in Table **4-18**, such dead time is low compared to the process time of 15 h. With this, a proper approximation of the MIMO PID control is obtained.

Table 4-18: Values of the linear approximation of the first-order system with delay and oscillation of the systems

System	**K**	**L (s)**	τ **(s)**
FR-T_2	0.37	1800	10000
FR-T_{14}	-448.05	8000	15200
BR-T_2	0.10	5000	9000
BR-T_{14}	1.02	3000	14000

where **K** is the proportional gain for the PID controller. **L** is the time delay in open-loop Ziegler-Nichols tuning, τ stands for the system's time constant, representing the time it takes

to reach approximately 63.2 % of its total change after a step input.

Table **4-19** presents the tuning parameters for the MIMO PID system. Within the characteristics obtained from the controllers, the over-peak Ov and the response time of the co-controller Ts. It can be observed that the controller presents a relatively high percentage of the references, this is due to the non-linearities of the system in certain regions of operation.

Table 4-19: PID controller parameters by CHR tuning method.

Controller	**Kp**	**Ki**	**Kd**	**Ov [%]**	**Ts (s)**
FR-T_2	14.22	0.0033	10748.86	19.08	20516.70
FR-T_{14}	-0.004	$-2.10x10^{-7}$	-13.54	0.00	63631.78
BR-T_2	17.03	0.0014	35772.01	0.00	42651.42
BR-T_{14}	4.33	0.0006	5456.64	20.35	62746.88

Section NMPC presents the results of the MIMO PID control compared to the LMPC and NMPC control and compares the performance indices.

4.4.2. LMPC

With the validated phenomenological model of the column, an LMPC controller model is proposed. With this linear model, it is possible to use the LMPC controller tuning proposal via the optimization technique of Giraldo et al. [2022].

The primary objective of this study is to address the challenge of implementing a 2×2 system using an LMPC. The system in question manipulates the feed and boilup ratio input variables. This manipulation aims to exert control over the condenser and reboiler temperatures, both output variables. These operations are based on a model validated from a reactive distillation column at the pilot scale. The linear model used in the controller was that obtained in the Equation 4-16

Given the complexity of the oversized nature of the pilot-plant RDC equipment, regulating these variables becomes a complex task. Consequently, a decision was made to confine the condenser temperature within the operational parameters of 359.3K and 361K. Simultaneously, the reboiler temperature has a designated setpoint of 440K to augment product quality.

The optimal LMPC's tuning parameters are delineated as follows: a sampling period of $T_s = 1000$s, a prediction horizon of $P = 23$, a control horizon of $M = 2$, and the semi-definite

weighting matrices are given by $Q = \text{diag}([0; 0.1127])$ and $W = \text{diag}([0.6013; 0.4027])$.

As the system output is capable of operating within a certain range, provided it adheres to the flexible constraints, the first element of the diagonal matrix Q is set to zero. The penalty weight for violation of the flexible constraint is defined as $\rho_\epsilon = 10000$. Section NMPC presenters the results of the LMPC compared with the MIMO PID and NMPC.

4.4.3. NMPC

This section compares MIMO PID, LMPC, and NMPC control strategies. Table **4-20** compares the parameters between LMPC and NMPC, where N is the prediction horizon, Nu is the control horizon, Q is the weights of the manipulated variables, W is the weights of the controlled variables and Ts is the sampling time. The same non-linear plant model was used as the NMPC controller model. The tuning of the NMPC controller parameters started from the optimized tuning, in the same way as the LMPC controller, and fine-tuning set manually.

Table 4-20: LMPC and NMPC control parameters.

Parameters/Control strategy	**LMPC**	**NMPC**
N	23	23
Nu	2	2
Q	[0.0 0.1127]	[0.0 0.1127]
W	[0.6013 0.4027]	[0.4811 0.3221]
Ts	1000	500

LMPC and NMPC have the same prediction horizon $N = 23$, which means both strategies aim to predict the same number of future steps and have the same control horizon $Nu = 2$, indicating both strategies will optimize the same number of future control moves. Both have the same state weighting matrix $Q = [0.00.1127]$, implying that both strategies assign the same importance to the system states. However, The values for LMPC and NMPC are $W = [0.6013\,0.4027]$ and $W = [0.4811\,0.3221]$, respectively. This means the LMPC places slightly more importance on control action changes than the NMPC. The values of T_S for LMPC and NMPC are 1000 and 500, respectively, implying that the calculations in NMPC are performed twice as often as in LMPC.

Based on these parameters, both LMPC and NMPC are trying to achieve the same control objective. However, they approach the control problem slightly differently due to differences in their control weighting matrices and sampling times. NMPC adjusts the control actions more frequently (higher sampling rate) but with less emphasis on changes in control actions (lower control weight) compared to LMPC.

Figure **4-35** compares the three proposed control strategies. It can be observed that the MIMO PID control works quickly saturated in the control limits of the manipulated variables and fails to meet the operating restrictions of the condenser temperature. The LMPC control addresses operational constraints; however, compared to the NMPC control, it has a slightly slower response time. At the simulation time t=50 h, there is an unmeasured disturbance in the lactic acid feed composition. All three strategies reduce the effect of such disturbance on the system. However, the LMPC and NMPC control are the ones that best manage to solve, being the NMPC which presents the best performance.

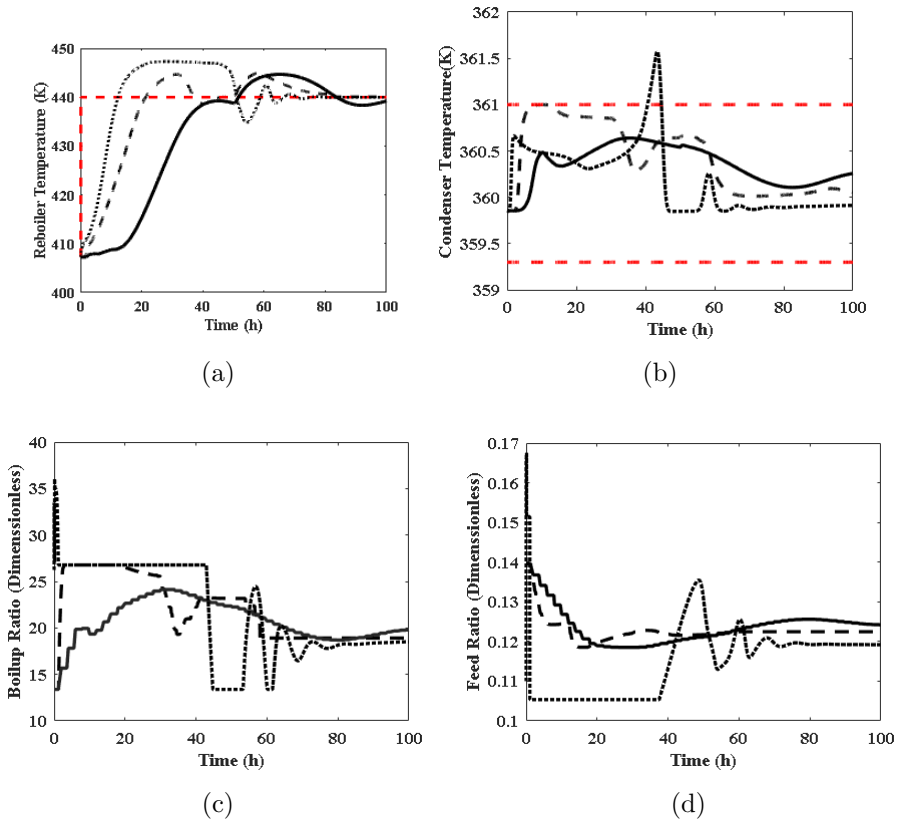

Figure 4-35: Control strategies comparison, (â€¢) PID, (−) LMPC, (−−) NMPC, (−−) reference limits, (a) Reboiler temperature. (b) Condenser temperature. (c) Boilup Ratio. (d) Feed Ratio.

Table **4-21** presents the performance indices of the three control strategies. It can be observed that the NMPC controller performs the best among all three controllers based on both metrics. It has the lowest ITSE and ITAE values, suggesting that it minimizes error over time most effectively. LMPC performs considerably better than the MIMO PID; this suggests that the LMPC and NMPC can control the system more effectively, leading to a smaller error over time than the MIMO PID.

However, the computational time for LMPC was approximately 10.1395 min compared with 2200 min using NMPC. It can be concluded that while the NMPC control performs best, the LMPC control is good enough to be evaluated in the pilot plant. This is also due to the operational restrictions that the plant presents, and that is related to oversizing some equipment, such as the reboiler. Based on this analysis, it is possible to evaluate the estimates of states and disturbances by ANN considering the LMPC control, which will be evaluated in the next section.

Table 4-21: Performance indices for proposed control strategies.

Performance Indices	**MIMO PID**	**LMPC**	**NMPC**
ITSE	5.10e+7	2.92e+5	7.16e+4
ITAE	5.03e+5	2.10e+4	9.28e+3
Computational Time	<1 min	<5 min	∼30 h

4.4.4. ANN state-estimator

As was described in Section State Estimator, the approach toward the design of an artificial neural network for noise signal filtering, disturbance, and end-product composition estimation involves data collection, where a large dataset containing instances of the noise signal, disturbance, and the corresponding end-product compositions was collected. Then, it was followed by the preprocessing and feature extraction, following the network architecture, training, and optimization. After defining the architecture, the network is trained, and finally, the validation and testing are performed.

In Figure **4-36** can be observed the regression (Figure **4-36** a)) and training state (Figure **4-36** b)) for the proposed ANN obtaining a R value of 99.89 %. In Figure **4-36** b), mu is the learning rate. It determines how big a step the network takes to update weights during

training. The network training uses some form of gradient descent optimization. At each training iteration, the error gradient concerning the weights is calculated using backpropagation. The gradient indicates how to change the weights to reduce the error. The learning rate mu determines the size of the weight update in the gradient descent direction.v It means that the obtained ANN represents the system with a good fitting.

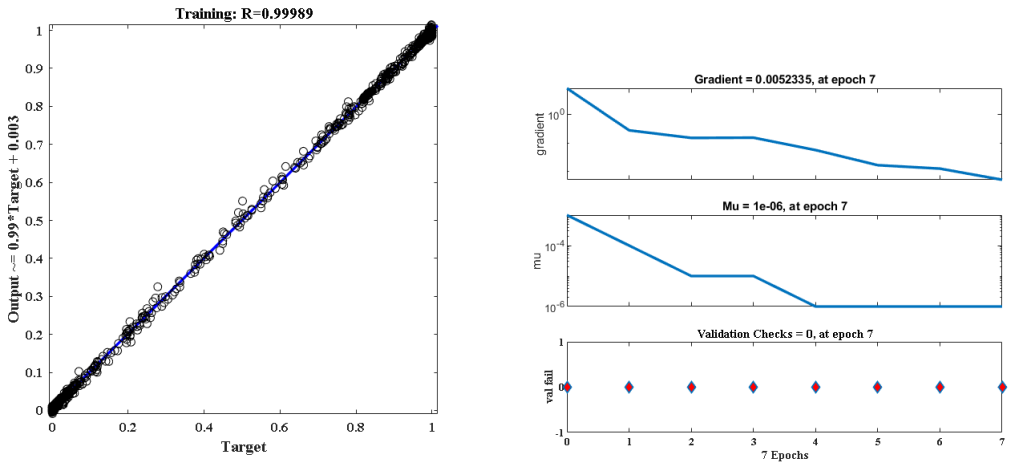

(a) (b)

Figure 4-36: ANN training performance, (a) Regression. (b) Training state.

Figure **4-37** presents the ANN response as a white noise filter for the condenser and reboiler temperatures for an LMPC control strategy, and the selected white noise was based on plant data attempting to represent reality at the pilot plant scale. It can be observed that the ANN can filter the entire noise in the controlled variables, having a good estimation of the controlled variables. In Table **4-22**, the performance indices related to the proposed control strategies, including the noise, can be observed. The ANN estimation presents similar indices concerning the LMPC without estimation.

Table 4-22: Performance indices for proposed control strategies.

Performance indices	MIMO PID	LMPC	NMPC	LMPC-ANN
ITSE	5.10e+07	2.92e+05	7.16e+04	3.47e+05
ITAE	5.03e+05	2.10e+04	9.28e+03	2.53e+04

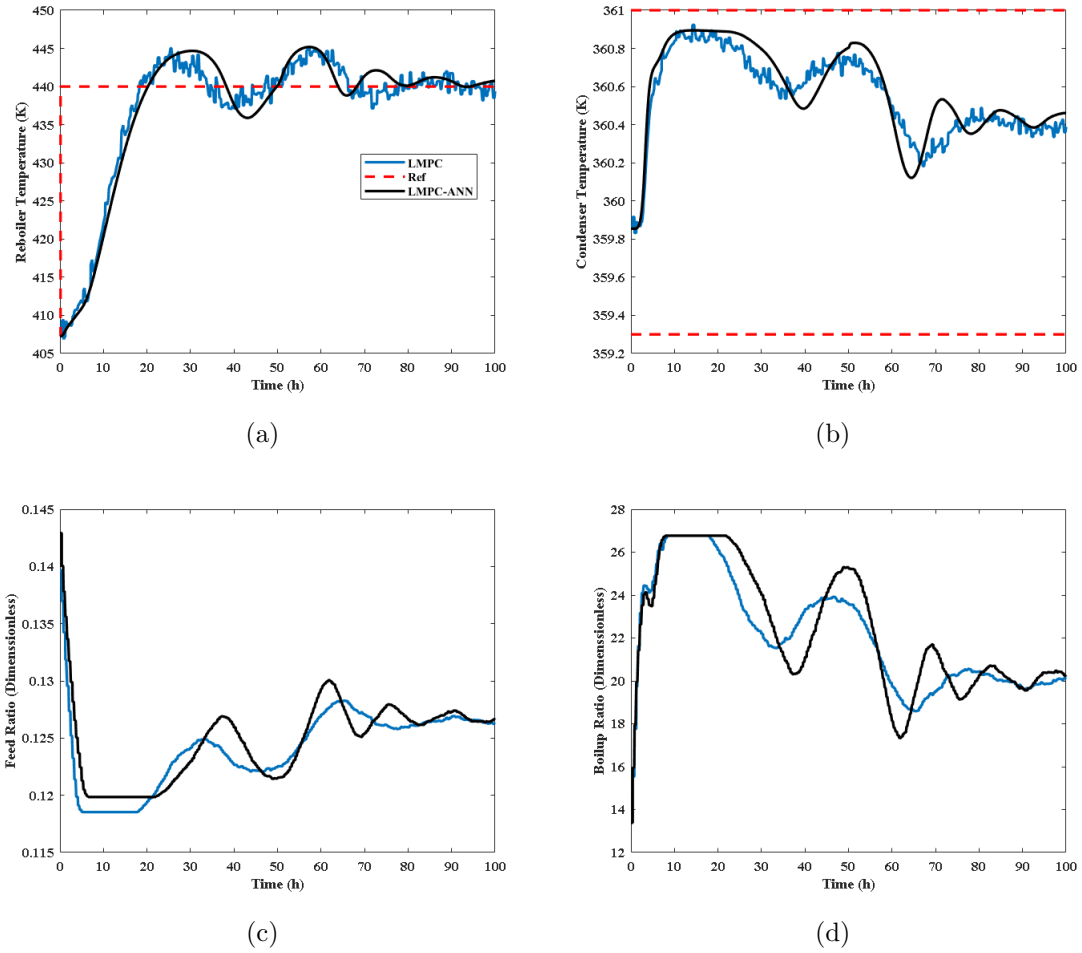

Figure 4-37: ANN noise filter, (−) LMPC with noise and disturbance, (−)LMPC with noise, disturbance, and ANN as a noise filter, (−−) reference limits, (a) Reboiler temperature. (b) Condenser temperature. (c) Feed ratio. (d) Boilup ratio.

With the obtained results, it was evaluated the disturbances estimation for the LMPC-ANN and the BuLa composition. In the operation of the pilot plant, there is an unmeasured disturbance related to the lactic acid composition in the feed. To generate simulation data and train the neural network to predict such an unmeasured disturbance, scenarios were generated where the lactic acid composition value changes to ± 20 % of the reference value as a constant or variable staggered disturbance. Figure **4-38** compares the LMPC-ANN control, including the aforementioned non-measured disturbance, which can now be used as a measured disturbance within the control strategy. The results are compared against a simple LMPC without any estimation. It can be observed that the LMPC-ANN addressed the disturbance more softly than the simple LMPC. It implies a more stable operation in a real process.

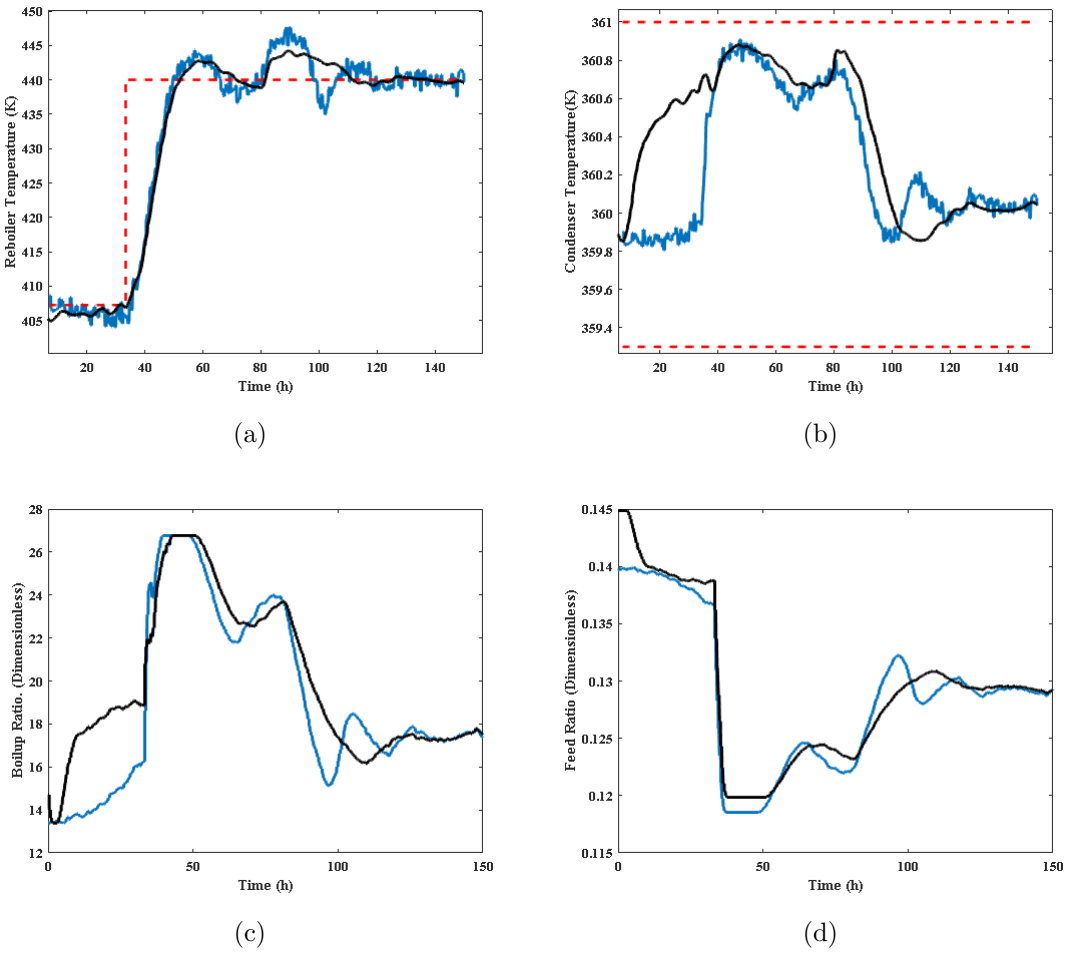

Figure 4-38: LMPC-ANN vs Simple LMPC, (−) simple LMPC with noise and non-disturbance estimation, (−) LMPC-ANN with measure disturbance, (−−) reference limits, (a) Reboiler temperature. (b) Condenser temperature. (c) Boilup Ratio. (d) Feed ratio.

Figure **4-39** presented the ANN disturbance and BuLa estimations along the control operation. Concerning ANN disturbance estimation, it can be observed (Figure **4-39** a) that the ANN can reproduce a variation in the LA feed composition. In the same sense, it can be observed in Figure **4-39** b) that the ANN can predict the BuLa composition reaching a final high-end-product composition. With the proposed control strategy, it is possible to operate, at least in *silico*, a stable reactive distillation column at the pilot plant scale to get BuLa with a high composition.

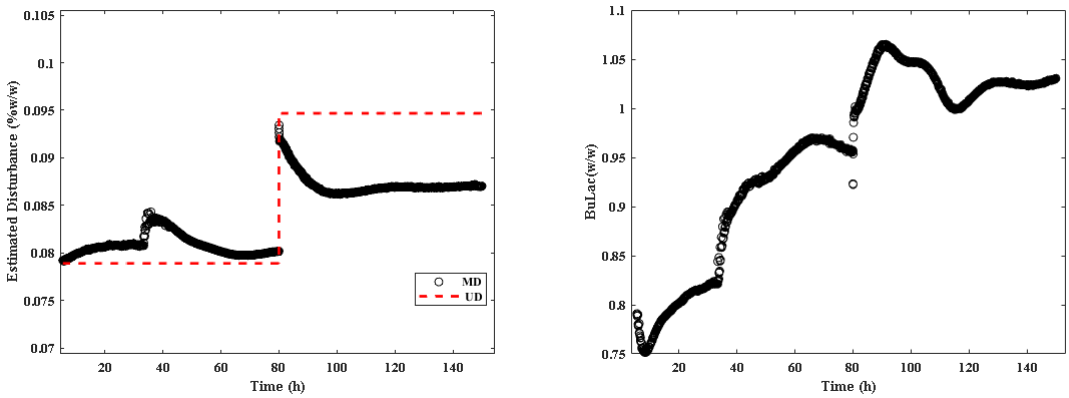

(a) (b)

Figure 4-39: (○) ANN disturbance estimation, (−−) forced disturbance, (a) Estimated Disturbance. (b) BuLa estimation.

4.4.5. Conclusions of the section

This section addressed the complexity of implementing a 2Ã—2 system using an LMPC controller on a model validated from a reactive distillation column at the pilot scale. The challenge is manifested due to oversized column equipment, making controlling condenser and reboiler temperatures daunting.

Compared with the MIMO PID and NMPC controllers, the proposed LMPC performs well under operational constraints. Based on the pilot plant operation, there are several challenges to consider in producing green solvents, such as n-butyl lactate. The oversizing of the reboiler, the high non-linear dynamics due to the reactive and separation processes, and the presence of several stable states make stabilizing the system, from a control point of view, difficult. As shown in this chapter, the advanced control proposals, LMPC and NMPC, allow the system to be operated stably, maintaining final product quality.

In particular, the NMPC adjusts control actions more frequently due to a higher sampling rate but places less emphasis on changes in control actions compared to the LMPC. Conversely, the LMPC places slightly more importance on control action changes, reflected in different weighting matrix values. Despite these differences, the LMPC and NMPC effectively reduced the impact of an unmeasured disturbance in the lactic acid feed composition at the 50-hour simulation mark. However, the computational time for LMPC (10.1395 min) compared with NMPC (2200 min) means that in terms of applicability, the LMPC control is more suitable for applications requiring fast response than the NMPC control.

These findings provide important insights for future control system design and highlight the superior performance of the NMPC under the given conditions. When developing an optimal control strategy for a system, it is essential to carefully consider the specific constraints and disturbance conditions that can affect that system. Recent research we have conducted highlights the importance of taking this factor into account Lima et al. [2023].

Finally, the ANN was analyzed as a noise filter for condenser and reboiler temperatures in an LMPC control strategy. The ANN exhibited good capabilities in filtering the entire noise within the controlled variables, presenting an accurate estimation of these variables.

Performance indices related to the proposed control strategies were assessed and are displayed in Table **4-22**. Notably, the ANN estimation provided similar performance indices to the LMPC control strategy without estimation. This similarity suggests that the ANN successfully filters out noise from the system and maintains the LMPC strategy's control performance.

Based on the findings illustrated in Figure **4-39**, it is evident that the ANN effectively reproduced a variation in the LA feed composition. Furthermore, the ANN presented a reliable prediction of the BuLa composition, ultimately achieving a high-end product composition.

These findings highlight the potential of using ANNs as noise filters in control strategies, particularly in complex variables such as condenser and reboiler temperatures. Furthermore, this research emphasizes integrating techniques like ANNs in control systems to enhance their robustness and performance, especially in significant noise and disturbances scenarios.

5 Conclusions and Suggestions for Future Works

This work presented extensive research and analysis on producing n-butyl lactate, an environmentally friendly solvent, using a reactive distillation process at a pilot plant scale. Thermodynamic modeling and simulation were leveraged to gain insights into this complex quaternary system involving lactic acid, n-butanol, n-butyl lactate, and water. The modeling results demonstrated adequate prediction capabilities and enabled the identification of feasible operating conditions and optimal configurations for reactive distillation.

Experimental data at the pilot scale was used to validate process simulations and dynamic models. The models showed good agreement with experimental results. Different control strategies were explored, including MIMO-PID, NMPC, and LMPC. LMPC exhibited good performance in maintaining product quality despite system constraints, disturbances, and computational time.

The integration of artificial neural networks was analyzed to filter noise in key process measurements. This approach demonstrated the potential for enhancing the robustness of model-based control systems in the face of significant noise and variability.

This work contributes to thermodynamic modeling, dynamic simulation, advanced process control, and machine learning techniques for n-butyl lactate production. The knowledge gained can inform and guide future research and development focused on similar reactive separation systems and sustainable solvent production. The presented models, data, and analysis techniques provide a strong foundation for ongoing efforts in this domain.

Evaluation of real-time control (RTO) applied to the LMPC control is recommended to determine optimal operating points while fulfilling restrictions as desired product quality and minimizing energy load on the reboiler.

It is important to be able to perform energy and economic analyses of this type of system. Operational life cycle analysis would be a good way to ensure the technical-economic viability of producing n-butyl lactate at the pilot plant scale.

Finally, it is recommended to implement and evaluate the advanced control strategies presented in this work for butyl lactate production in the pilot plant. This work was developed in the interface of simulink to facilitate the connection with the pilot plant via OPC.

Bibliografía

Afreen, A. Kumar, and R. Gupta. Lactic acid esters as green solvents for organic synthesis: A critical review. *Chemosphere*, 272(129605), 2021.

Afaq Ahmad, Weihua Gao, and Sebastian Engell. A study of model adaptation in iterative real-time optimization of processes with uncertainties. *Computers and Chemical Engineering*, 122:218–227, 2019. ISSN 00981354. doi: 10.1016/j.compchemeng.2018.08.001.

Hyunsoo Ahn, Kwang Soon Lee, Mansuk Kim, and Juhyun Lee. Control of a reactive batch distillation process using an iterative learning technique. *Korean Journal of Chemical Engineering*, 31(1):6–11, 2014. ISSN 02561115. doi: 10.1007/s11814-013-0192-7.

J. R. Almeida, M. S. Río, H. Pereira, and D. V. Evtuguin. Lactate esters as green solvents for lignocellulose processing: A review. *Journal of Cleaner Production*, 215:1261–1272, 2019.

M. A. Ammar, M. A. El-Ansari, and A. H. M. Elwahy. Lactate esters as bio-based solvents for the extraction of bioactive compounds from natural sources. *Separation and Purification Technology*, 221:223–235, 2019.

S. S. Anand, B. K. Philip, and H. M. Mehendale. Volatile Organic Compounds. In *Encyclopedia of Toxicology: Third Edition*, pages 967–970. 2014. ISBN 9780123864543. doi: 10.1016/B978-0-12-386454-3.00358-4.

P.T Anastas and Warner. Green Chemistry: Theory and Practice. *Oxford University Press*, 2000.

F. A. Andersen. Safety assessment of cosmetic ingredients. *International Journal of Toxicology*, 17(SUPPL. 1):1–241, 1998. ISSN 10915818. doi: 10.1177/109158189801700101.

Santiago Aparicio and Rafael Alcalde. The green solvent ethyl lactate: An experimental and theoretical characterization. *Green Chemistry*, 11(1):65–78, 2009. ISSN 14639262. doi: 10.1039/b811909k.

Dhia Y. Aqar, Nejat Rahmanian, and Iqbal M. Mujtaba. Methyl lactate synthesis using batch reactive distillation: Operational challenges and strategy for enhanced performance. *Separation and Purification Technology*, 158:193–203, 2016. ISSN 18733794. doi: 10.1016/j.seppur.2015.12.023.

Navinchandra Asthana, Aspi Kolah, Dung T. Vu, Carl T. Lira, and Dennis J. Miller. A continuous reactive separation process for ethyl lactate formation. *Organic Process Research and Development*, 9(5):599–607, 2005. ISSN 10836160. doi: 10.1021/op0500640.

Navinchandra S. Asthana, Aspi K. Kolah, Dung T. Vu, Carl T. Lira, and Dennis J. Miller. A kinetic model for the esterification of lactic acid and its oligomers. *Industrial and Engineering Chemistry Research*, 45(15):5251–5257, 2006. ISSN 08885885. doi: 10.1021/ie0513604.

Alexandru T Balaban. Process Design Principles: Synthesis and Analysis, 2000. ISSN 0095-2338.

Domingos Barbosa and Michael F. Doherty. The simple distillation of homogeneous reactive mixtures. *Chemical Engineering Science*, 43(3):541–550, 1988. ISSN 00092509. doi: 10.1016/0009-2509(88)87015-5.

Paola Andrea Bastidas Jiménez. *Diseño y montaje de un sistema piloto de destilación - reacción para la producción de acetato de isoamilo*. PhD thesis, Universidad Nacional de Colombia, 2014.

Lloyd Berg and Bozeman. Mont. Separation of lactate esters by extractive destillation, 1990.

Dominik Bykowski, Agnieszka Grala, and Piotr Sobota. Conversion of lactides into ethyl lactates and value-added products. *Tetrahedron Letters*, 2014. ISSN 18733581. doi: 10.1016/j.tetlet.2014.07.103.

Eduardo F. Camacho and Carlos Bordons. *Model Predictive Control*. Springer, 2nd edition, 2004.

M. Nataly Castrillon and C. Silvia Ochoa. Design and control integration of a reactive distillation column for ethyl lactate production. *2017 IEEE 3rd Colombian Conference on Automatic Control, CCAC 2017 - Conference Proceedings*, 2018-Janua:1–6, 2018. doi: 10.1109/CCAC.2017.8276470.

Gabriel Charles and Bogin Charles. Normal butyl lactate, 1928.

Dong Woo Cho, Jungin Shin, Moon Sam Shin, Won Bae, and Hwayong Kim. High-pressure phase behavior of propyl lactate and butyl lactate in supercritical carbon dioxide. *Journal of Chemical Thermodynamics*, 47:177–182, 2012. ISSN 00219614. doi: 10.1016/j.jct.2011.10.010.

James H. Clark, Fabien E I Deswarte, and Thomas J. Farmer. The integration of green chemistry into future biorefineries, 2009. ISSN 1932104X.

James H. Clark, Thomas J. Farmer, Andrew J. Hunt, and James Sherwood. Opportunities for bio-based solvents created as petrochemical and fuel products transition towards renewable resources, 2015. ISSN 14220067.

G. H. Cohen and G. A. Coon. Discussion: â€œOn the Automatic Control of Generalized Passive Systemsâ€. *Trans. ASME.*, 64:1–3, 1952.

European comission. http://ec.europa.eu/environment/industry/stationary /ied/legislation.htm, 2017.

Cesar Augusto Correa Sanchez. *Producción de Acetato de Fusel Por Destilación Reactiva Producción de Acetato de Fusel Por Destilación Reactiva*. PhD thesis, Universidad nacional de Colombia, 2015.

Shi Bao Dai, Hao Yeh Lee, and Cheng Liang Chen. Design and Economic Evaluation for Production of Ethyl Lactate via Reactive Distillation Combined with Various Separation Configurations. In *Computer Aided Chemical Engineering*, volume 44, pages 127–132. 2018. doi: 10.1016/B978-0-444-64241-7.50016-1.

Stephane Dassy, Hughes Wiame, and Fernand C. Thyrion. Kinetics of the liquid phase synthesis and hydrolysis of butyl lactate catalysed by cation exchange resin. *Journal of Chemical Technology Biotechnology*, 59(2):149–156, 1994. ISSN 10974660. doi: 10.1002/jctb.280590206.

Patricia Delgado, María Teresa Sanz, Sagrario Beltrán, and Luis Alberto Núñez. Ethyl lactate production via esterification of lactic acid with ethanol combined with pervaporation. *Chemical Engineering Journal*, 165(2):693–700, 2010. ISSN 13858947. doi: 10.1016/j.cej.2010.10.009.

M. F. Doherty and J. D. Perkins. On the dynamics of distillation processes-III. The topological structure of ternary residue curve maps. *Chemical Engineering Science*, 34(12): 1401–1414, 1979. ISSN 00092509. doi: 10.1016/0009-2509(79)85164-7.

Lucas Domingues, Phylipe Andrian Cussolin, Julio Lopes da Silva, Leonardo Hadlich de Oliveira, and Martín Aznar. Liquid-liquid equilibrium data for ternary systems of water+lactic acid+C4-C7 alcohols at 298.2K and atmospheric pressure. *Fluid Phase Equilibria*, 354:12–18, 2013. ISSN 03783812. doi: 10.1016/j.fluid.2013.06.007.

David Duque, Jessica Arroyave, and Luisa Correa. Diseño conceptual, simulación y optimización del proceso de producción de Lactato de Etilo. *Revista Virtual de Procesos Industriales*, 2016. URL `https://www.revistavirtualpro.com/biblioteca/diseno-conceptual-simulacion-y-optimizacion-del-proceso-de-produccion-de-lactato-de-etilo`.

Martyn J. Earle and Kenneth R. Seddon. Ionic liquids. Green solvents for the future. *Pure and Applied Chemistry*, 72(7):1391–1398, 2000. ISSN 1365-3075. doi: 10.1351/pac200072071391. URL http://www.degruyter.com/view/j/pac.2000.72.issue-7/pac200072071391/pac200072071391.

Elmahboub A. Edreder, Iqbal M. Mujtaba, and Mansour Emtir. Optimization of Batch Reactive Distillation Process : Production of Lactic Acid. *20th European Symposium on Computer Aided Process Engineering â€“ ESCAPE20*, 2010.

Peter Eyerer, Martin Weller, and Christof Hubner. *Polymers â€“ Opportunities and Risks II*. 12 edition, 2010. ISBN 978-3-642-02796-3.

M. Francisco, Vega, and O Pérez. Optimización Dinámica para el Diseño Integrado de procesos en Lazo Cerrado. *XXIII Jornadas de Automática,*, 2000.

Ji Fuquan. Room-temperature curing ethyl lactate removal type silicone sealant, 2017.

Cesar Garcia, Jessica Velandia, Mario Céspedes, Gerardo Rodríguez, and Iván D. Gil. Isobaric Vaporâˆ'Liquid Equilibrium for the Binary Mixture of 1â€˜Butanol + Butyl Lâ€˜Lactate at 1 and 5 kPa. *Journal of Chemical and Engineering Data*, pages 1–6, 2021. doi: 10.1021/acs.jced.0c01068.

J. George Hayden and John P. O'Connell. A Generalized Method for Predicting Second Virial Coefficients. *Industrial and Engineering Chemistry Process Design and Development*, 14 (3), 1975. ISSN 01964305. doi: 10.1021/i260055a003.

Martino Gauchi Georges and Teissier Remy. Continuous production of ethyl lactate, useful as solvent for cleaning and degreasing surfaces, involves esterifying lactic acid with ethanol and removing water by molecular sieve adsorption and distillation, 2004.

Sergio A. C. Giraldo, PrÃamo A. Melo, and Argimiro R. Secchi. Tuning of model predictive controllers based on hybrid optimization. *Processes*, 10(2), 2022. ISSN 2227-9717. doi: 10.3390/pr10020351. URL https://www.mdpi.com/2227-9717/10/2/351.

Fred Glover. A template for scatter search and path relinking. In *Lecture Notes in Computer Science (including subseries Lecture Notes in Artificial Intelligence and Lecture Notes in Bioinformatics)*, volume 1363, pages 3–51, 1998. ISBN 3540641696. doi: 10.1007/bfb0026589.

Grand View Research. Grand View Research, 2015. URL https://www.grandviewresearch.com/industry-analysis/bio-solvents-market.

Grand View Research. Grand View Research, 2016. URL https://www.grandviewresearch.com/industry-analysis/green-bio-based-solvents-market.

Devin W. Griffith, Lorenz T. Biegler, and Sachin C. Patwardhan. Robustly stable adaptive horizon nonlinear model predictive control. *Journal of Process Control*, 70:109–122, 2018. ISSN 09591524. doi: 10.1016/j.jprocont.2018.07.014.

Katharina Häckl and Werner Kunz. Some aspects of green solvents. *Comptes Rendus Chimie*, 21(6):572–580, 2018. ISSN 16310748. doi: 10.1016/j.crci.2018.03.010.

Daniel Haßkerl, Clemens Lindscheid, Sankaranarayanan Subramanian, Patrick Diewald, Alexandru Tatulea-Codrean, and Sebastian Engell. Economics optimizing control of a multiproduct reactive distillation process under model uncertainty. *Computers and Chemical Engineering*, 118:25–48, 2018a. ISSN 00981354. doi: 10.1016/j.compchemeng.2018.07.003. URL `https://doi.org/10.1016/j.compchemeng.2018.07.003`.

Daniel Haßkerl, Clemens Lindscheid, Sankaranarayanan Subramanian, Steven Markert, Andrzej Górak, and Sebastian Engell. Application of Economics Optimizing Control to a Two-step Transesterification Reaction in a Pilot-Scale Reactive Distillation Column. *IFAC-PapersOnLine*, 51(18):67–72, 2018b. ISSN 24058963. doi: 10.1016/j.ifacol.2018.09.252. URL `https://doi.org/10.1016/j.ifacol.2018.09.252`.

Daniel Haßkerl, Sankaranarayanan Subramanian, Steven Markert, Stefanie Kaiser, and Sebastian Engell. Multi-rate state estimation applied to a pilot-scale reactive distillation process. *Chemical Engineering Science*, 185:256–281, 2018c. ISSN 00092509. doi: 10.1016/j.ces.2018.04.018.

Henrique Steinherz Hippert, Carlos Eduardo Pedreira, and Reinaldo Castro Souza. Neural networks for short-term load forecasting: A review and evaluation. *IEEE Transactions on Power Systems*, 16(1):44–55, 2001. ISSN 08858950. doi: 10.1109/59.910780.

Qiuming Hu, Yinglan Li, Yan Li, Jianhong Xie, Jinbin Zhang, Renyi Xu, and Sun Tianwei. Energy-saving production process and apparatus of ethyl lactate, 2019.

Koichi Iwakabe and Hitoshi Kosuge. Isobaric vapor-liquid-liquid equilibria with a newly developed still. *Fluid Phase Equilibria*, 192(1-2):171–186, 2001. ISSN 03783812. doi: 10.1016/S0378-3812(01)00631-8.

Koichi Iwakabe and Hitoshi Kosuge. A correlation method for isobaric vapor-liquid and vapor-liquid-liquid equilibria data of binary systems. *Fluid Phase Equilibria*, 266(1-2): 202–210, 2008. ISSN 03783812. doi: 10.1016/j.fluid.2008.01.019.

Amiya K. Jana and Sudip Banerjee. Neuro estimator-based inferential extended generic model control of a reactive distillation column. *Chemical Engineering Research and Design*, 130:284–294, 2018. ISSN 02638762. doi: 10.1016/j.cherd.2017.12.041.

Philip G. Jessop. Searching for green solvents, 2011. ISSN 14639270.

Zhongkai Jiang, Jumei Xu, Zuoxiang Zeng, Weilan Xue, and Shating Li. Kinetics of the esterification between lactic acid and isoamyl alcohol in the presence of silica gel-supported sodium hydrogen sulphate. *Canadian Journal of Chemical Engineering*, 96(9):1972–1978, 2018. ISSN 1939019X. doi: 10.1002/cjce.23127.

Liu Jianwu, Zhang Yue, Yan Shenghu, and Shen Jiefa. Catalyst for preparing acrylic acid and butyl ester using lactic acid method and preparation method thereof, 2009.

Yang Jichu, Ma Li, and Zhang Yang. Process for synthesizing ethyl lactate by catalytic rectifying method, 2005.

Suleyman Karacan. Biodiesel production using reactive distillation column: Real time model predictive control in Matlab Simulink. *International Journal of Energy Applications and Technologies*, pages 107–114, 2018. doi: 10.31593/ijeat.437998.

Rohit Kawathekar and James B. Riggs. Nonlinear model predictive control of a reactive distillation column. *Control Engineering Practice*, 15(2):231–239, 2007. ISSN 09670661. doi: 10.1016/j.conengprac.2006.07.004.

Tobias Keller. Reactive Distillation. In *Distillation: Equipment and Processes*, pages 261–294. 2014. ISBN 9780123868794. doi: 10.1016/B978-0-12-386878-7.00008-5.

V. N. Kiva, E. K. Hilmen, and S. Skogestad. Azeotropic phase equilibrium diagrams: A survey. *Chemical Engineering Science*, 58(10):1903–1953, 2003. ISSN 00092509. doi: 10.1016/S0009-2509(03)00018-6.

Rakesh Kumar and Sanjay M. Mahajani. Esterification of lactic acid with n-butanol by reactive distillation. In *Industrial and Engineering Chemistry Research*, volume 46, pages 6873–6882, 2007. doi: 10.1021/ie061274j.

I. Kuan Lai, Shih Bo Hung, Wan Jen Hung, Cheng Ching Yu, Ming Jer Lee, and Hsiao Ping Huang. Design and control of reactive distillation for ethyl and isopropyl acetates production with azeotropic feeds. *Chemical Engineering Science*, 62(3):878–898, 2007. ISSN 00092509. doi: 10.1016/j.ces.2006.10.019.

Ming Jer Lee, Ju Yin Chiu, and Ho Mu Lin. Kinetics of catalytic esterification of propionic acid and n-butanol over Amberlyst 35. *Industrial and Engineering Chemistry Research*, 41(12):2882–2887, 2002. ISSN 08885885. doi: 10.1021/ie0105472.

Fernando Arrais Romero Dias Lima, Ruan De Rezende Faria, Rodrigo Curvelo, Matheus Calheiros Fernandes Cadorini, César Augusto García Echeverry, Maurício Bezerra de Souza, and Argimiro Resende Secchi. Influence of Estimators and Numerical Approaches on the Implementation of NMPCs. *Processes*, 11(4):1102, apr 2023. ISSN 2227-9717. doi: 10.3390/pr11041102. URL `https://www.mdpi.com/2227-9717/11/4/1102`.

Laura Lomba, Beatriz Giner, Estefanía Zuriaga, Ignacio Gascón, and Carlos Lafuente. Thermophysical properties of lactates. *Thermochimica Acta*, 575:305–312, 2014. ISSN 00406031. doi: 10.1016/j.tca.2013.11.010.

Álvaro Orjuela Londoño, Fernando Leiva Lenis, Luis Alejandro, Boyacá Mendivelso, Gerardo Rodríguez Niño, Luis María, and Carballo Suárez. Obtención de mapas de curvas residuales para la síntesis de acetato de butilo. *Ingeniería e Investigación*, 26(3):26–34, 2006.

Michael L Luyben and William L. Luyben. *Essentials of Process Control*. 1997.

Jan M. Maciejowski. *Predictive Control with Constraints*. Pearson Education, 2002.

Raj Ganesh Manivannan, Sayeed Mohammad, Ken McCarley, Tony Cai, and Clint Aichele. A New Test System for Distillation Efficiency Experiments at Elevated Liquid Viscosities: Vapor-Liquid Equilibrium and Liquid Viscosity Data for Cyclopentanol + Cyclohexanol. *Journal of Chemical and Engineering Data*, 64(2):696–705, 2019. ISSN 15205134. doi: 10.1021/acs.jced.8b00929.

Antonio Marcilla, María Del Mar Olaya, María Dolores Serrano, and María Angeles Garrido. Pitfalls in the evaluation of the thermodynamic consistency of experimental VLE data sets. *Industrial and Engineering Chemistry Research*, 52(36):13198–13208, 2013. ISSN 08885885. doi: 10.1021/ie401646j.

Zion market research. Zion market research, 2017. URL `https://www.zionmarketresearch.com/market-analysis/bio-solvents-market`.

Alejandro Marquez-Ruiz, Carlos S. Méndez-Blanco, and Leyla Özkan. Modeling of reactive batch distillation processes for control. *Computers and Chemical Engineering*, pages 86–98, 2019. ISSN 00981354. doi: 10.1016/j.compchemeng.2018.10.010.

Andrés F. Martínez, Juan S. Rodríguez, Cesar A. Sánchez, Alvaro Orjuela, and Gerardo Rodríguez. Isobutyl acetate by reactive distillation. Part III. Conceptual design, simulation and optimization. *Chemical Engineering and Processing - Process Intensification*, 155, 2020a. ISSN 02552701. doi: 10.1016/j.cep.2020.108059.

Andrés F. Martínez, César A. Sánchez, Alvaro Orjuela, and Gerardo Rodríguez. Isobutyl acetate by reactive distillation. Non-reactive phase equilibrium and topological analysis. *Fluid Phase Equilibria*, page 112612, 2020b. ISSN 03783812. doi: 10.1016/j.fluid.2020.112612.

Mathworks. https://www.mathworks.com/help/gads/how-globalsearch-and-multistart-work.html.

David Q. Mayne, James B. Rawlings, CV Rao, and POM Scokaert. Constrained model predictive control: Stability and optimality. *Automatica*, 36(6):789–814, 2000.

Brian C. McDonald, Joost A. De Gouw, Jessica B. Gilman, Shantanu H. Jathar, Ali Akherati, Christopher D. Cappa, Jose L. Jimenez, Julia Lee-Taylor, Patrick L. Hayes, Stuart A. McKeen, Yu Yan Cui, Si Wan Kim, Drew R. Gentner, Gabriel Isaacman-VanWertz, Allen H. Goldstein, Robert A. Harley, Gregory J. Frost, James M. Roberts, Thomas B. Ryerson, and Michael Trainer. Volatile chemical products emerging as largest petrochemical source of urban organic emissions. *Science*, 359(6377):760–764, 2018. ISSN 10959203. doi: 10.1126/science.aaq0524.

Michael Michelsen. The isothermal flash problem. Part I. Stability. 9, 1982.

Michael L. Michelsen. Phase equilibrium calculations. What is easy and what is difficult? *Computers and Chemical Engineering*, 16:S19–S29, 1992. ISSN 00981354. doi: 10.1016/S0098-1354(09)80006-9.

Dennis J. Miller, Navinchandra Asthana, Aspi Kolah, and Carl T. Lira. Process for production of organic acid ester, 2006.

Liu Mo, Jiang Shao-Tong, Pan Li-Jun, Zheng Zhi, and Luo Shui-Zhong. Design and control of reactive distillation for hydrolysis of methyl lactate. *Chemical Engineering Research and Design*, 89(11):2199–2206, 2011. ISSN 02638762. doi: 10.1016/j.cherd.2011.03.001.

Ali Mohammad and Inamuddin. *Green solvents I: Properties and applications in chemistry*. 2012. ISBN 9789400717121. doi: 10.1007/978-94-007-1712-1.

Jørgen Mollerup and M L Michelsen. *Thermodynamic Models: Fundamentals Computational Aspects*. 2004. ISBN 8798996134.

Natalia Montoya, Jairo Durán, Fernando Córdoba, Iván Darío Gil, Carlos Alexander Trujillo, and Gerardo Rodríguez. Colombian fusel oil. *Ingenieria e Investigacion*, 36(2):21–27, 2016. ISSN 22488723. doi: 10.15446/ing.investig.v36n2.52369.

Alexander Nann, Christoph Held, and Gabriele Sadowski. Liquid âˆ' Liquid Equilibria of 1 â€‘ Butanol / Water / IL Systems. 2013.

William M. Nelson. Choosing Solvents That Promote Green Chemistry. pages 313–328. 2009. doi: 10.1021/bk-2000-0767.ch024.

Matthew J. Okasinski and Michael F. Doherty. Thermodynamic Behavior of Reactive Azeotropes. *AIChE Journal*, 43(9):2227–2238, 1997. ISSN 00011541. doi: 10.1002/aic.690430909.

Aykut Özgülsün, Filiz KaraosmanÇ'glu, and Melek Tüter. Esterification reaction of oleic acid with a fusel oil fraction for production of lubricating oil. *JAOCS, Journal of the American Oil Chemists' Society*, 77(1):105–109, 2000. ISSN 0003021X. doi: 10.1007/s11746-000-0017-5.

Susana Peña-Tejedor, Ruth Murga, Maria Teresa Sanz, and Sagrario Beltrán. Vapor-liquid equilibria and excess volumes of the binary systems ethanol + ethyl lactate, isopropanol + isopropyl lactate and n-butanol + n-butyl lactate at 101.325 kPa. *Fluid Phase Equilibria*, 230(1-2):197–203, 2005a. ISSN 03783812. doi: 10.1016/j.fluid.2005.02.015.

Susana Peña-Tejedor, Ruth Murga, Maria Teresa Sanz, and Sagrario Beltrán. Vapor-liquid equilibria and excess volumes of the binary systems ethanol + ethyl lactate, isopropanol + isopropyl lactate and n-butanol + n-butyl lactate at 101.325 kPa. *Fluid Phase Equilibria*, 2005b. ISSN 03783812. doi: 10.1016/j.fluid.2005.02.015.

Carla S.M. Pereira, Viviana M.T.M. Silva, and Alírio E. Rodrigues. Ethyl lactate as a solvent: Properties, applications and production processes - A review, 2011. ISSN 14639262.

Domenico Pirozzi and Guido Greco. Lipase-catalyzed transformations for the synthesis of butyl lactate: A comparison between esterification and transesterification. *Biotechnology Progress*, 22(2):444–448, 2006. ISSN 87567938. doi: 10.1021/bp0503033.

P. Swapna Reddy, K. Yamuna Rani, and Sachin C. Patwardhan. Multi-objective optimization of a reactive batch distillation process using reduced order model. *Computers and Chemical Engineering*, 106:40–56, 2017. ISSN 00981354. doi: 10.1016/j.compchemeng.2017.05.017.

C. E. Rehberg, Marion B. Dixon, and C. H. Fisher. Mixed esters of lactic and carbonic acids. reaction of chloroformates with esters of lactic acid. *Journal of Organic Chemistry*, 13(2): 254–264, 1948. ISSN 15206904. doi: 10.1021/jo01160a013.

Guo Rui and Zhang Weilue. Method for synthesizing high-purity butyl lactate, 2018.

Cesar A. Sánchez, Orlando A. Sánchez, Alvaro Orjuela, Iván D. Gil, and Gerardo Rodríguez. Vapor-liquid equilibrium for binary mixtures of acetates in the direct esterification of fusel oil. *Journal of Chemical and Engineering Data*, 62(1):11–19, 2017. ISSN 15205134. doi: 10.1021/acs.jced.6b00221.

Cesar A. Sánchez, Andrés A. Herrera, Julio C. Vargas, Iván D. Gil, and Gerardo Rodríguez. Isobaric Vapor Liquid Equilibria for Binary Mixtures of Isoamyl Acetate + Ethyl Acetate at 50 and 100 kPa. *Journal of Chemical and Engineering Data*, 64(5):2110–2115, 2019. ISSN 15205134. doi: 10.1021/acs.jced.8b01053.

Cesar A Sánchez, Iván D. Gil, and Gerardo Rodríguez. Fluid phase equilibria for the isoamyl acetate production by reactive distillation. *Fluid Phase Equilibria*, pages 2–30, 2020.

Maria Teresa Sanz, Sagrario Beltrán, Beatriz Calvo, Jose Luis Cabezas, and Jose Coca. Vapor Liquid Equilibria of the Mixtures Involved in the Esterification of Lactic Acid with Methanol. *Journal of Chemical and Engineering Data*, 48(6):1446–1452, 2003. ISSN 00219568. doi: 10.1021/je034028c.

William H. Schulz, Henry E. Schulz, Winter Haven, Woodrow Richardson, W. Fla. Auburndale, and William H. Schulz. Process of esterfying butyl lactate, 1955.

Boelo Schuur, Thomas Brouwer, Dion Smink, and Lisette M.J. Sprakel. Green solvents for sustainable separation processes. *Current Opinion in Green and Sustainable Chemistry*, 18:57–65, 2019. ISSN 24522236. doi: 10.1016/j.cogsc.2018.12.009.

Tretjak Serge, Burtin Elie, and Teissier Remy. Continuous production of ethyl lactate by esterifying lactic acid with ethanol, comprises using a flash column and distillation column for product recovery, 2004.

Mayank Shah, Anton A. Kiss, Edwin Zondervan, and André B. De Haan. A systematic framework for the feasibility and technical evaluation of reactive distillation processes. *Chemical Engineering and Processing: Process Intensification*, 60:55–64, 2012. ISSN 02552701. doi: 10.1016/j.cep.2012.05.007.

Bass Shailer L. and Fenn Howard N. Secondary butyl lactate, 1934.

Neha Sharma and Kailash Singh. Neural network and support vector machine predictive control of tert-amyl methyl ether reactive distillation column. *Systems Science and Control Engineering*, 2(1):512–526, 2014. ISSN 21642583. doi: 10.1080/21642583.2014.924082.

Sonali R Sharma. Green Chemistry, Green Solvents and Alternative Techniques in Organic Synthesis SONALI R. SHARMA Green Chemistry, Green Solvents and Alternative Techniques in Organic Synthesis. *International Journal of Chemical and Physical Sciences*, 4: 2319–6602, 2015.

Hong Xin Shen, Lorenzo Casalino, and Ya Zhong Luo. Global search capabilities of indirect methods for impulsive transfers. *Journal of the Astronautical Sciences*, 62(3):212–232, 2015. ISSN 21950571. doi: 10.1007/s40295-015-0073-x.

Skogestad Sigurd and Postlethwaite Ian. *MULTIVARIABLE FEEDBACK CONTROL Analysis and design*, volume 20. Second edition, 1979.

J. M. Smith. Introduction to chemical engineering thermodynamics. *Journal of Chemical Education*, 27(10):584, 1950. ISSN 0021-9584. doi: 10.1021/ed027p584.3.

Smith J. Van Ness and H. Abbott. *Introducción a la Termodinámica en Ingeniería Química*. 2009. ISBN 9780521191333. doi: 10: 0-8400-5444-0.

M Smith, J. Van Ness, H. Abbott. *Introducción a la Termodinámica en Ingeniería Química*. 2009. ISBN 9780521191333. doi: 10: 0-8400-5444-0.

Andrzej I. Stankiewicz and Jacob A. Moulijn. Process Intensification: Transforming Chemical Engineering - Netherlands Enterprise Agency. *Process Design Trends*, page 13, 2013. ISSN 03607275.

Sirivimon Tintavon and Paisan Kittisupakorn. EKF composition estimation and GMC control of a reactive distillation column. *AIP Conference Proceedings*, 1879, 2017. ISSN 15517616. doi: 10.1063/1.5000457.

Özge Tirpanalan, Michael Reisinger, Marina Smerilli, Florian Huber, Markus Neureiter, Wolfgang Kneifel, and Senad Novalin. Wheat bran biorefinery - An insight into the process chain for the production of lactic acid. *Bioresource Technology*, 180:242–249, 2015. ISSN 18732976. doi: 10.1016/j.biortech.2015.01.021.

Zsolt Ugray, Leon Lasdon, John Plummer, Fred Glover, James Kelly, and Rafael Marti. Scatter search and local NLP solvers: A multistart framework for global optimization. *INFORMS Journal on Computing*, 19(3):328–340, 2007. ISSN 15265528. doi: 10.1287/ijoc.1060.0175.

Sophie Ung and Michael F. Doherty. Vapor-liquid phase equilibrium in systems with multiple chemical reactions. *Chemical Engineering Science*, 50(1):23–48, 1995. ISSN 00092509. doi: 10.1016/0009-2509(94)00180-Y.

Olga Valerica Taga, Claudia Irina Koncsag, Ana Maria Sirvriu, and Gheorghita Jinescu. Isopropyl Lactate Obtaining by Transesterification in Reactive Distillation System. *revista de chimie*, 70(1), 2019.

Jayaram Valluru and Sachin C. Patwardhan. An Integrated Frequent RTO and Adaptive Nonlinear MPC Scheme Based on Simultaneous Bayesian State and Parameter Estimation. *Industrial and Engineering Chemistry Research*, 58(18):7561–7578, 2019. ISSN 15205045. doi: 10.1021/acs.iecr.8b05327.

Jayaram Valluru, Jalesh L. Purohit, Sachin C. Patwardhan, and Sanjay M. Mahajani. Adaptive optimizing control of an ideal reactive distillation column. In *IFAC-PapersOnLine*, volume 28, pages 489–494, 2015a. doi: 10.1016/j.ifacol.2015.09.015.

Jayaram Valluru, Jalesh L. Purohit, Sachin C. Patwardhan, and Sanjay M. Mahajani. Adaptive optimizing control of an ideal reactive distillation column. In *IFAC-PapersOnLine*, volume 28, pages 489–494, 2015b. doi: 10.1016/j.ifacol.2015.09.015.

Jessica J. Velandia, César A. García, Mario A. Céspedes, Gerardo Rodríguez, and Iván D. Gil. Reactive and non-reactive residue curve maps analysis to produce Butyl Lactate by catalytic distillation. *Chemical Engineering and Processing - Process Intensification*, 168, 2021. ISSN 02552701. doi: 10.1016/j.cep.2021.108558.

Ganesh Venimadhavan, George Buzad, Michael F. Doherty, and Michael F. Malone. Effect of kinetics on residue curve maps for reactive distillation. *AIChE Journal*, 40(11):1814–1824, 1994. ISSN 15475905. doi: 10.1002/aic.690401106.

A. Wahid and I. G.E.P. Putra. Multivariable model predictive control design of reactive distillation column for Dimethyl Ether production. In *IOP Conference Series: Materials Science and Engineering*, volume 334, 2018. doi: 10.1088/1757-899X/334/1/012018.

Henk Walpot. *Theoretical modeling of residue curve maps for a reactive distillation concept for the production of n -propyl propionate*. PhD thesis, Delf University, Delf, 2011.

Y. Wei, Y., Yu, Z. Wu, L. Zhang, S. Yang, and Z. Liu. A novel synthesis of ethyl lactate from bio-based lactic acid using sulfonated resin as catalyst. *Journal of Molecular Liquids*, 314(113609), 2020.

Charles Edmund Wood, John Edward Such, and Frank Scarf. CCLVI. - The rotatory dispersion of the esters of lactic acid. Part II. The isomeric butyl esters. *Journal of the Chemical Society (Resumed)*, 129:1928–1938, 1926. ISSN 03681769. doi: 10.1039/JR9262901928.

Anna Wypych and George Wypych. *Databook of green solvents*. ChemTec Publishing, Toronto, 2014. ISBN 9781895198829. doi: 10.1016/B978-1-895198-82-9.50001-4.

Anna George Wypych. No Title. In *Databook of Green Solvents*, chapter 1, pages 1–575. ChemTec Publishing, Toronto, 2014. ISBN 978-1-895198-82-9.

Jumei Xu, Shating Li, Zuoxiang Zeng, and Weilan Xue. Isobaric Vapor-Liquid Equilibrium for Binary System of Isoamyl dl -Lactate and Isoamyl Alcohol at 25.0, 50.0, and 101.3 kPa. *Journal of Chemical and Engineering Data*, 2020. ISSN 15205134. doi: 10.1021/acs.jced.9b00757.

Liang Yuming and Zhang Yong. Preparation method of high-purity food standard butyl lactate, 2015.

Qingrui Zhang, Sen Yan, Haiying Li, and Pengfei Xu. Optimization and control of a reactive and extractive distillation process for the synthesis of isopropyl acetate. *Chemical Engineering Communications*, 206(5):559–571, 2019. ISSN 15635201. doi: 10.1080/00986445.2018.1511982.

Lourdes Zumalacarregui. *Evaluación de métodos de consistencia termodinámica de datos experimentales de ELV a presión constante*. PhD thesis, UNIVERSIDAD TECNOLÓGICA DE LA HABANA, 2018.